

UNIVERSITY OF OKLAHOMA
GRADUATE COLLEGE

DESIGN AND IMPLEMENTATION OF A LOSS-PROGRAMMABLE
FILTERING ATTENUATOR

A THESIS
SUBMITTED TO THE GRADUATE FACULTY
in partial fulfillment of the requirements for the
Degree of
MASTER OF SCIENCE

By
JONATHAN KNOWLES
Norman, Oklahoma
2022

DESIGN AND IMPLEMENTATION OF A LOSS-PROGRAMMABLE
FILTERING ATTENUATOR

A THESIS APPROVED FOR THE
SCHOOL OF ELECTRICAL AND COMPUTER ENGINEERING

BY THE COMMITTEE CONSISTING OF

Dr. Jay McDaniel, Chair

Dr. Hjalti Sigmarsson

Dr. Caleb Fulton

© Copyright by JONATHAN KNOWLES 2022

All Rights Reserved.

Acknowledgments

I would not have been able to achieve all that I have in my time at the University of Oklahoma without the help of many wonderful people. I would first like to thank my advisor, Dr. Jay McDaniel. He saw my my potential and has guided and advised me since my Junior year. This sometimes involved basic questions about why some things are done as well as some less basic questions. He has not only helped me become a better engineer but has also taught me to be a better researcher as well as shown me how to present my work. Anytime I say that I would like to become better at something, he takes it as a personal mission to find opportunities for me to improve. I am better for having him as my advisor.

I would also like to thank the other two members of my committee, Dr. Hjalti Sigmarsson and Dr. Caleb Fulton. Dr. Sigmarsson has helped me understand microwave engineering in general and filter design specifically, better than I could have ever hoped. Dr. Fulton has taught me how the power of intuition can help when all else fails. He has also shown me that you can't keep a good dragon down. Both Dr. Sigmarsson and Dr. Fulton have shown me several tips and tricks that are extremely helpful and cannot be found in any book on microwave engineering.

I would also like to thank the many people at the Advanced Radar Research Center (ARRC) who have helped me in various ways throughout my time there. I would like to thank Clayton Blosser, Patrick O'Connor-Lynch, and Eric Wells for going through this process of graduate school with me and helping me in various

ways throughout this journey. I would also like to thank Paul Hartline, Russell Kenney, Rylee Mattingly, Rachel Jarvis, Grant Karber, Marc Thibodeau, Ashley Palmer, Stephen Bass, Chris Walker, Thomas Brachtenbach, Adrian Bauer, Kurt Konyalioglu, Randall Summers, Alex Pham, and many others at the ARRC who have assisted me academically and otherwise.

Finally, I would like to thank those who supported me in a non-academic way. My parents, Jim and Paula Knowles for always believing in me telling me I can do whatever I put my mind to. My brother, Joshua Knowles for being good at the things I am not good at and being willing to help me with them. My sister and brother in-law Jamie and Jerod Harris as well as my nephews Aiden and Colton for always trying to get me to relax and play some video games. And last but not least, the Council for being the best group of friends I could have hoped for. I am fortunate to have family and friends who support my goals like they all have.

This work is funded by the Department of Energy's Kansas City National Security Campus, operated by the Honeywell Federal Manufacturing Technologies, LLC under contract number DE-NA0002839.

Table of Contents

Acknowledgment	iv
Table of Contents	vi
List of Tables	ix
List of Figures	x
Abstract	xv
1 Introduction and Background	1
1.1 Filters	2
1.2 Attenuators	3
1.3 Filtering Attenuators	4
1.4 Thesis Outline	6
2 Theory	8
2.1 Generalized Math	8
2.2 Generalized Results	18
2.3 Resonator Quality Factor	24
2.4 Expansion to Higher Orders	27
2.4.1 Resistor Placement in Higher-Order Filtenuators	28
2.5 Summary	33

3	Static Filtenuator Design	34
3.1	Design of a Third-Order Static Filtenuator	34
3.1.1	Low-Pass Prototype	35
3.1.2	Lowpass to Bandpass Transformation	37
3.2	Simulations	41
3.2.1	Ideal Simulation	42
3.2.2	Adding Non-Ideal Inductor Models	43
3.2.3	Adding Non-Ideal Capacitor Models	45
3.2.4	Adding Non-Ideal Resistor Models	46
3.2.5	Effects of Traces Between Series Resonators	48
3.2.6	Adding Microstrip Traces and Vias	56
3.3	Fabrication	58
3.4	Measured Results	60
3.5	Summary	64
4	Tunable Filtenuator Design	65
4.1	Tunable Resistors	65
4.2	Simulation	67
4.2.1	Adding Non-Ideal Diode Models	67
4.2.1.1	Diode Biasing	69
4.2.2	Adding Non-Ideal RF Choke Models	71
4.2.3	Adding Non-Ideal Inductor Models	72
4.2.4	Adding Non-Ideal Capacitor Models	74
4.2.5	Adding Microstrip Traces and Vias	75
4.2.6	Multiple Levels of Attenuation	78
4.3	Fabrication	80
4.4	Measured Results	82
4.5	Summary	92

5	Conclusions and Future Work	93
5.1	Conclusions	93
5.2	Scientific Impact	94
5.3	Future Work	94
	References	97

List of Tables

2.1 Table of common attenuator values and associated resistance values
to achieve desired attenuation 18

3.1 Table of calculated g-coefficients 36

3.2 Table of values used for the static filtenuator 62

4.1 Table of filtenuator losses and the corresponding biasing voltages
and currents 92

List of Figures

1.1	A traditional RF receive chain found in wireless systems	2
1.2	The four main types of microwave filters, from [1]	3
1.3	A traditional RF receive chain with the filter and attenuator combined	4
1.4	Effect of added loss to filter on filter shape, from [2]	5
2.1	Generalized third-order filtering attenuator circuit schematic	9
2.2	Generalized third-order filtenuator circuit schematic with defined resistances	11
2.3	Generalized third-order filtenuator circuit schematic at resonance . .	13
2.4	Circuit schematic for solving for the input impedance of the filtenuator at resonance	13
2.5	Circuit schematic for solving for the transfer function of the filtenuator at resonance, adapted from [3]	15
2.6	Example circuit schematic of a lowpass filtenuator	19
2.7	S-parameters of a lowpass filtenuator	20
2.8	Example circuit schematic of a highpass filtenuator	20
2.9	S-parameters of a highpass filtenuator	21
2.10	Example circuit schematic of a bandpass filtenuator	22
2.11	S-parameters of a bandpass filtenuator	22
2.12	Example circuit schematic of a bandstop filtenuator	23
2.13	S-parameters of a bandstop filtenuator	23
2.14	Circuit for calculating series resonator quality factor	25

2.15	Quality factor as a function of resistance	26
2.16	Bandwidth as a function of resistance	26
2.17	Generalized schematic of a fifth-order filtenuator circuit	27
2.18	Generalized schematic of a fifth-order filtenuator circuit at resonance	28
2.19	fifth-order filtenuator schematic with only central resonator resistively loaded	29
2.20	S-parameters for a fifth-order filtenuator with 3, 6, and 10 dB of loss with the resistance added to only the center-most resonator . . .	29
2.21	Fifth-order filtenuator schematic with resistance spread among series resonators	30
2.22	S-parameters for a fifth-order filtenuator with 3, 6, and 10 dB of loss with the resistance spread out along the series resonators	31
2.23	Fifth-order filtenuator schematic with resistance only on outer-most series resonators	32
2.24	S-parameters for a fifth-order filtenuator with 3, 6, and 10 dB of loss with the resistance added to only the outer-most resonators . . .	32
3.1	Lowpass filter prototype schematic	37
3.2	Lowpass filter prototype S-parameters	37
3.3	Schematic of the lowpass filter scaled to the system impedance . . .	38
3.4	Table of filter transformations found in [4]	39
3.5	Frequency scaled and bandpass transformed lowpass prototype . . .	39
3.6	Final designed third-order Chebyshev bandpass filter	40
3.7	S-parameters of the designed third-order Chebyshev bandpass filter .	41
3.8	ADS simulation setup of the ideal filtenuator	42
3.9	S-parameters for the ideal filtenuator simulation	43
3.10	ADS simulation setup of the filtenuator after adding real measured inductor S-parameters	44

3.11	S-parameters for the ADS simulation after adding real inductor S-parameters compared to the ideal simulation	44
3.12	ADS simulation setup of the filtenuator after adding real measured capacitor S-parameters	45
3.13	S-parameters for the ADS simulation after adding real capacitor S-parameters compared to the ideal simulation	46
3.14	ADS simulation setup of the filtenuator after adding an equivalent circuit for the resistors	47
3.15	S-parameters for the ADS simulation after adding resistor equivalent circuit compared to the ideal simulation	47
3.16	Ideal circuit of the series LC resonator	48
3.17	Simulated S-parameters of the ideal series LC resonator	49
3.18	Schematic of the series LC resonator with a transmission line in-between components	50
3.19	Simulated S-parameters of the series LC resonator with a transmission line in-between components compared to the ideal LC resonator	50
3.20	Equivalent circuit of the series resonator with transmission line . . .	51
3.21	Simulated S-parameters of the series LC resonator with the added inductance compensated for compared to the ideal LC resonator . .	53
3.22	Model of the series resonator used to solve for C_{new}	54
3.23	Simulated S-parameters of the series LC resonator with the added capacitance compensated for compared to the ideal LC resonator . .	55
3.24	S-parameters for the fully non-ideal ADS simulation	57
3.25	S-parameters for the ADS simulation after adding microstrip traces compared to the ideal simulation	58
3.26	EAGLE layout of the static filtenuator	59
3.27	Fabricated and populated PCB of the static filtenuator	60
3.28	Measured results of the static filtenuator compared to ADS simulation	61

3.29	Measured S_{11} of the static filtenuator with 3, 4, 5, 6, and 7 dB of passband attenuation	62
3.30	Measured S_{21} of the static filtenuator with 3, 4, 5, 6, and 7 dB of passband attenuation	63
3.31	Measured group delay of the static filtenuator with 3, 4, 5, 6, and 7 dB of passband attenuation	64
4.1	Filtenuator schematic with diodes added	67
4.2	Filtenuator ADS schematic after adding PIN diode equivalent circuit	68
4.3	Filtenuator simulation S-parameters after adding PIN diode equivalent circuit	68
4.4	Filtenuator schematic with biasing circuitry added	70
4.5	DC analysis of filtenuator schematic with biasing circuitry	70
4.6	Filtenuator ADS schematic after adding biasing circuitry	71
4.7	Filtenuator simulation S-parameters after adding RF choke measured S-parameters compared to non-ideal diode S-parameters . . .	72
4.8	Filtenuator ADS schematic after adding measured inductor S-parameters	73
4.9	Filtenuator simulation S-parameters after adding measured inductor S-parameters compared to non-ideal diode S-parameters	73
4.10	Filtenuator ADS schematic after adding measured capacitor S-parameters	74
4.11	Filtenuator simulation S-parameters after adding measured capacitor S-parameters compared to non-ideal diode S-parameters	75
4.12	Filtenuator ADS schematic after adding microstrip trace and via models	76
4.13	Filtenuator simulation S-parameters after adding microstrip trace and via models	77
4.14	S_{21} of the final ADS simulation with 3, 4, 5, 6, and 7 dB of loss . . .	78
4.15	Zoomed-In S_{21} of the final ADS simulation with 3, 4, 5, 6, and 7 dB of loss	79

4.16	S_{11} of the final ADS simulation with 3, 4, 5, 6, and 7 dB of loss	80
4.17	Layout of the tunable filtenuator	81
4.18	Fabricated and populated PCB of the tunable filtenuator	82
4.19	Measured S-parameters of the filtenuator with both diodes sharing a power supply	82
4.20	S-parameters of the filtenuator ADS simulation with both diodes sharing a power supply	83
4.21	Measured S-parameters after using separate power supplies for shunt diodes	84
4.22	Simulated S-parameters of the single inductor bias line compared to the inductor and capacitor bias line	85
4.23	Measured S-parameters after adding bypass capacitor to bias lines	86
4.24	S-parameters of the filtenuator simulation compared to the mea- sured results	87
4.25	S_{21} of the final filtenuator measurements with 3, 4, 5, 6, and 7 dB of loss	88
4.26	Zoomed-In S_{21} of the final filtenuator measurements with 3, 4, 5, 6, and 7 dB of loss	89
4.27	S_{11} of the measured results with 3, 4, 5, 6, and 7 dB of loss	90
4.28	Group delay of the measured filtenuator with 3, 4, 5, 6, and 7 dB of loss	91
5.1	Calculated group delay of a symmetric filtenuator simulation with 3, 7, and 10 dB of attenuation	95
5.2	Calculated group delay of an asymmetric filtenuator simulation with 3, 7, and 10 dB of attenuation	96

Abstract

With the increased demand for modern wireless systems in various applications, the need for adaptable radio frequency (RF) systems has greatly increased. These modern systems rely on the ability to operate in the microwave frequency spectrum (1 GHz to 1 THz) without interference from other devices while also retaining the ability to detect very low and very high power signals simultaneously. There is also an ever-increasing demand for the reduction of cost, size, weight, and power (C-SWaP) of these modern RF systems that drives an ever-increasing demand for more agile filters in the microwave frequency spectrum. A filtering attenuator (filtenuator) is a device that combines the frequency-selective characteristics of a filter and the loss-programmable characteristics of an attenuator into a single component. In this thesis, a generalized theory of filtenuators is presented. A loss-programmable, third-order filtenuator is also designed to verify the generalized theory. The design of the filtenuator is based on tuning the resistance of a π -network of resistors. The tuning of the resistances is achieved through the use of PIN diodes. The π -network of resistances is built around a third-order filter that provides the filter response of the filtenuator. The filtenuator is designed to operate at 1 GHz and have a tunable attenuation range of 2-10 dB. This filtenuator demonstrates the feasibility of a tunable, low C-SWaP solution to increase RF system dynamic range as well as demonstrating a design process that allows for future development of filtenuators.

Chapter 1

Introduction and Background

In the modern world, there is an increasing demand for and reliance on wireless data transfer, power transfer, and sensing which is due to the increased prevalence of 5G, the Internet of Things, self-driving cars, imaging, and many other new and exciting technologies. Because there are so many new technologies that rely on access to the frequency spectrum and because the frequency spectrum is a finite resource, there is a ubiquitous need to carefully manage the use of the spectrum by these different technologies. All of these amazing new technologies which rely on the ability of modern RF systems to operate in the microwave frequency spectrum (1 GHz to 1 THz) also need to be able to detect very low power signals as well as very high power signals. There is also simultaneously an ever-increasing demand for the reduction of cost, size, weight, and power (C-SWaP) of modern RF systems.

Traditionally, an RF receiver (Rx) consists of an antenna, a filter, an attenuator, and an amplifier. In the system, the antenna receives signals by utilizing its intrinsic spacial filtering properties. The filter then allows only the signals within the band of frequencies which it has been designed for to pass while attenuating the out-of-band signals. The attenuator then lowers the power level of the received signal to a level that the amplifier can handle while also providing a broadband match between the filter and the amplifier. The amplifier then amplifies the signal that is now, ideally,

at the correct frequency and power level to the analog to digital converter (ADC). A schematic of a traditional RF front end is shown in Figure 1.1.

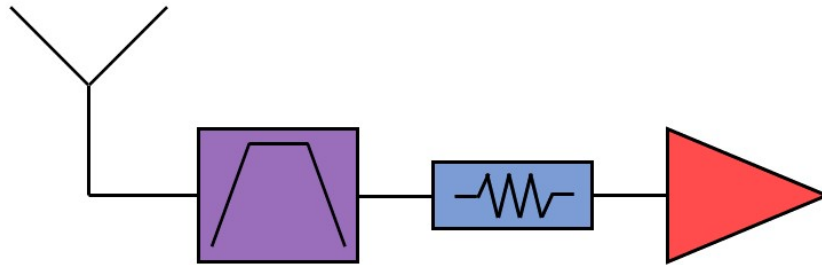


Figure 1.1: A traditional RF receive chain found in wireless systems

1.1 Filters

To ensure that these devices operate in their desired frequency band, filters are used. Filters are electrical components that have frequency-dependent properties that allow a certain group of frequencies to be transmitted while at the same time stopping the transmission of other frequencies. This component allows devices to operate without interfering with one another.

There are four different types of microwave filters: lowpass, highpass, bandpass, and bandstop. A lowpass filter allows frequencies below the cutoff frequency to be passed while attenuating frequencies higher than the cutoff frequency. Highpass filters do the opposite and allow frequencies above the cutoff frequency to be passed while attenuating frequencies lower than the cutoff frequency. Bandpass filters allow a band of frequencies to pass while attenuating frequencies above and below that band. Bandstop filters attenuate a band of frequencies while allowing frequencies above and below that band to pass. An illustration of the four main

types of microwave filters is shown in Figure 1.2.

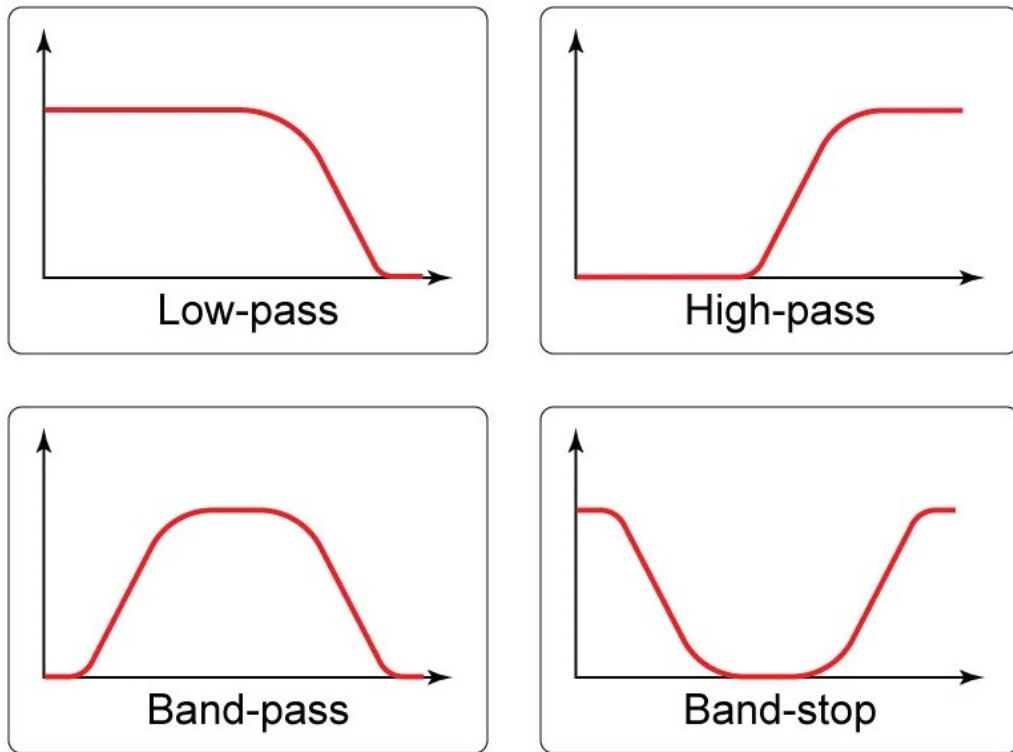


Figure 1.2: The four main types of microwave filters, from [1]

1.2 Attenuators

In RF and microwave systems, attenuators also serve multiple purposes. Often-times a signal needs to be attenuated in order to avoid over-driving an amplifier. Attenuators are also used in radar systems to provide a broadband match for unmatched components such as filters (matched in the passband and reflective in the stopband) and amplifiers by placing the attenuator between these two components. There are three basic types of attenuator: fixed attenuators, variable attenuators, and step attenuators [5]. Fixed attenuators are passive devices which provide a fixed attenuation levels. The drawback of a fixed attenuator is that they must be switched

out of a system when a different attenuation level is necessary. Step attenuators allow the attenuation to be modified in discrete fixed steps. The drawback of a step attenuator is that the attenuation level necessary for your system may be a value that it is not capable of providing. Variable attenuators are active devices which allow for continuous tuning of the attenuation of the device by changing the voltage. A drawback of variable attenuators is that they are not frequency-selective. An ideal scenario would be to have a continuously tunable attenuator with the frequency-selective capability of a filter.

1.3 Filtering Attenuators

A possible solution is to create a component that combines the function of a filter and an attenuator into a single component. Another addition to this component would be to make the passband attenuation of this new component loss-programmable to accommodate for different power levels of received signals. This would serve to lower the overall system SWaP while also increasing the dynamic range of the system by allowing the system to receive a wider range of inputs. A

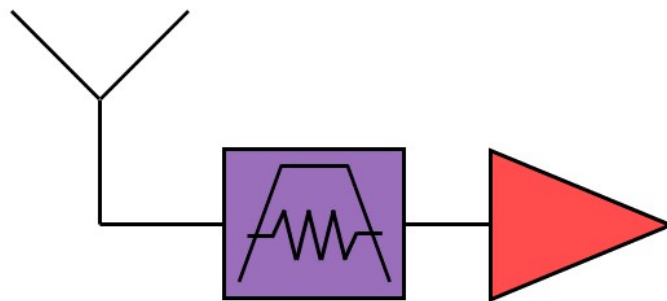


Figure 1.3: A traditional RF receive chain with the filter and attenuator combined

schematic of a RF front end with the filter and attenuator combined to decrease system SWaP is shown in Figure 1.3.

There is limited literature on filters that serve a dual purpose of attenuating while filtering. One method used to combine the frequency selective characteristics of a filter with the attenuation properties of an attenuator is done by intentionally introducing loss into the filter. This added loss has the added effect of causing the filter to begin losing its shape due to this loss causing a reduction in the quality factor of the resonators. The quality factor (Q) of a resonator is a unit-less figure of merit defined as the time-averaged stored energy in a resonator divided by the energy lost per second in that resonator [2]. There is some literature on methods to correct for this loss of shape [6, 7]. These methods still require the design of a separate filter for each amount of desired attenuation within a system. An illustration of the effect that decreasing the unloaded quality factor of the resonators of a filter has on the shape of the filter is shown in Figure 1.4.

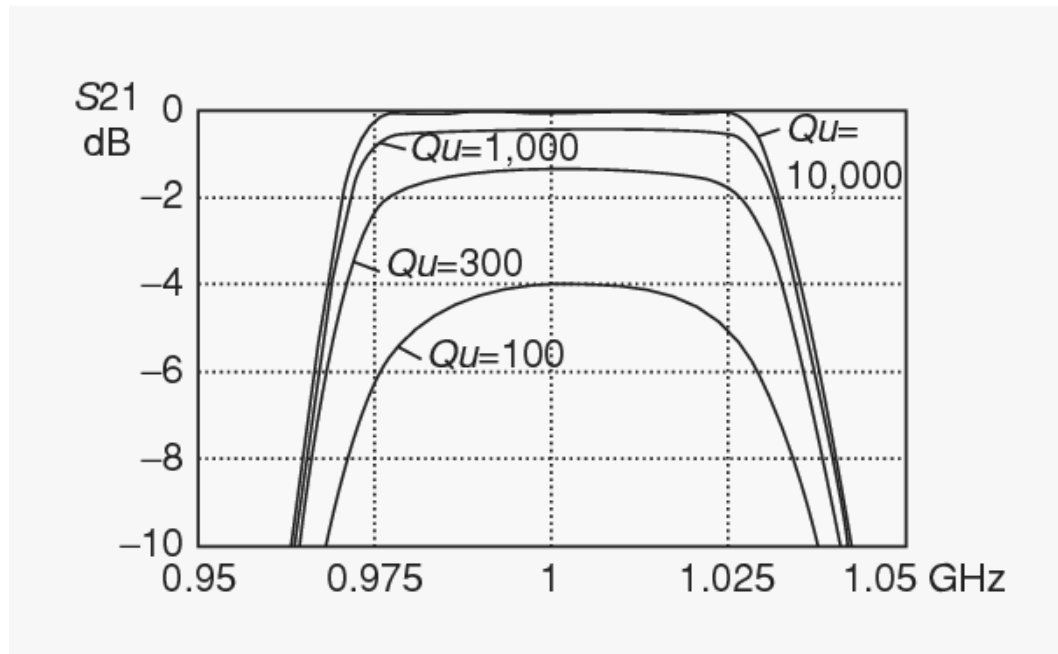


Figure 1.4: Effect of added loss to filter on filter shape, from [2]

There have been other attempts to design filters that serve a dual purpose of attenuating while filtering. These include higher frequency, on-chip implementations using field-effect transistors [8, 9] or graphene [10]-[14], and a bandstop filter application where the stopband attenuation is controlled [15, 16]. The on-chip filtering attenuator (filtenuator) is limited to discrete values of attenuation and the graphene version suffers from the series resistance added to the resonators resulting in a poor match. A filtenuator that remains well-matched, has the utility to be modified to accommodate different filter types, and also is reproducible using traditional fabrication methods using lumped-element LC components at low frequencies to reduce cost and integrated circuit (IC) fabrication lead times would be an ideal technology to mitigate the aforementioned problems.

1.4 Thesis Outline

The goal of this thesis is to demonstrate the theory, design, simulation, and fabrication of loss-programmable filtenuators. Because of that, this thesis will be broken down into several sections to cover these areas.

Chapter 2 covers the generalized theory of filtenuators. A generalized circuit topology is chosen and used to derive a set of generalized design equations for the filtenuator concept. Several different types of filtenuators are demonstrated including: lowpass, highpass, bandpass, and bandstop filtenuators. The effect on resonator Q of resistively loading resonators is also explored. Finally, the generalized topology is expanded to higher-order filtenuators and the effects of resistor placement are explored.

Chapter 3 covers the design, simulation, and fabrication of a static filtenuator design. A third-order bandpass filtenuator is designed as a proof-of-concept. This

circuit is then designed step-by-step in Keysight Advanced Design System (ADS) using non-ideal component models. The design is finally fabricated and tested to validate the filtenuator theory in Chapter 2.

Chapter 4 focuses on the design, simulation, and fabrication of a tunable filtenuator design. A third-order tunable bandpass filtenuator is designed using PIN diodes as tunable resistances. This design is then designed step-by-step in ADS using non-ideal component models. An evaluation of the effects of bias lines configuration on the out of band performance of the filtenuator is also performed. The design is then fabricated and tested.

Chapter 5 provides a summary of work and the scientific impact of the work. This chapter also discusses potential improvements to the design and areas of the research that should be explored in the future.

Chapter 2

Theory

To have a good understanding of the filtering attenuator (filtenuator) operation, a strong theoretical foundation is necessary. This is accomplished by solving for the generalized filtenuator structure. These results are then evaluated at the resonant frequency to show that the structure breaks down into a π -resistor circuit. Design equations are derived by solving the resulting circuit for its input impedance and transfer function. These derived equations are then used to show a theoretical foundation for the design of lowpass, highpass, bandpass, and bandstop filtenuators. This mathematical basis is then expanded to the case of higher-order filtenuator circuit structures.

2.1 Generalized Math

In deciding on a general circuit structure for the filtenuator concept, several factors must be considered. The structure must enable tunability of the circuit, allow for the filtenuator to remain well-matched, and be realizable. With these factors in mind, it was decided to take a traditional π -resistor attenuator circuit and superimpose a series-shunt-series lumped-element ladder filter structure into that traditional circuit model. A generalized schematic of the filtenuator has been

designed and is shown in Figure 2.1. In this schematic, $Z_1, Z_3, Z_5,$ and Z_7 are impedances determined by mathematics, which are derived later, while $Z_2, Z_4,$ and Z_6 are resonators for the type of filter to be implemented.

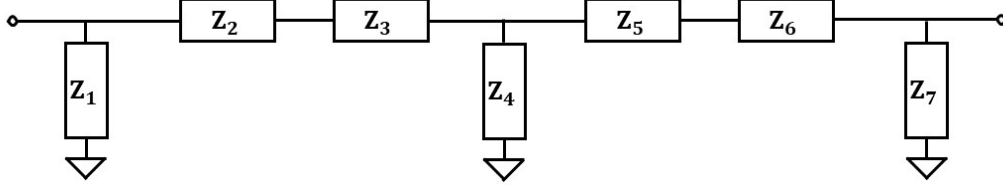


Figure 2.1: Generalized third-order filtering attenuator circuit schematic

The ABCD Matrix for a shunt admittance is

$$\begin{bmatrix} A_N & B_N \\ C_N & D_N \end{bmatrix} = \begin{bmatrix} 1 & 0 \\ Y_N & 1 \end{bmatrix} = \begin{bmatrix} 1 & 0 \\ \frac{1}{Z_N} & 1 \end{bmatrix} \quad (2.1)$$

while the ABCD Matrix for a series impedance is

$$\begin{bmatrix} A_N & B_N \\ C_N & D_N \end{bmatrix} = \begin{bmatrix} 1 & Y_N \\ 0 & 1 \end{bmatrix} = \begin{bmatrix} 1 & \frac{1}{Z_N} \\ 0 & 1 \end{bmatrix}. \quad (2.2)$$

The full matrix for the structure is

$$\begin{bmatrix} A & B \\ C & D \end{bmatrix} = \begin{bmatrix} A_1 & B_1 \\ C_1 & D_1 \end{bmatrix} \begin{bmatrix} A_2 & B_2 \\ C_2 & D_2 \end{bmatrix} \begin{bmatrix} A_3 & B_3 \\ C_3 & D_3 \end{bmatrix} \begin{bmatrix} A_4 & B_4 \\ C_4 & D_4 \end{bmatrix} \begin{bmatrix} A_5 & B_5 \\ C_5 & D_5 \end{bmatrix} \begin{bmatrix} A_6 & B_6 \\ C_6 & D_6 \end{bmatrix} \begin{bmatrix} A_7 & B_7 \\ C_7 & D_7 \end{bmatrix} \quad (2.3)$$

which is a cascade of the components within the general circuit structure. Using the ABCD matrices for the shunt admittance and the series impedance and substituting into (2.3) yields

$$\begin{bmatrix} A & B \\ C & D \end{bmatrix} = \begin{bmatrix} 1 & 0 \\ \frac{1}{Z_1} & 1 \end{bmatrix} \begin{bmatrix} 1 & Z_2 \\ 0 & 1 \end{bmatrix} \begin{bmatrix} 1 & Z_3 \\ 0 & 1 \end{bmatrix} \begin{bmatrix} 1 & 0 \\ \frac{1}{Z_4} & 1 \end{bmatrix} \begin{bmatrix} 1 & Z_5 \\ 0 & 1 \end{bmatrix} \begin{bmatrix} 1 & Z_6 \\ 0 & 1 \end{bmatrix} \begin{bmatrix} 1 & 0 \\ \frac{1}{Z_7} & 1 \end{bmatrix}. \quad (2.4)$$

The next several steps in the derivation process involve stepping through the matrix multiplications to solve for the combined ABCD parameter matrix of the circuit. The matrix multiplies are shown below, starting from the left and proceeding to the right

$$\begin{bmatrix} A & B \\ C & D \end{bmatrix} = \begin{bmatrix} 1 & Z_2 \\ \frac{1}{Z_1} & \frac{Z_2}{Z_1} + 1 \end{bmatrix} \begin{bmatrix} 1 & Z_3 \\ 0 & 1 \end{bmatrix} \begin{bmatrix} 1 & 0 \\ \frac{1}{Z_4} & 1 \end{bmatrix} \begin{bmatrix} 1 & Z_5 \\ 0 & 1 \end{bmatrix} \begin{bmatrix} 1 & Z_6 \\ 0 & 1 \end{bmatrix} \begin{bmatrix} 1 & 0 \\ \frac{1}{Z_7} & 1 \end{bmatrix}$$

$$\begin{bmatrix} A & B \\ C & D \end{bmatrix} = \begin{bmatrix} 1 & Z_2 + Z_3 \\ \frac{1}{Z_1} & \frac{Z_2}{Z_1} + \frac{Z_3}{Z_1} + 1 \end{bmatrix} \begin{bmatrix} 1 & 0 \\ \frac{1}{Z_4} & 1 \end{bmatrix} \begin{bmatrix} 1 & Z_5 \\ 0 & 1 \end{bmatrix} \begin{bmatrix} 1 & Z_6 \\ 0 & 1 \end{bmatrix} \begin{bmatrix} 1 & 0 \\ \frac{1}{Z_7} & 1 \end{bmatrix}$$

$$\begin{bmatrix} A & B \\ C & D \end{bmatrix} = \begin{bmatrix} \frac{Z_2+Z_3}{Z_4} + 1 & Z_2 + Z_3 \\ \frac{\frac{Z_2}{Z_1} + \frac{Z_3}{Z_1} + 1}{Z_4} + \frac{1}{Z_1} & \frac{Z_2}{Z_1} + \frac{Z_3}{Z_1} + 1 \end{bmatrix} \begin{bmatrix} 1 & Z_5 \\ 0 & 1 \end{bmatrix} \begin{bmatrix} 1 & Z_6 \\ 0 & 1 \end{bmatrix} \begin{bmatrix} 1 & 0 \\ \frac{1}{Z_7} & 1 \end{bmatrix}$$

$$\begin{bmatrix} A & B \\ C & D \end{bmatrix} = \begin{bmatrix} \frac{Z_2+Z_3}{Z_4} + 1 & Z_2 + Z_3 + Z_5 \left(\frac{Z_2+Z_3}{Z_4} + 1 \right) \\ \frac{\frac{Z_2}{Z_1} + \frac{Z_3}{Z_1} + 1}{Z_4} + \frac{1}{Z_1} & Z_5 \left(\frac{\frac{Z_2}{Z_1} + \frac{Z_3}{Z_1} + 1}{Z_4} + \frac{1}{Z_1} \right) + \frac{Z_2}{Z_1} + \frac{Z_3}{Z_1} + 1 \end{bmatrix} \begin{bmatrix} 1 & Z_6 \\ 0 & 1 \end{bmatrix} \begin{bmatrix} 1 & 0 \\ \frac{1}{Z_7} & 1 \end{bmatrix}$$

$$\begin{bmatrix} A & B \\ C & D \end{bmatrix} = \begin{bmatrix} \frac{Z_2+Z_3}{Z_4} + 1 & Z_2 + Z_3 + Z_5 \left(\frac{Z_2+Z_3}{Z_4} + 1 \right) + Z_6 \left(\frac{Z_2+Z_3}{Z_4} + 1 \right) \\ \frac{\frac{Z_2}{Z_1} + \frac{Z_3}{Z_1} + 1}{Z_4} + \frac{1}{Z_1} & Z_5 \left(\frac{\frac{Z_2}{Z_1} + \frac{Z_3}{Z_1} + 1}{Z_4} + \frac{1}{Z_1} \right) + Z_6 \left(\frac{\frac{Z_2}{Z_1} + \frac{Z_3}{Z_1} + 1}{Z_4} + \frac{1}{Z_1} \right) + \frac{Z_2}{Z_1} + \frac{Z_3}{Z_1} + 1 \end{bmatrix} \begin{bmatrix} 1 & 0 \\ \frac{1}{Z_7} & 1 \end{bmatrix}$$

$$A = \frac{Z_2 + Z_3}{Z_4} + \frac{Z_2 + Z_3 + Z_5 \left(\frac{Z_2+Z_3}{Z_4} + 1 \right) + Z_6 \left(\frac{Z_2+Z_3}{Z_4} + 1 \right)}{Z_7} + 1 \quad (2.5)$$

$$B = Z_2 + Z_3 + Z_5 \left(\frac{Z_2 + Z_3}{Z_4} + 1 \right) + Z_6 \left(\frac{Z_2 + Z_3}{Z_4} + 1 \right) \quad (2.6)$$

$$C = \frac{\frac{Z_2}{Z_1} + \frac{Z_3}{Z_1} + 1}{Z_4} + \frac{1}{Z_1} + \frac{Z_5 \left(\frac{\frac{Z_2}{Z_1} + \frac{Z_3}{Z_1} + 1}{Z_4} + \frac{1}{Z_1} \right) + Z_6 \left(\frac{\frac{Z_2}{Z_1} + \frac{Z_3}{Z_1} + 1}{Z_4} + \frac{1}{Z_1} \right) + \frac{Z_2}{Z_1} + \frac{Z_3}{Z_1} + 1}{Z_7} \quad (2.7)$$

$$D = Z_5 \left(\frac{\frac{Z_2}{Z_1} + \frac{Z_3}{Z_1} + 1}{Z_4} + \frac{1}{Z_1} \right) + Z_6 \left(\frac{\frac{Z_2}{Z_1} + \frac{Z_3}{Z_1} + 1}{Z_4} + \frac{1}{Z_1} \right) + \frac{Z_2}{Z_1} + \frac{Z_3}{Z_1} + 1. \quad (2.8)$$

Now that the matrix multiplications have been stepped through and the combined ABCD parameters of the circuit have been solved for, it is necessary to define which blocks within the circuit will be resistances. A symmetric circuit is assumed and so $Z_1 = Z_7 = R_A$ and $Z_3 = Z_5 = \frac{R_B}{2}$. A figure of the generalized third-order filtenuator circuit with defined resistances is shown in Figure 2.2.

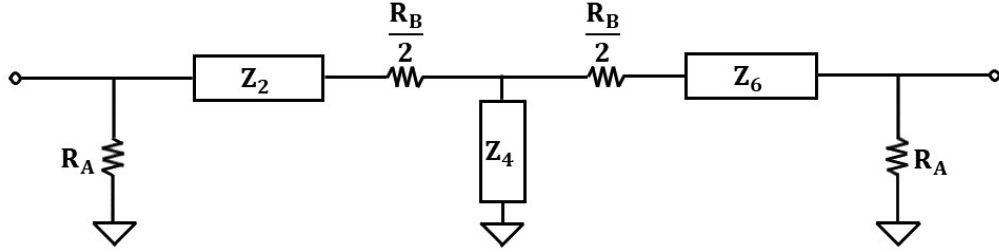


Figure 2.2: Generalized third-order filtenuator circuit schematic with defined resistances

The new values that have been decided on for Z_1 , Z_3 , Z_5 , and Z_7 can then be substituted into (2.5-2.8) which yields

$$A = \alpha + \frac{\frac{R_B}{2} + Z_2 + \frac{R_B(\alpha+1)}{2} + Z_6(\alpha+1)}{R_A} + 1 \quad (2.9)$$

$$B = \frac{R_B}{2} + Z_2 + \frac{R_B(\alpha+1)}{2} + Z_6(\alpha+1) \quad (2.10)$$

$$C = \frac{\alpha}{R_A} + \frac{1}{Z_4} + \frac{\frac{R_B}{2} \left(\frac{\alpha+1}{R_A} + \frac{1}{Z_4} \right) + Z_6 \left(\frac{\alpha+1}{R_A} + \frac{1}{Z_4} \right) + \frac{R_B}{2R_A} + \frac{Z_2}{R_A} + 1}{R_A} + \frac{1}{R_A} \quad (2.11)$$

$$D = \frac{R_B}{2} \left(\frac{\alpha+1}{R_A} + \frac{1}{Z_4} \right) + Z_6 \left(\frac{\alpha+1}{R_A} + \frac{1}{Z_4} \right) + \frac{R_B}{2R_A} + \frac{Z_2}{R_A} + 1 \quad (2.12)$$

where $\alpha = \frac{R_B + Z_2}{Z_4}$, R_A is the shunt resistances of the π -network, and R_B is the series resistance of the π -network. Note that R_B is divided by 2 to enforce symmetry within the circuit. At the resonant frequency Z_2 and Z_6 will act as short circuit and Z_4 will act as an open circuit. Because this is true, the limit is taken as Z_2 and Z_6 approach 0 and as Z_4 approaches ∞ . This allows (2.9-2.12) to be simplified as

$$\begin{bmatrix} A & B \\ C & D \end{bmatrix} = \begin{bmatrix} \frac{R_B}{R_A} + 1 & R_B \\ \frac{1}{R_A} + \frac{R_B + 1}{R_A} & \frac{R_B}{R_A} + 1 \end{bmatrix}. \quad (2.13)$$

The ABCD parameters are then converted to S-parameters [4] using

$$\begin{bmatrix} S_{11} & S_{12} \\ S_{21} & S_{22} \end{bmatrix} = \begin{bmatrix} \frac{A + \frac{B}{Z_0} - CZ_0 - D}{A + \frac{B}{Z_0} + CZ_0 + D} & \frac{2(AD - BC)}{A + \frac{B}{Z_0} + CZ_0 + D} \\ \frac{2}{A + \frac{B}{Z_0} + CZ_0 + D} & \frac{-A + \frac{B}{Z_0} - CZ_0 + D}{A + \frac{B}{Z_0} + CZ_0 + D} \end{bmatrix} \quad (2.14)$$

where Z_0 is the characteristic impedance of the system and A, B, C, and D are defined in (2.13). Putting (2.13) into (2.14) yields

$$S_{11} = \frac{\frac{R_B}{Z_0} - Z_0 \left(\frac{1}{R_A} + \frac{R_B + 1}{R_A} \right)}{\frac{2R_B}{R_A} + \frac{R_B}{Z_0} + Z_0 \left(\frac{1}{R_A} + \frac{R_B + 1}{R_A} \right) + 2} \quad (2.15)$$

$$S_{21} = \frac{2}{\frac{2R_B}{R_A} + \frac{R_B}{Z_0} + Z_0 \left(\frac{1}{R_A} + \frac{R_B + 1}{R_A} \right) + 2} \quad (2.16)$$

$$S_{21} = \frac{2}{\frac{2R_B}{R_A} + \frac{R_B}{Z_0} + Z_0 \left(\frac{1}{R_A} + \frac{R_B + 1}{R_A} \right) + 2} \quad (2.17)$$

$$S_{22} = \frac{\frac{R_B}{Z_0} - Z_0 \left(\frac{1}{R_A} + \frac{R_B + 1}{R_A} \right)}{\frac{2R_B}{R_A} + \frac{R_B}{Z_0} + Z_0 \left(\frac{1}{R_A} + \frac{R_B + 1}{R_A} \right) + 2}. \quad (2.18)$$

The S-parameters are now in terms of the resistances R_A and R_B as well as the system impedance Z_0 .

This shows that at the operating frequency of the designed filter, the intrinsic loss of the filter will be affected primarily by the chosen resistances R_A and R_B . These resistances are chosen such that the circuit is matched to the impedance of

the system at the operating frequency of the filter as well as providing the desired amount of attenuation.

At the operating frequency of the filter, the circuit will break down into a π -resistor network which can be solved using traditional circuit theory. The resulting π network is shown in Figure 2.3.

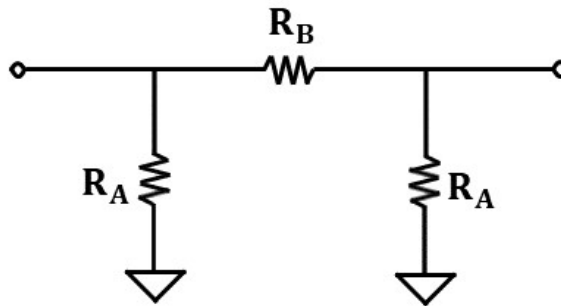


Figure 2.3: Generalized third-order fltenuator circuit schematic at resonance

To find the values of R_A and R_B that will result in a matched circuit while also providing the desired amount of attenuation, the input impedance of the circuit in

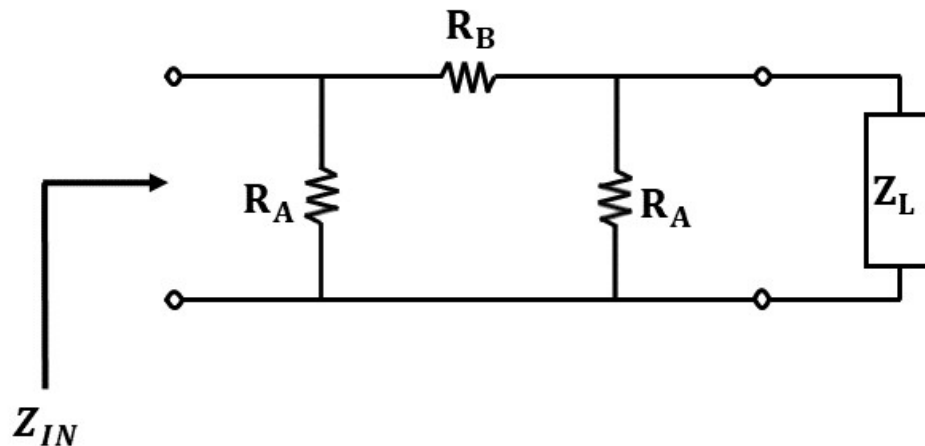


Figure 2.4: Circuit schematic for solving for the input impedance of the fltenuator at resonance

Figure 2.3 is solved to find an expression for R_A and R_B that is matched to the system impedance. The circuit that is used to solve for the input impedance is shown in Figure 2.4.

The input impedance (Z_{IN}) of the π -network is solved for by solving the parallel combination of the π -network loaded with an arbitrary load impedance (Z_L)

$$Z_{IN} = R_A \parallel (R_B + R_A \parallel Z_L) . \quad (2.19)$$

Putting the mathematical expression for a series and parallel combination of impedances into (2.19) yields

$$Z_{IN} = \frac{R_A R_B + \frac{R_A^2 Z_L}{R_A + Z_L}}{R_A + R_B + \frac{R_A Z_L}{R_A + Z_L}} . \quad (2.20)$$

Solving (2.20) for R_B yields

$$\frac{Z_{IN} R_A^2 + Z_{IN} Z_L R_A + Z_{IN} R_A Z_L + R_A^2 Z_L}{R_A^2 + Z_L R_A - Z_{IN} R_A - Z_{IN} Z_L} = R_B . \quad (2.21)$$

When a component is put into a system designed to a certain system impedance, Z_{IN} and Z_L are assumed to be the same as the system impedance (Z_0). This allows for the assumption that $Z_L = Z_{IN} = Z_0$ which yields

$$\frac{2Z_0^2 R_A}{R_A^2 - Z_0^2} = R_B . \quad (2.22)$$

Solving (2.22) for R_A yields

$$R_B R_A^2 - 2Z_0^2 R_A - R_B Z_0^2 = 0 . \quad (2.23)$$

Because (2.23) is in the form of a quadratic equation, the formula

$$\frac{-b \pm \sqrt{b^2 - 4ac}}{2a} \quad (2.24)$$

can be used to solve for R_A , where

$$a = R_B \quad (2.25)$$

$$b = -2Z_0^2 \quad (2.26)$$

$$c = -R_B Z_0^2 . \quad (2.27)$$

Substituting (2.25-2.27) into (2.24) yields

$$R_A = \frac{2Z_0^2 \pm \sqrt{(2Z_0^2)^2 + 4(R_B)(R_B Z_0^2)}}{2R_B} . \quad (2.28)$$

This results in an expression for R_A in terms of the system impedance Z_0 and the series resistance R_B .

Now that an expression for R_A in terms of R_B and Z_0 has been solved for, an expression for R_B can be found. This is done by solving for the transfer function (H) of the circuit using Kirchoff's Current Law (KCL). The schematic that is used to solve for the transfer function is shown in Figure 2.5. In this schematic V_{IN} is

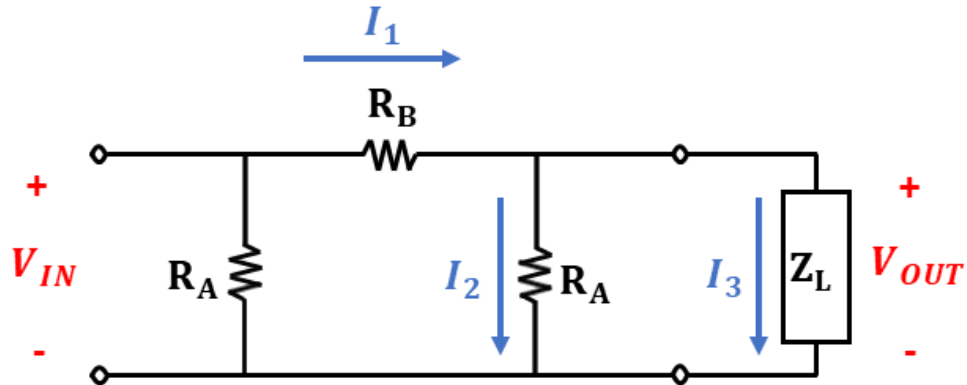


Figure 2.5: Circuit schematic for solving for the transfer function of the filter attenuator at resonance, adapted from [3]

the input voltage, V_{OUT} is the output voltage, I_1 is the current entering the output node, I_2 and I_3 are the currents leaving the output node, and Z_L is an arbitrary load impedance that the circuit is terminated into.

The transfer function of a circuit describes what the output of a system looks like, depending on the input to that system. The transfer function is defined as $H = \frac{V_{OUT}}{V_{IN}}$. The transfer function of the circuit is solved for by using KCL. In KCL the sum of the currents entering a node must equal the sum of the currents exiting a node. For this particular circuit

$$KCL : I_1 = I_2 + I_3 . \quad (2.29)$$

The currents are defined based on Figure 2.5 as $I_1 = \frac{V_{OUT}-V_{IN}}{R_B}$, $I_2 = \frac{V_{OUT}-0}{R_A}$, and $I_3 = \frac{V_{OUT}-0}{Z_0}$. These values for the individual currents are then put into (2.29) which yields

$$\frac{V_{OUT} - V_{IN}}{R_B} = \frac{V_{OUT} - 0}{R_A} + \frac{V_{OUT} - 0}{Z_0} . \quad (2.30)$$

Equation (2.30) is then solved for the transfer function H , which yields

$$H = \frac{V_{OUT}}{V_{IN}} = \frac{R_A \parallel Z_0}{R_A \parallel Z_0 + R_B} . \quad (2.31)$$

Solving (2.31) for R_B yields

$$R_B = \frac{R_A Z_0 (1 - H)}{H R_A + H Z_0} . \quad (2.32)$$

This results in an expression for R_B in terms of the system impedance (Z_0), the shunt resistance (R_A), and the transfer function (H) where $H = 10^{-\frac{A_{dB}}{20}}$ and A_{dB} is the desired attenuation in decibels.

Although an expression for R_B has been solved for, an expression for R_A still needs to be derived. This is accomplished by setting (2.28) and (2.32) equal to each other and solving for R_A

$$R_B = \frac{2Z_0^2 R_A}{R_A^2 - Z_0^2} = \frac{R_A Z_0 (1 - H)}{H (R_A + Z_0)} . \quad (2.33)$$

This results in an expression for R_A that is based solely on the system impedance Z_0 and the transfer function H . After some algebra, (2.33) is massaged into the form of a quadratic equation

$$Z_0 (1 - H) R_A^2 - 2H Z_0^2 R_A + (-2H Z_0^3 - Z_0^3 (1 - H)) = 0 . \quad (2.34)$$

Because (2.34) is in the form of a quadratic equation, (2.24) can be used to solve for R_A , where

$$a = Z_0 (1 - H) \quad (2.35)$$

$$b = -2H Z_0^2 \quad (2.36)$$

$$c = -2H Z_0^3 - Z_0^3 (1 - H) . \quad (2.37)$$

Substituting (2.35-2.37) into (2.24) yields

$$R_A = \frac{2H Z_0^2 \pm \sqrt{(-2H Z_0^2)^2 + 4(Z_0 (1 - H)) (-2H Z_0^3 - Z_0^3 (1 - H))}}{2Z_0 (1 - H)} . \quad (2.38)$$

Now a little bit of algebra and the positive result of (2.38) are used to yield

$$R_A = \frac{Z_0 (H + 1)}{1 - H} . \quad (2.39)$$

The result from (2.39) is then put into (2.32) to yield

$$R_B = \frac{Z_0(1 - H^2)}{2H} . \quad (2.40)$$

Equations (2.39) and (2.40) are now in terms of Z_0 and H and can be used to find values for R_A and R_B that will give the desired amount of loss while maintaining a match. A table of common attenuator values and the corresponding resistances needed to achieve a matched response is shown in Table 2.1.

Table 2.1: Table of common attenuator values and associated resistance values to achieve desired attenuation

Loss (dB)	R_A	R_B
1	869.5482	5.7692
2	436.2116	11.6149
3	292.4022	17.6148
6	150.4760	37.3519
8	116.1425	52.8445
12	83.545	93.2471
18	64.4024	195.4347
24	56.7345	394.6459
30	53.2655	789.7788
32	52.5766	994.64

2.2 Generalized Results

Now that the theoretical foundation has been laid, it is mathematically possible to make a filter for an arbitrary system impedance and frequency. The impedances Z_2 , Z_4 , and Z_6 can also be designed to operate as a lowpass, highpass, bandpass, or bandstop filter. The derived analytical results and the generalized

structure described in Figure 2.2 are used to present several different types of fil-
tenuators.

The first type of filtenuator that will be shown is the lowpass filtenuator. This
type of filtenuator can be realized by making Z_2 and Z_6 inductors and Z_4 a capacitor
using the well-known filter synthesis design procedure [2] and (2.32) and (2.39).
The resulting circuit is shown in Figure 2.6.

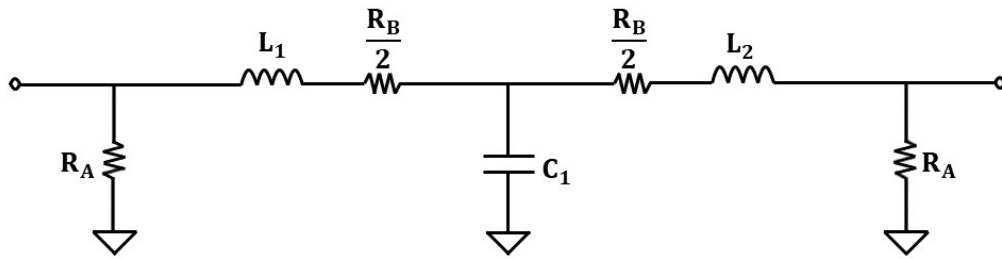


Figure 2.6: Example circuit schematic of a lowpass filtenuator

An ideal lowpass filtenuator circuit is designed and simulated in ADS. The filtenuator
is designed to have a cutoff frequency of 1 GHz, 20 dB of return loss, and
2.5 dB of intended passband attenuation. The resulting S-parameters are shown in
Figure 2.7. The S_{21} shows that the lowpass response has the 2.5 dB of passband
attenuation that was designed for. The S_{11} shows that the return loss ripple is more
than the designed 20 dB which is due to the increase in the intrinsic loss of the filter.

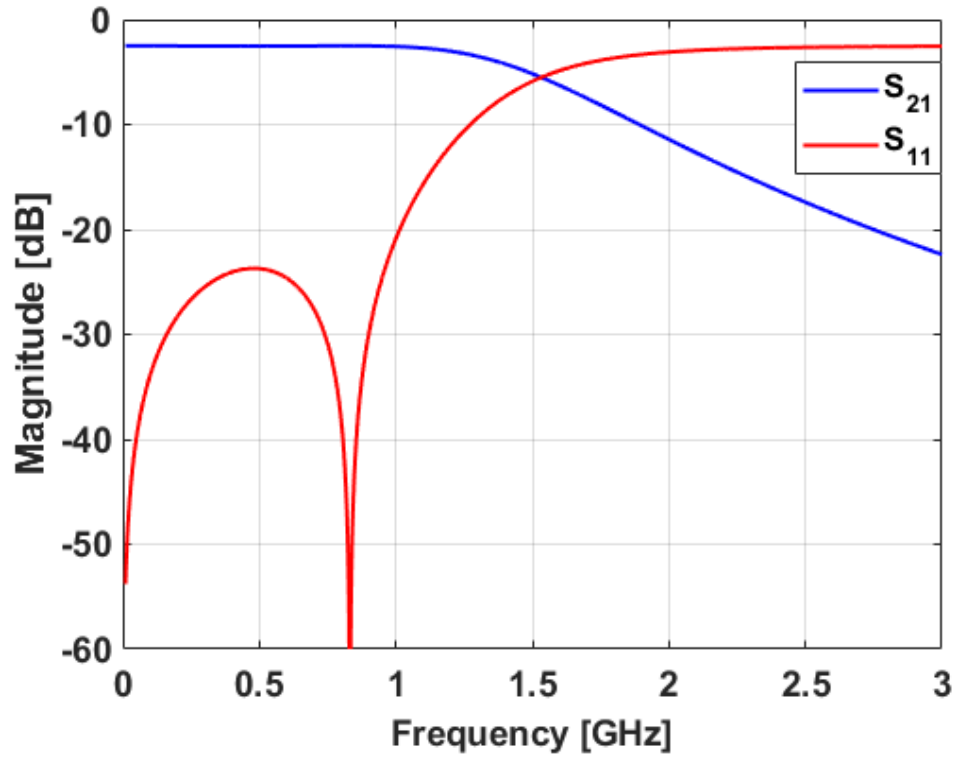


Figure 2.7: S-parameters of a lowpass filtenuator

The next type of filtenuator to discuss is the highpass filtenuator. This type of filtenuator is realized by making Z_2 and Z_6 capacitors and Z_4 an inductor using the well-known filter synthesis design procedure [2] and (2.32) and (2.39). The resulting circuit is shown in Figure 2.8.

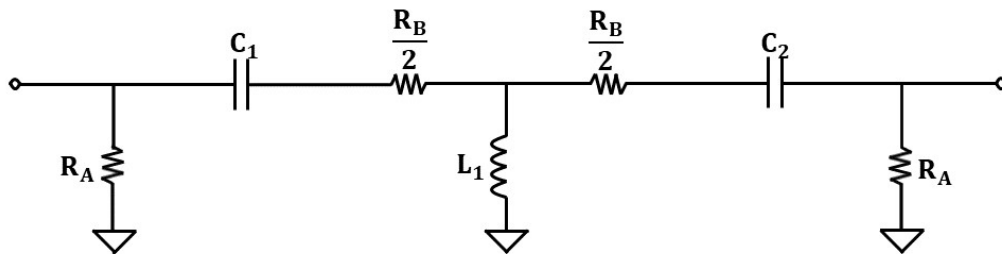


Figure 2.8: Example circuit schematic of a highpass filtenuator

An ideal highpass filtenuator circuit is designed and simulated in ADS. The filtenu-

ator is designed to have a cutoff frequency of 1 GHz, 20 dB of return loss, and 2.5 dB of intended passband attenuation. The resulting S-parameters are shown in Figure 2.9. The S_{21} shows that the highpass response has the 2.5 dB of passband attenuation that was designed for, while the S_{11} shows that the return loss ripple is more than the designed 20 dB which is due to the increase in the intrinsic loss of the filter.

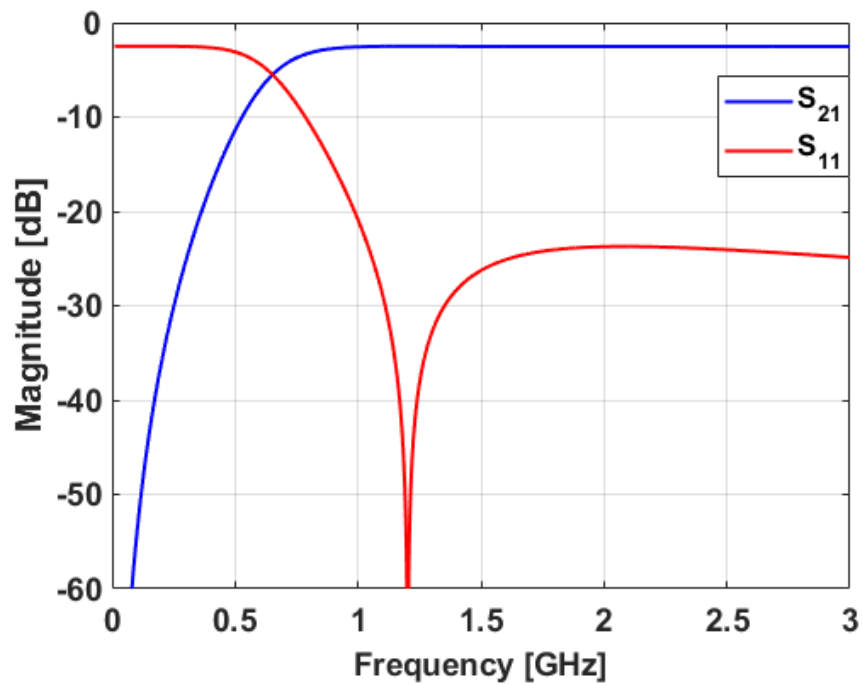


Figure 2.9: S-parameters of a highpass filtenuator

The next type of filtenuator to discuss is the bandpass filtenuator. This type of filtenuator is realized by making Z_2 and Z_6 series LC resonators and Z_4 a parallel LC resonator using the well-known filter synthesis design procedure [2] and (2.32) and (2.39). The resulting circuit is shown in Figure 2.10.

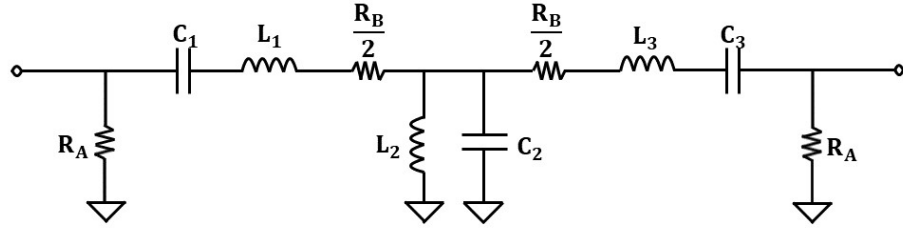


Figure 2.10: Example circuit schematic of a bandpass filter

An ideal bandpass filter circuit is designed and simulated in ADS. The filter is designed to have a center frequency of 1 GHz, 20 dB of return loss, and 2.5 dB of intended passband attenuation. The resulting S-parameters are shown in Figure 2.11. The S_{21} shows that the bandpass response has the 2.5 dB of passband attenuation that was designed for. The S_{11} shows that the return loss ripple is more than the designed 20 dB which is due to the increase in the intrinsic loss of the filter.

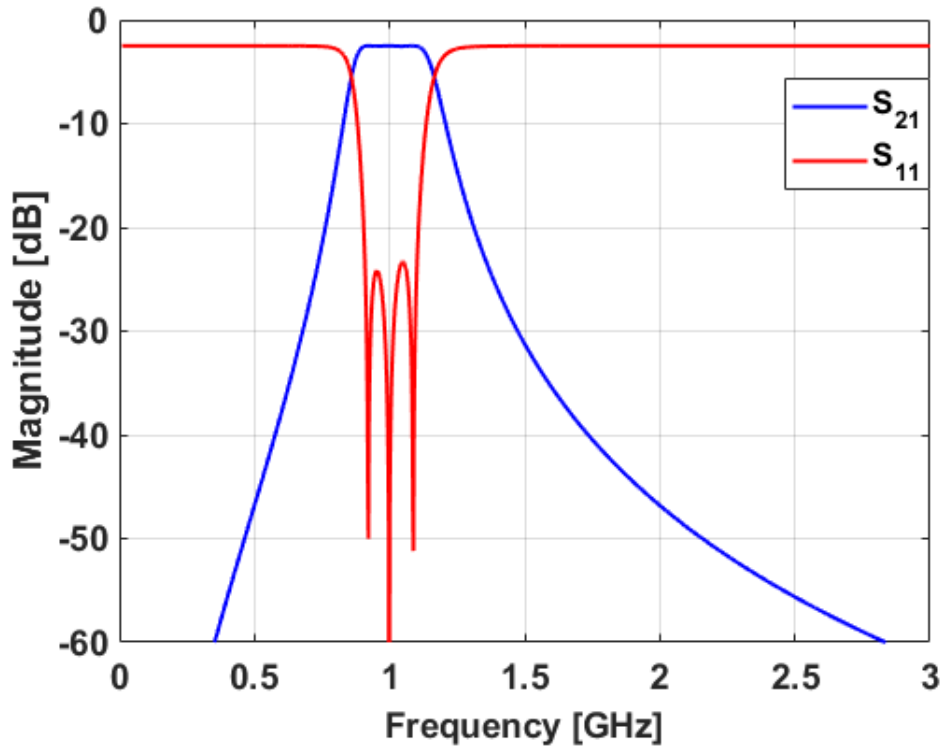


Figure 2.11: S-parameters of a bandpass filter

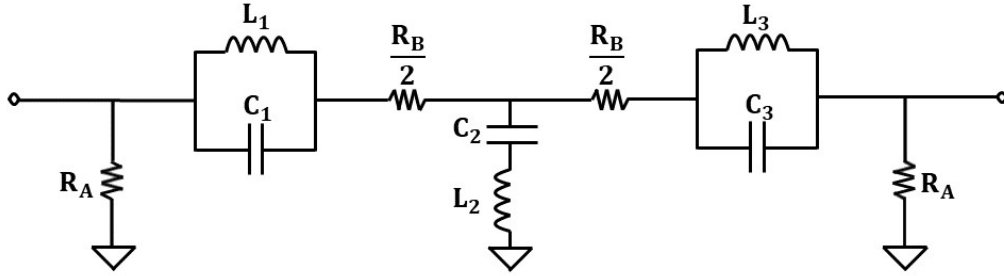


Figure 2.12: Example circuit schematic of a bandstop filter

Finally, the last type of filter to discuss is the bandstop filter. This type of filter is realized by making Z_2 and Z_6 parallel LC resonators and Z_4 a series LC resonator using the well-known filter synthesis design procedure [2] and (2.32) and (2.39). The resulting circuit is shown in Figure 2.12.

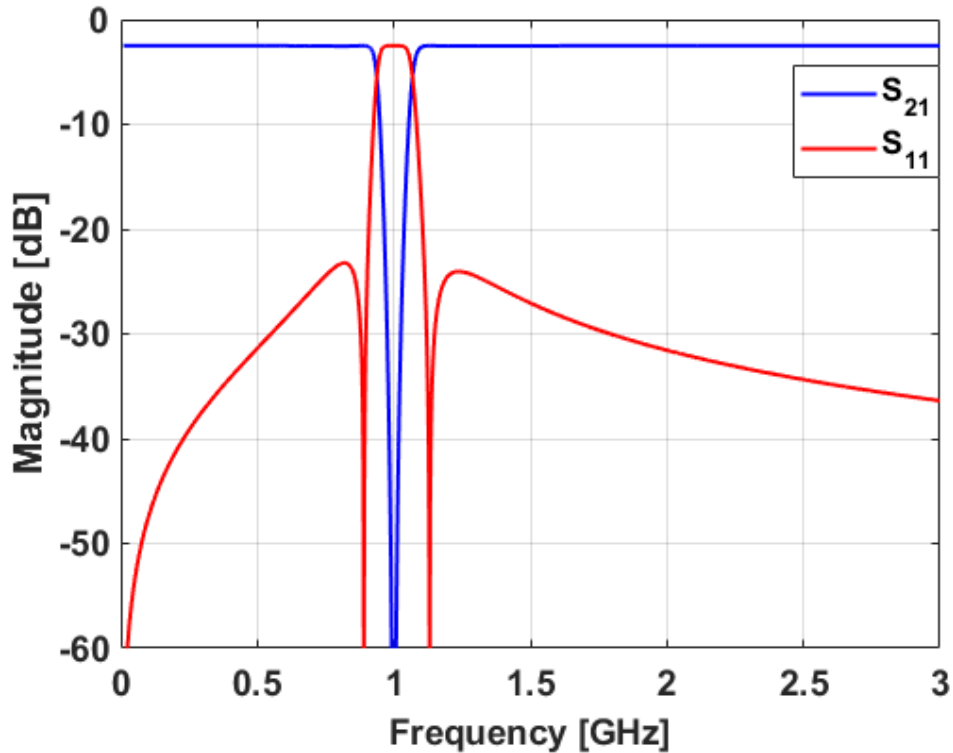


Figure 2.13: S-parameters of a bandstop filter

An ideal bandstop filtenuator circuit is designed and simulated in ADS. The filter is designed to have a center frequency of 1 GHz, 20 dB of return loss, and 2.5 dB of intended passband attenuation. The resulting S-parameters are shown in Figure 2.13. The S_{21} shows that the bandstop response has the 2.5 dB of passband attenuation that was designed for. The S_{11} shows that the return loss ripple is more than the designed 20 dB which is due to the increase in the intrinsic loss of the filter.

Several different filtenuators are presented including a lowpass, highpass, bandpass, and bandstop filtenuator. This demonstrates the flexibility of the proposed filtenuator structure. Although the structure affords some flexibility, this could come at the cost of resonator Q.

2.3 Resonator Quality Factor

In a filter with intended loss added to it, like the proposed filtenuator, it is important to understand the trade-offs that are involved in the design of such a filter. One of these trade-offs is the degradation in the resonator Q as the passband attenuation of the filtenuator is increased. References [2]-[4] and [17, 18], were used in the creation of the material in this section.

In microwave engineering, the Q of a resonant structure is extremely important for this structure to perform as designed. In a general sense, a higher Q is indicative of a more selective resonant structure and a narrower bandwidth, while a lower Q is indicative of a less selective resonant structure and wider bandwidth. For the proposed filtenuator, only the series resonators have a resistance added to them. Because of this, the Q of the series resonators will become degraded while the shunt resonator will remain unaffected. Due to this, only the Q of a loaded series LC resonator is evaluated. The circuit used to calculate the Q of a series resonator

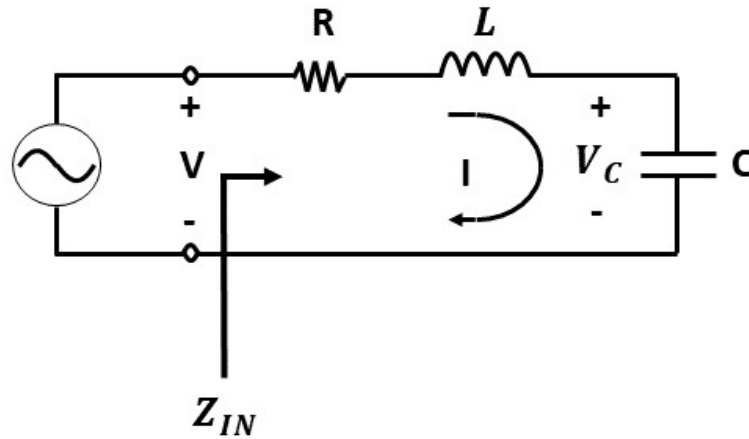


Figure 2.14: Circuit for calculating series resonator quality factor

is shown in Figure 2.14.

To get an understanding of the limits of the proposed filter, the Q of a series resonator is evaluated at 1 GHz for an inductor value of 30 nH by using

$$Q = \frac{\omega_0 L}{R} = \frac{1}{\omega_0 RC} . \quad (2.41)$$

The Q of a series resonator is then observed as a function of the series resistance of the resonator. A plot of the quality factor of a series resonator as a function of resistance is shown in Figure 2.15. The Q of the series resonator has a sharp decrease for resistances of more than a few ohms and decreases to less than 25 for resistances of more than 6 ohms before eventually leveling out to the single digits. This decrease in Q as a function of resistance also has a great impact on the bandwidth (BW) of the resonator due to the relationship of

$$Q = \frac{1}{BW} . \quad (2.42)$$

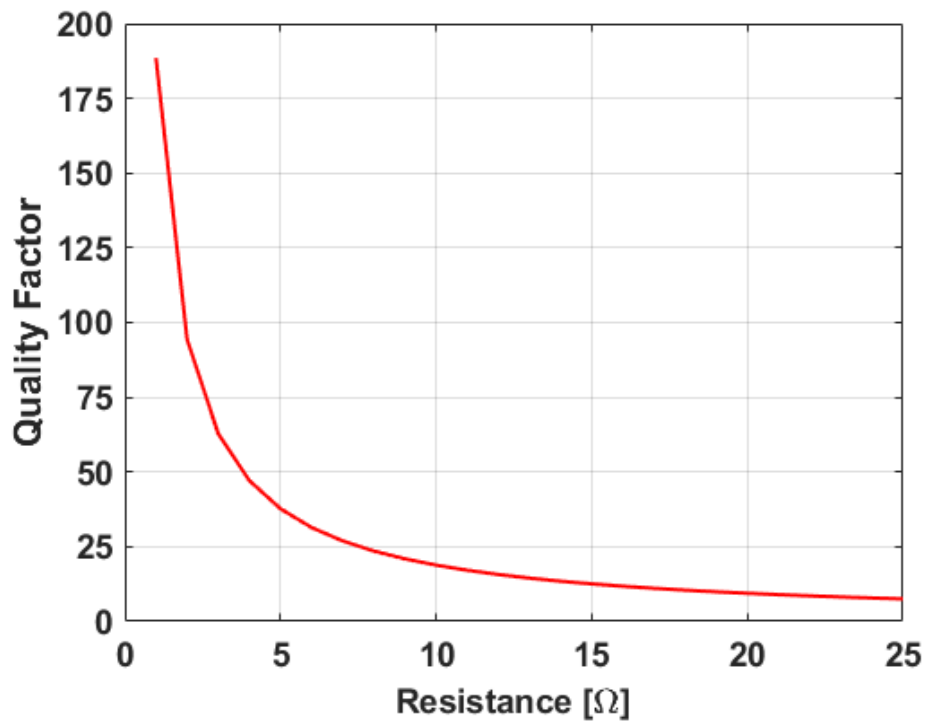


Figure 2.15: Quality factor as a function of resistance

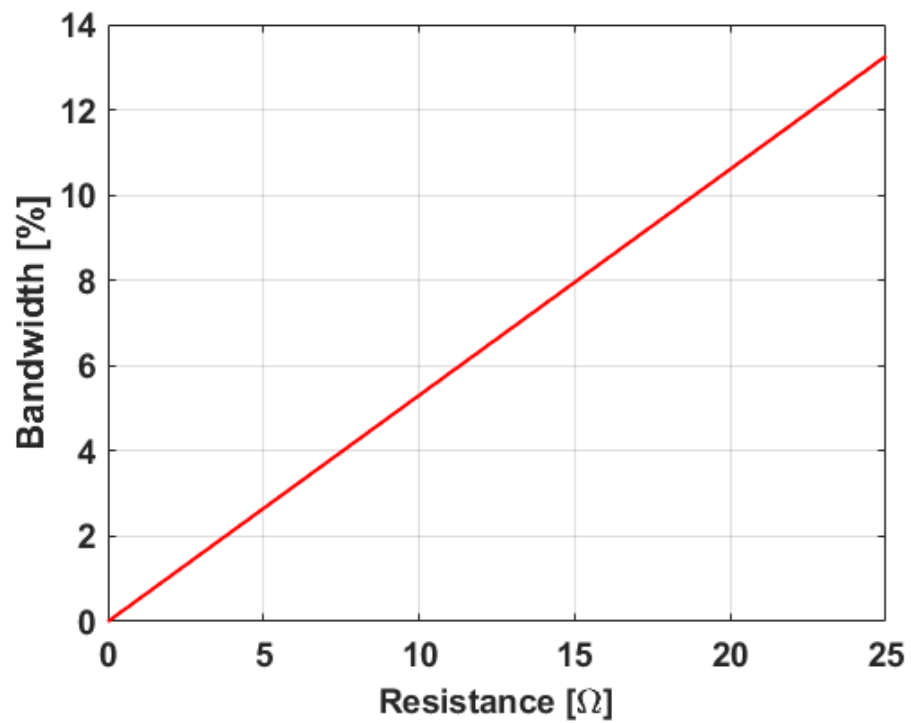


Figure 2.16: Bandwidth as a function of resistance

This relation means that as resistance in the series resonator is increased, and by extension loss is increased, the resonator Q decreases while resonator bandwidth increases as shown in Figure 2.16. This increase in bandwidth could make it difficult to realize a filter with a narrow passband. Because of this decrease in Q as a function of resistance in series resonators, the degradation of resonator bandwidth, and the increase in resonator impedance, the amount of loss that can be designed for is limited in a third-order filter. Because of this, an evaluation of higher-order filters is necessary.

2.4 Expansion to Higher Orders

Now that the theory for a third-order generalized filter has been derived and the possibility of several different types of filters has been shown, the expansion of the theoretical results to higher-order filter structures is necessary. A generalized schematic for a fifth-order filter is shown in Figure 2.17.

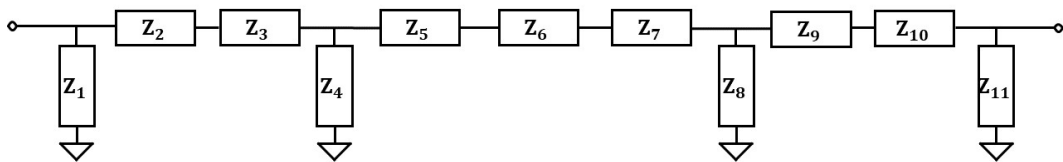


Figure 2.17: Generalized schematic of a fifth-order filter circuit

For a generalized fifth-order filter circuit, such as the one shown in Figure 2.17, while at resonance, impedances $Z_3, Z_6,$ and Z_9 become short circuits while impedances Z_4 and Z_8 become open circuits. This is shown in Figure 2.18.

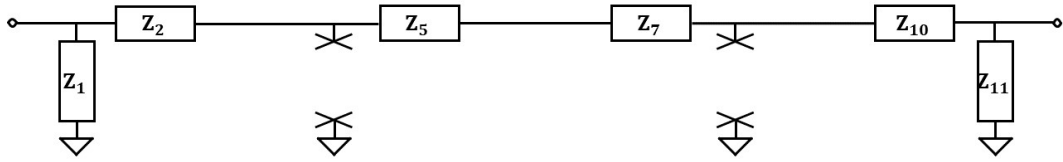


Figure 2.18: Generalized schematic of a fifth-order filter circuit at resonance

At resonance, all that remains is Z_1 , Z_2 , Z_5 , Z_7 , Z_{10} , and Z_{11} . If those blocks are assumed to be purely real (resistances), then this circuit also breaks down into a π -network of resistors similarly to the third-order filter. Using logical induction, it follows that for odd orders of filters with an initial series component configuration, the theory previously used to design a third-order filter can also be used to design higher-order filters.

2.4.1 Resistor Placement in Higher-Order Filters

At resonance, blocks Z_1 , Z_2 , Z_5 , Z_7 , Z_{10} , and Z_{11} remain, as shown in Figure 2.18. It is found that this offers a certain degree of freedom with which to explore the effect of different symmetric configurations of resistor locations within the filter circuit. Changing the location of resistors could also affect how the Q of each of the resonators will be affected by increased filter loss. To show the effect that resistor placement has on a higher-order filter, a fifth-order band-pass filter (BPF) with 20% fractional bandwidth and 20 dB of passband return loss is designed at 1 GHz. In all of the following configurations, Z_1 and Z_{11} will be shunt resistances R_A .

The first resistor configuration that is explored is when only the central resonator is loaded symmetrically with the series resistance, while the rest of the resonators are left unloaded as shown in Figure 2.19.

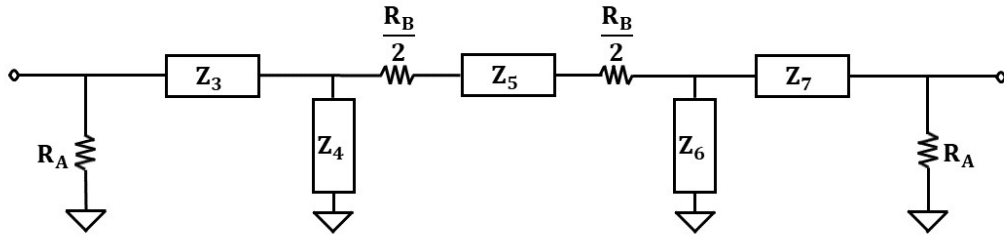


Figure 2.19: fifth-order filter schematic with only central resonator resistively loaded

The S-parameters for this configuration are shown in Figure 2.20. This resistor configuration allows the circuit to provide the intended passband attenuation; however, there are some unintended consequences. In S_{21} , the passband of the filter shows a dip at the center frequency that increases with increased passband attenuation.

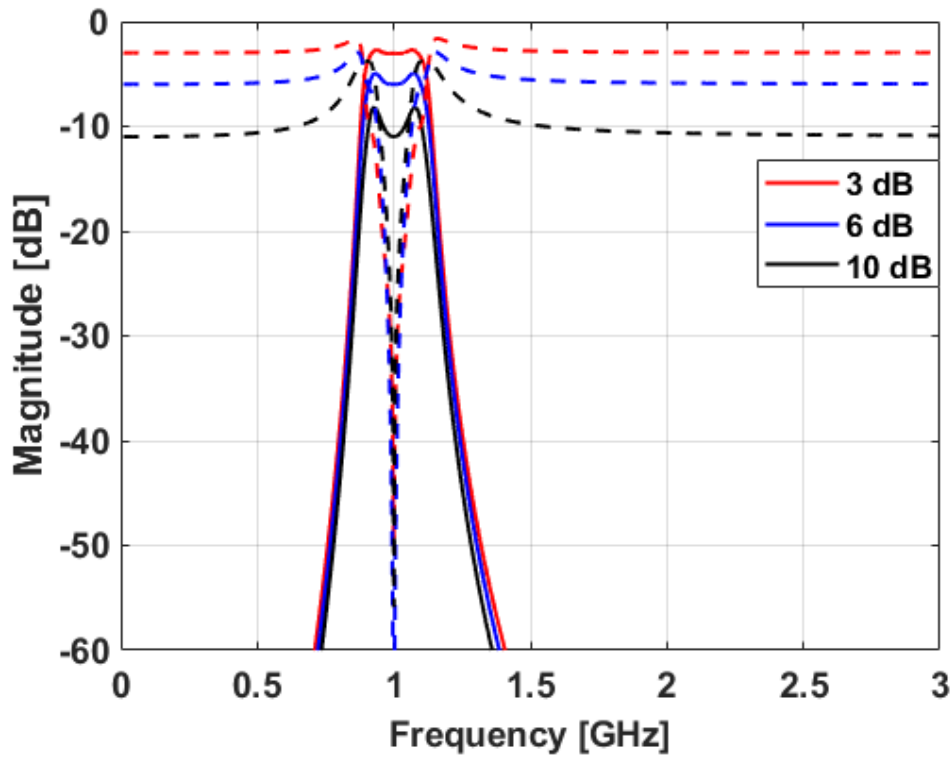


Figure 2.20: S-parameters for a fifth-order filter with 3, 6, and 10 dB of loss with the resistance added to only the center-most resonator

In S_{11} , the return loss is degraded at lower levels of loss and gets worse at higher levels of passband attenuation in the filtenuator. The effect in S_{21} could be due to the central resonator being highly loaded while the other resonators are not loaded at all, resulting in an uneven loss across the passband and degradation of the return loss away from the center frequency of the filter. The change in S_{11} could be due to the reflection zeros of the filtenuator collapsing onto each other and creating more of a Butterworth type response.

The next resistor configuration to be explored is the series resistance R_B spread out equally along all the series resonators. A potential benefit of such a configuration is the resistance is spread out among the resonators; therefore, the Q of no single resonator becomes severely degraded as loss is increased. This resistor configuration is shown in Figure 2.21.

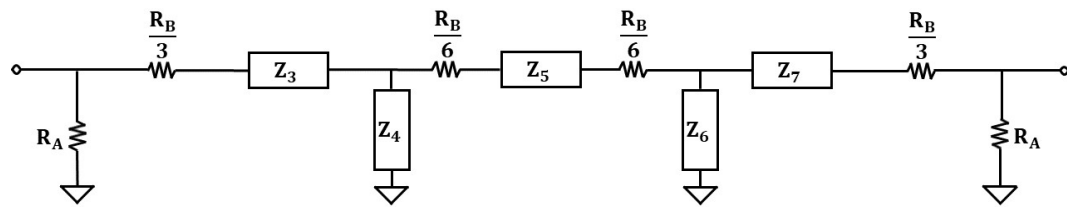


Figure 2.21: Fifth-order filtenuator schematic with resistance spread among series resonators

The S-parameters for this configuration are shown in Figure 2.22. This configuration of resistors also provides the intended passband attenuation; however, there are still some unintended effects caused by this method. In S_{21} , the dip at the center frequency is no longer present for any level passband attenuation, although the passband becomes less flat and more rounded at the edge of the passband. In S_{11} , the return loss still looks degraded; however, as passband attenuation is increased, the effect on the return loss is not as dramatic as the case of the central resonator

being the only one loaded with resistance. Note that the S_{21} of this configuration look similar to that of Figure 1.4 where the Q of the filter resonators are being decreased. This could be because three of the five resonators are being loaded rather than the single resonator in the first case.

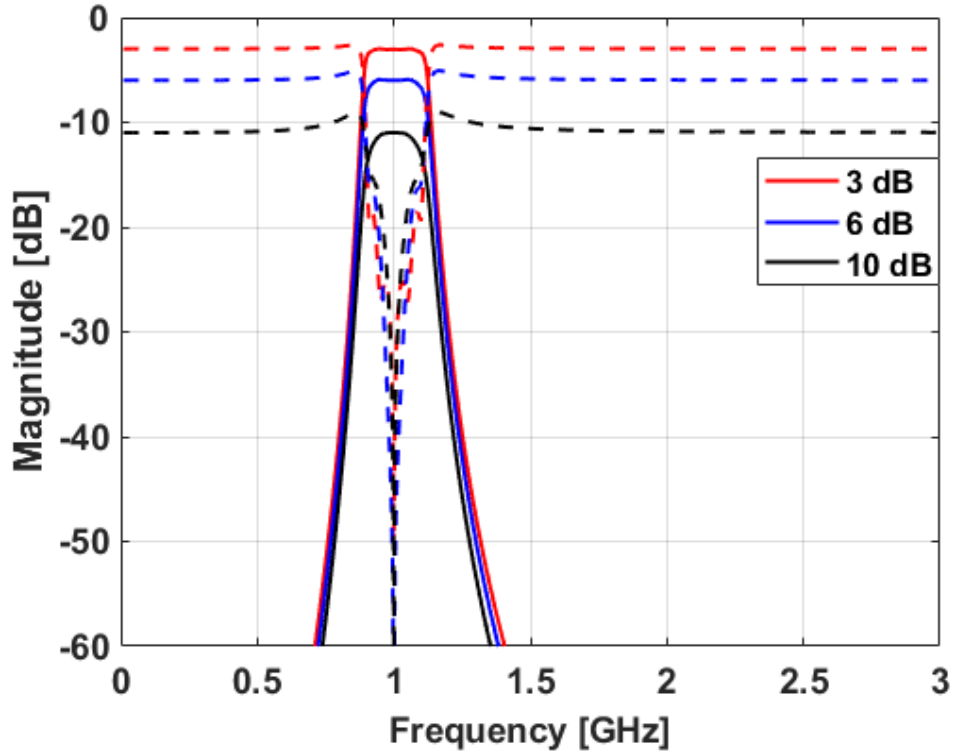


Figure 2.22: S-parameters for a fifth-order filter with 3, 6, and 10 dB of loss with the resistance spread out along the series resonators

The last resistor configuration to be explored is the series resistance R_B placed on the two outermost resonators. This configuration is a good trade-off between the previous configurations as no single resonator becomes severely degraded. At higher levels of passband attenuation, only two resonators face a large degradation in resonator Q. This configuration has the potential to lead to a flatter response at higher losses and better retention of the filter shape in comparison to the other two configurations. This resistor configuration is shown in Figure 2.23.

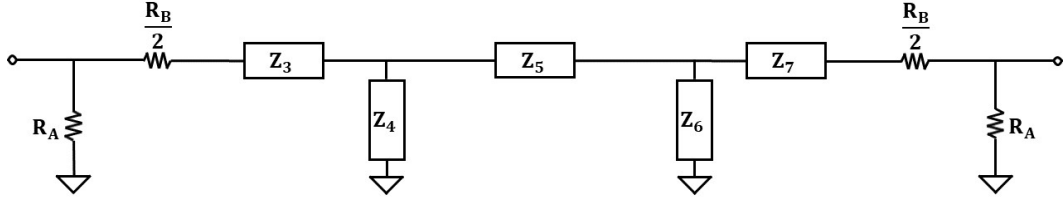


Figure 2.23: Fifth-order filter schematic with resistance only on outer-most series resonators

The S-parameters for this configuration are shown in Figure 2.24. This configuration of resistors provides the intended passband attenuation while also losing the unintended consequences from the previous two configurations. In S_{21} , the rounded passband is no longer present for low loss and is barely noticeable at higher levels

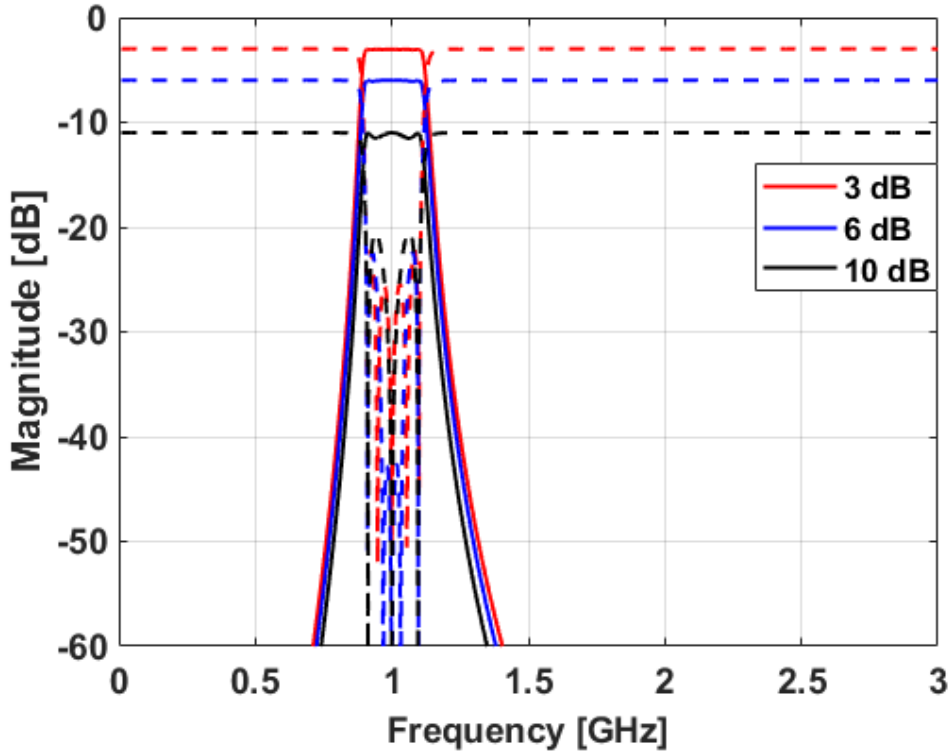


Figure 2.24: S-parameters for a fifth-order filter with 3, 6, and 10 dB of loss with the resistance added to only the outer-most resonators

of attenuation. In S_{11} , the return loss looks much less degraded than in the previous configurations. The filter shows an $N-2$ effect in the return loss of the 10 dB filter. This could be because two of the reflection zeros are being shifted due to the added resistance to the resonators.

2.5 Summary

In this chapter, a generalized circuit topology was chosen and used to derive a set of generalized design equations for the filter concept. Several different types of filters were demonstrated including: lowpass, highpass, bandpass, and bandstop filters. The effect on resonator quality factor (Q) of resistively loading resonators was also explored. The generalized topology was also expanded to include higher-order filters. Finally, the effects of resistor placement on higher-order filters was explored.

The lessons learned from this chapter can be used as a theoretical foundation for the design of future filters. The theoretically derived S-parameters and design equations provide valuable insight into the operation and design of filters. This theoretical framework paves the way for the design and fabrication of future filter circuits. With this framework, a proof-of-concept static filter was designed, simulated, and fabricated.

Chapter 3

Static Filtenuator Design

In the first step of any new component design, it is important to design a prototype that is as simple as possible while also verifying that the theory holds when realized. In this chapter, a static filtenuator prototype using the basic structure outlined in Chapter 2 is designed, simulated, fabricated, and tested. Lumped-element resistors, inductors, and capacitors are used in this initial design to keep the design simple. The filtenuator is designed at a center frequency of 1 GHz allowing for lumped-element components to be used for the resonators while also being a high enough frequency to validate its application in radio frequency (RF) circuits. A bandpass filter is chosen for this thesis, as it is the most applicable in the context of a receiver front end.

3.1 Design of a Third-Order Static Filtenuator

The first step in the design of a third-order filtenuator is to design a third-order filter as the basis for the desired filter response. Before this can be synthesized, a few parameters must first be decided on. The most fundamental parameter is the filter response type. Two basic filter response types that are relatively easy to synthesize are the maximally flat response (Butterworth) and the equi-ripple response

(Chebyshev). For this design, a Chebyshev response is chosen. The next parameter to be decided is the filter order (N). The filter is designed to be a third-order to keep the filter symmetric while also remaining as simple as possible. The next parameter to be decided is the fractional bandwidth of the filter (FBW). The filter is designed to have a 20% FBW to facilitate the selection of realizable lumped-element component values. The last parameter to decide before synthesis can begin is the ripple of the filter. This ripple can be based on either the passband ripple in the insertion loss (L_A) or the passband ripple in the return loss (L_R). A return loss ripple of 20 dB is chosen to ensure that the filter remains matched at the passband. References [2]-[4], [17], and [19] are used for the creation of this material.

The design of a lowpass prototype filter is based on a set of values called g-coefficients. Once the g-coefficients have been calculated, the filter must then be frequency and impedance scaled. For this simple design, the frequency will be 1 GHz while the system impedance that the filter will be design for will be 50 ohms.

3.1.1 Low-Pass Prototype

The first step of the filter design is to create a lowpass prototype filter. The lowpass prototype filter is defined by calculated g-coefficients. The g-coefficients are calculated by using the order (N) and the ripple (L_R). The order of the filter is $N = 3$ and the prescribed ripple is $L_R = 20$ dB. Now that the basic parameters of the base filter for the filter have been decided on, the g-coefficients can be calculated recursively using (3.1 - 3.4)

$$g_0 = 1 \tag{3.1}$$

$$g_1 = \frac{2 \sin 2/2n}{\eta} \tag{3.2}$$

$$g_{r+1} = \frac{4 \sin\left(\frac{(2r-1)\pi}{2n}\right) \sin\left(\frac{(2r+1)\pi}{2n}\right)}{g_r \left(\eta^2 + \sin^2\left(\frac{r\pi}{n}\right)\right)} \text{ for } r = 1, 2, \dots, n-1 \quad (3.3)$$

$$g_{n+1} = \begin{cases} 1, & \text{for } n \text{ odd} \\ \epsilon + \sqrt{1 + \epsilon^2}, & \text{for } n \text{ even and } S_{11}(0) \geq 0 \\ \frac{1}{\epsilon + \sqrt{1 + \epsilon^2}}, & \text{for } n \text{ even and } S_{11}(0) \leq 0 \end{cases} \quad (3.4)$$

where η is defined as

$$\eta = \sinh\left(\frac{\sinh^{-1}(\epsilon^{-1})}{n}\right) \quad (3.5)$$

and the ripple factor (ϵ), which controls the return loss ripple, is defined as

$$\epsilon = \frac{1}{\sqrt{10^{-\frac{L_R}{10}} - 1}} \quad (3.6)$$

Table 3.1: Table of calculated g-coefficients

g_0	g_1	g_2	g_3	g_4
1	0.8534	1.1039	0.8534	1

These calculated g-coefficients are used to design a prototype lowpass filter with a cutoff frequency of 1 rad/s and a source and load impedance of 1 ohm. The calculated g-coefficients for the lowpass filter prototype are shown in Table 3.1 and the general schematic for a normalized prototype lowpass filter is shown in Figure 3.1. The scattering-parameters (S-parameters) of the lowpass prototype are shown in Figure 3.2.

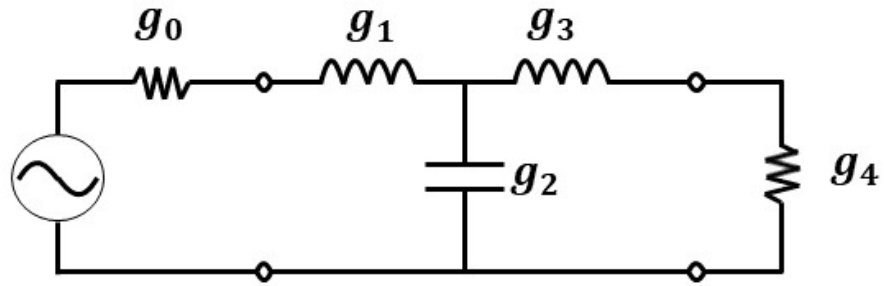


Figure 3.1: Lowpass filter prototype schematic

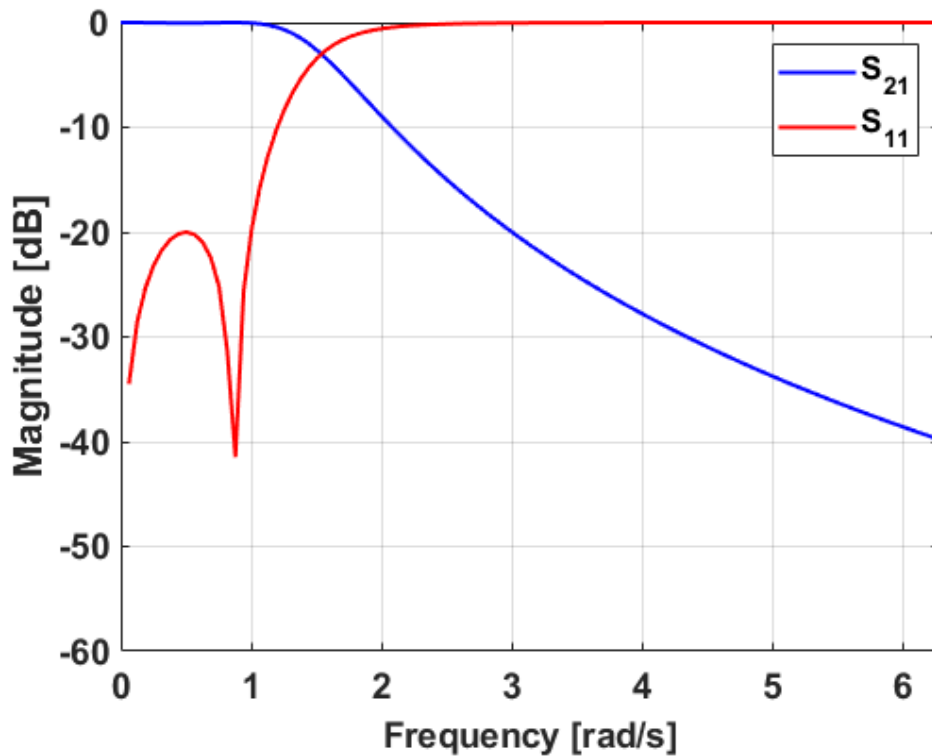


Figure 3.2: Lowpass filter prototype S-parameters

3.1.2 Lowpass to Bandpass Transformation

Once the g -coefficients have been calculated and the lowpass filter prototype has been designed, the next step in the process is to transform the filter from a lowpass

filter with a cutoff frequency (ω_c or f_c) of 1 rad/s (or 0.159 Hz) with a normalized source and load impedance of 1 ohm into a filter with a center frequency of 1 GHz and a load impedance of 50 ohms.

The first step of this process is to impedance scale the components in the low-pass filter prototype to allow the filter to operate within a 50 ohm system. This is done by multiplying the source and load impedance as well as the inductors by the 50 ohm system impedance and dividing the capacitor by the 50 ohm system impedance. The lowpass filter schematic after impedance scaling is shown in Figure 3.3.

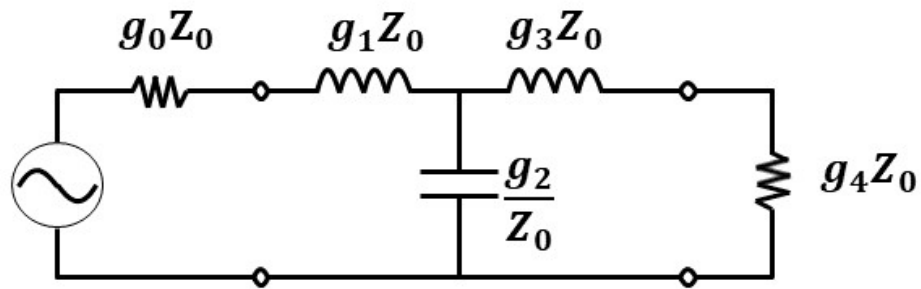


Figure 3.3: Schematic of the lowpass filter scaled to the system impedance

The next step after the lowpass prototype filter has been impedance scaled, is to frequency scale and perform a lowpass to bandpass transformation on the prototype. The lowpass filter prototype is transformed into a bandpass filter by replacing the inductors in the prototype with an inductor and capacitor in series and the capacitors in the prototype with an inductor and capacitor in parallel. The required transformations to go from a lowpass prototype to a highpass, bandpass, and bandstop filter are shown in Figure 3.4.

TABLE 8.6 Summary of Prototype Filter Transformations $\left(\Delta = \frac{\omega_2 - \omega_1}{\omega_0}\right)$

Low-pass	High-pass	Bandpass	Bandstop

Figure 3.4: Table of filter transformations found in [4]

Now that the inductors and capacitors have been replaced with LC resonators, the resonators can be frequency scaled so that the bandpass filter operates in the appropriate frequency band. To do this, the series inductors are divided by the center frequency (ω_0) and the fractional bandwidth (Δ) of the proposed filter. The series capacitors are multiplied by Δ and divided by ω_0 . The parallel inductors are mul-

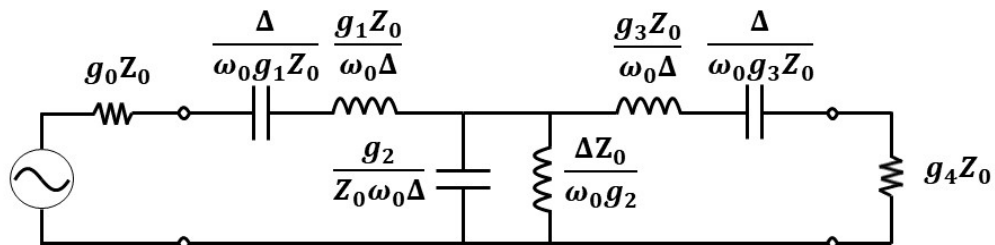


Figure 3.5: Frequency scaled and bandpass transformed lowpass prototype

multiplied by Δ and divided by ω_0 while the parallel capacitors are divided by both Δ and ω_0 . A circuit schematic showing the calculations necessary for each component is shown in Figure 3.5 for convenience.

The final step in the synthesis of the filter is to calculate each of the components needed to create this filter. After calculation, it was found that a 0.745 pF and a 17.96 pF capacitor are needed as well as a 33.96 nH and a 1.44 nH inductor. These values are of a magnitude that are realizable with discrete lumped-element components that are commercially available. A circuit schematic with the final ideal values of the components is shown in Figure 3.6.

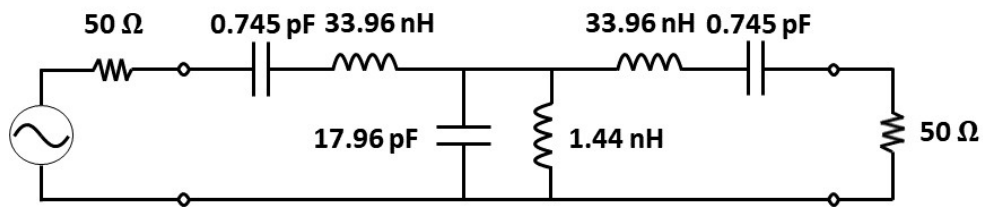


Figure 3.6: Final designed third-order Chebyshev bandpass filter

The circuit with the ideal components shown in Figure 3.6 is then simulated in ADS to verify the process was completed correctly. The filter has a center frequency of 1 GHz with a 20 % fractional bandwidth passband and a return loss ripple of 20 dB. The S-parameters of the final designed and simulated filter are shown in Figure 3.7.

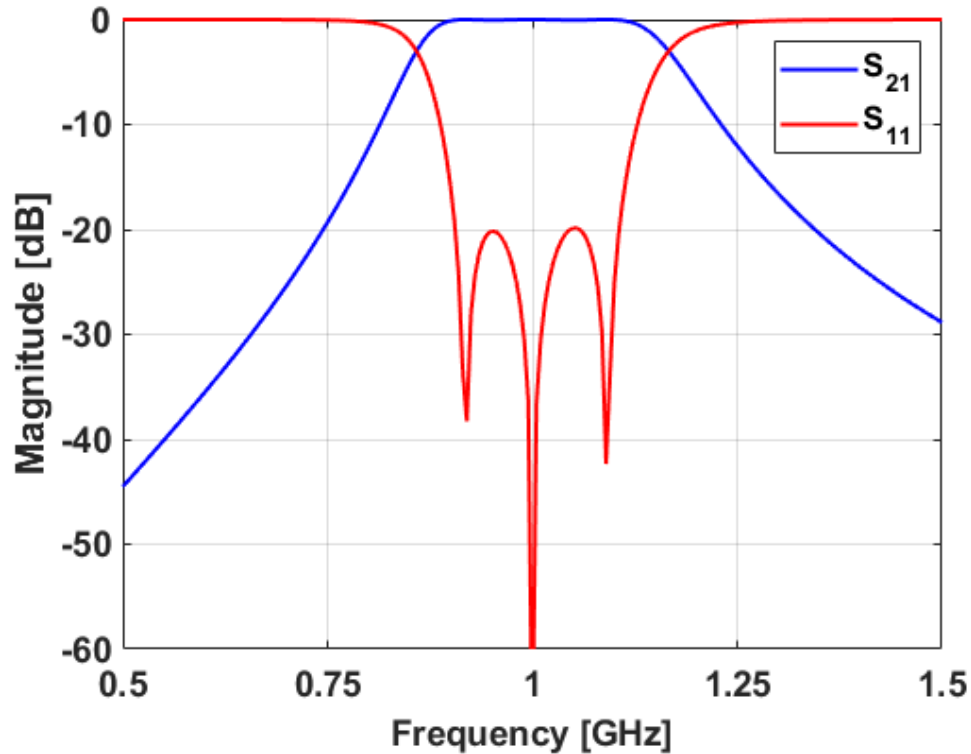


Figure 3.7: S-parameters of the designed third-order Chebyshev bandpass filter

3.2 Simulations

Now that the bandpass filter is designed, the next step in the design process is to integrate that base filter into the overall filtenuator design. The theory for this has already been outlined in Chapter 2, and so the component values from Figure 3.6 can simply be placed in the general bandpass filtenuator structure in Figure 2.10.

Now that the general schematic for the filtenuator has been decided, it will be simulated in ADS. The best way to ensure a relatively straightforward fabrication process is to design simulations that are as accurate as possible. Real measured component S-parameters, equivalent circuits, and non-ideal models of PCB components are commonly used to more accurately model components in simulation

and enhance the probability of success during the fabrication process.

The process of adding non-ideal models is an important aspect of accurately modeling an RF circuit. The method used to design this circuit is starting with a simulation that exclusively uses ideal models of the RLC components. Next, non-ideal models for the inductors, then capacitors, and finally, resistors will be sequentially added to the simulation. Lastly, non-ideal models of microstrip traces and vias are added to the simulation to minimize the effect that the components have on the performance of the design.

3.2.1 Ideal Simulation

The first step in the design process is to simulate the ideal circuit in ADS. For this simulation, the priority is on keeping the filtenuator at the correct frequency and attenuation while also remaining well-matched in S_{11} . For the initial simulations, a single attenuation value will be designed to keep the design process as simple as possible. The shunt resistance R_A will be set to 1000 ohms and the series resistances R_B will be set to 10 ohms. These values were selected because the largest available resistance value for the high frequency resistor series used is 1000 ohms while the smallest available value in that series is 10 ohms. These values should result in a matched circuit and passband attenuation of around 2 dB at the passband. The ideal ADS schematic is shown in Figure 3.8.

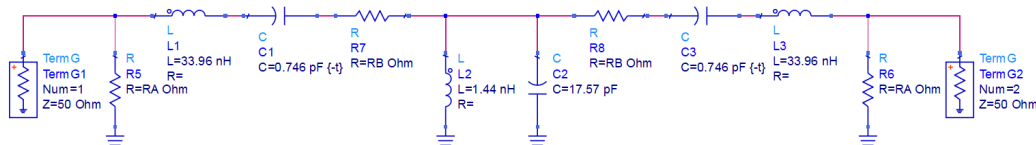


Figure 3.8: ADS simulation setup of the ideal filtenuator

The S-parameters of the ideal ADS simulation are shown in Figure 3.9. The S_{21} of the filter shows the prescribed amount of passband attenuation that it was designed for while the S_{11} shows that the filter is well-matched across the passband, although with about 18 dB of return loss in comparison to the 20 dB of the original filter. A slight degradation in the filter ripple is also observed.

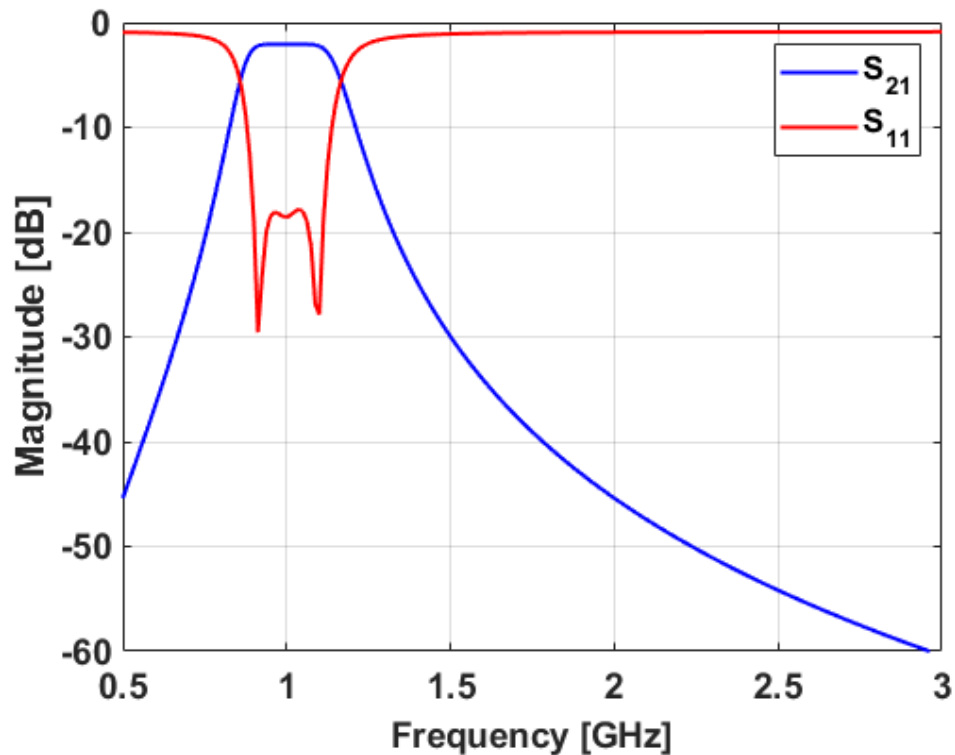


Figure 3.9: S-parameters for the ideal filter simulation

3.2.2 Adding Non-Ideal Inductor Models

The next step in the design process is to add real measured inductor S-parameters to the ADS simulation. These are added to the simulation first because it is more difficult to find specific values of inductors than it is to find other components. This scarcity makes it much more difficult to tune the values of inductors than ca-

capacitors. The ADS schematic after adding real inductor S-parameters is shown in Figure 3.10.

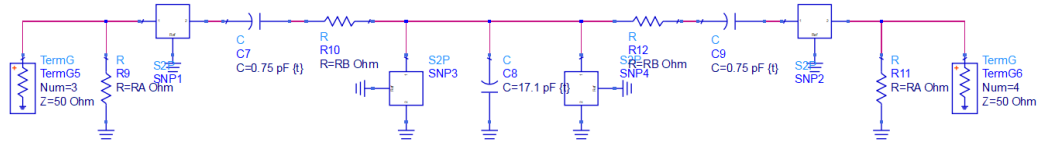


Figure 3.10: ADS simulation setup of the filtenuator after adding real measured inductor S-parameters

The S-parameters of the ADS simulation with real measured inductor S-parameters are shown in Figure 3.11. The S_{21} of the filter shows about 1 dB more loss than the ideal simulation as well as a more rounded passband edge. This is due to the

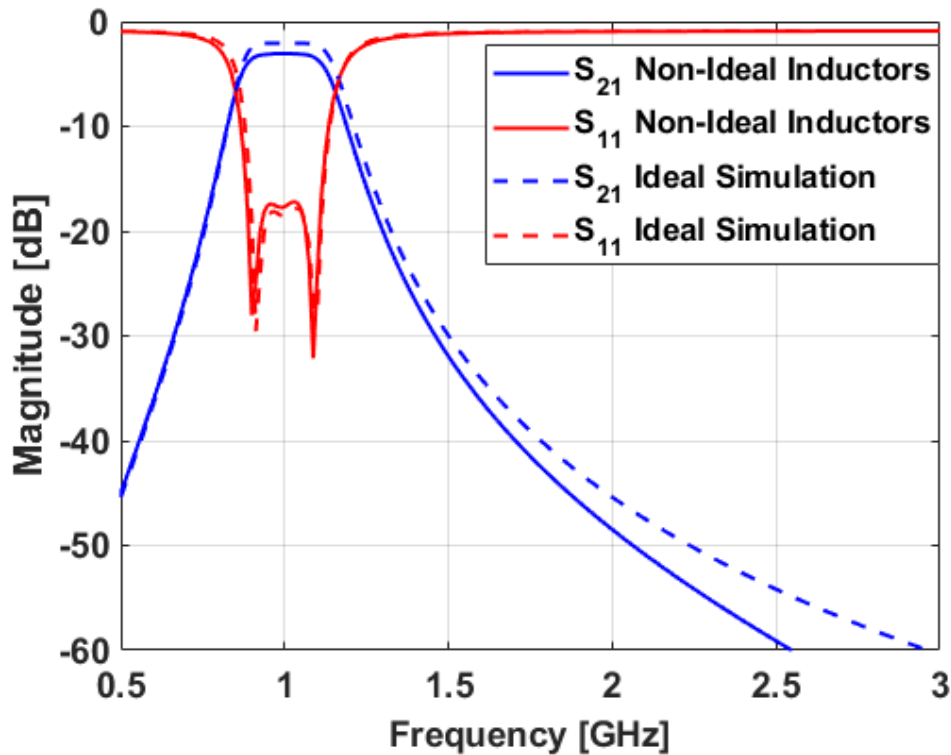


Figure 3.11: S-parameters for the ADS simulation after adding real inductor S-parameters compared to the ideal simulation

DC resistance of the inductors adding additional loss to the filter and contributing to a decrease in resonator Q . The bandwidth is also narrower due to the lack of availability of components that meet the exact specifications of the calculated component values. The S_{11} of the filter shows the same degradation of the filter ripple as the ideal filtenuator simulation with a slightly lopsided response.

3.2.3 Adding Non-Ideal Capacitor Models

The next step in the design process is to add real measured capacitor S-parameters to the ADS simulation. The capacitors are added after the inductors because there is greater availability of capacitor values to choose from which makes it much easier to tune the capacitors than the inductors. Due to limited choices of inductor values, the center frequency of the filter is slightly shifted. This frequency shift necessitates tuning the capacitor values to attain the desired center frequency. The ADS schematic after adding real capacitor S-parameters is shown in Figure 3.12.

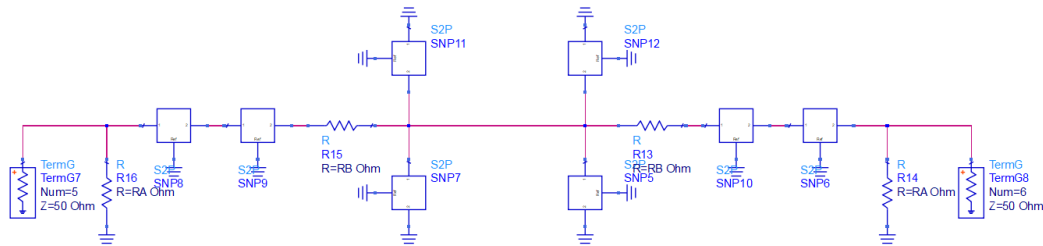


Figure 3.12: ADS simulation setup of the filtenuator after adding real measured capacitor S-parameters

The S-parameters of the ADS simulation with real measured capacitor S-parameters are shown in Figure 3.13. The S_{21} of the filter shows an additional 0.3 dB of loss after adding the real measured capacitor S-parameters. There is also a slight reduction in bandwidth which is due to tuning the capacitors to compensate for the

non-ideal inductor values used. The return loss of the filter continues to show some ripple degradation.

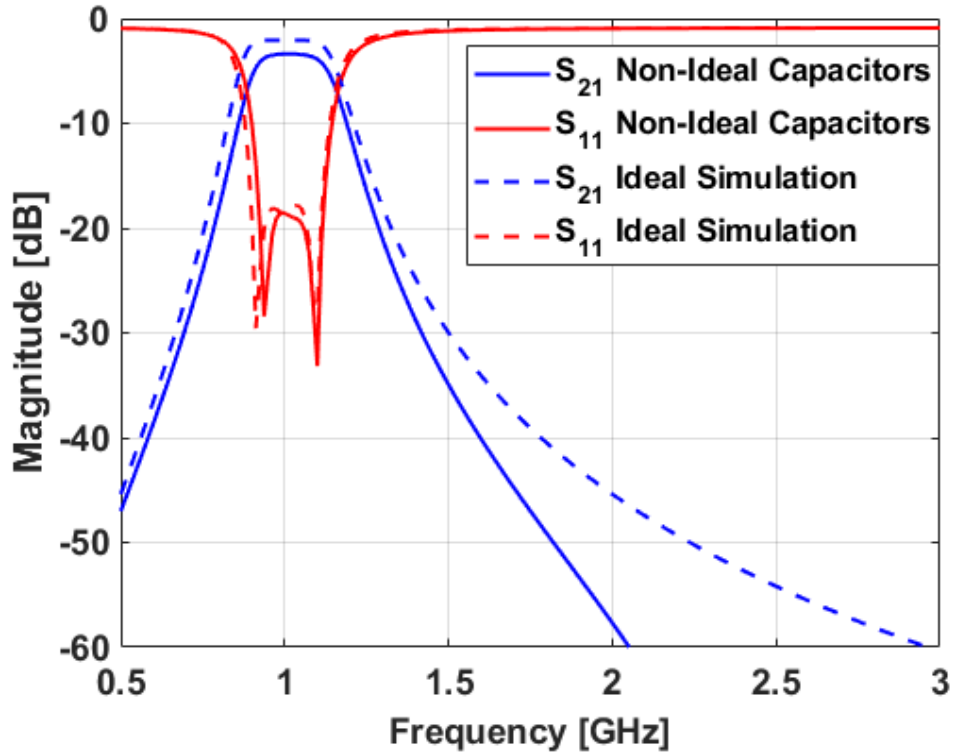


Figure 3.13: S-parameters for the ADS simulation after adding real capacitor S-parameters compared to the ideal simulation

3.2.4 Adding Non-Ideal Resistor Models

The next step in the design process is to add a non-ideal model of the resistors into the ADS simulation. The chosen resistors did not have the measured S-parameter data necessary to use for a more accurate simulation. Because of this, an equivalent circuit model of the resistors was used in the place of measured S-parameters. The equivalent circuit consisted of the value of the resistor in series with a 0.129 nH inductance. This series combination was then in parallel with a 0.0392 pF capacitance. The ADS simulation after adding the resistor equivalent

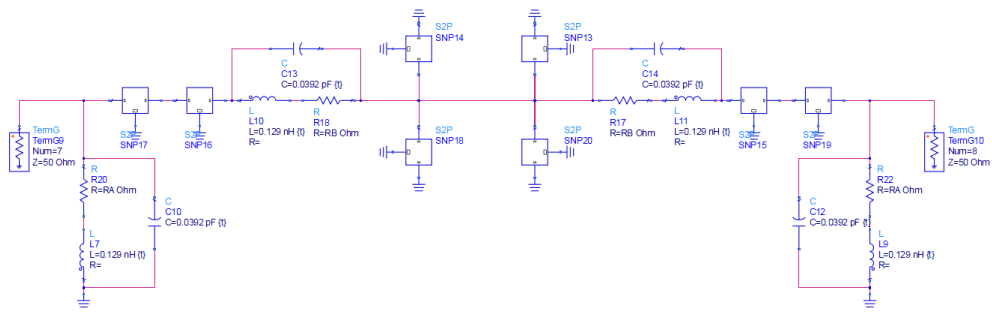


Figure 3.14: ADS simulation setup of the filtenuator after adding an equivalent circuit for the resistors

circuit model to it is shown in Figure 3.14 while the S-parameters of the ADS simulation with the resistor equivalent circuit are shown in Figure 3.15. The addition of the resistor equivalent circuit to the simulation does not noticeably affect the response of the filtenuator. This is not a surprise as the amount of inductance and

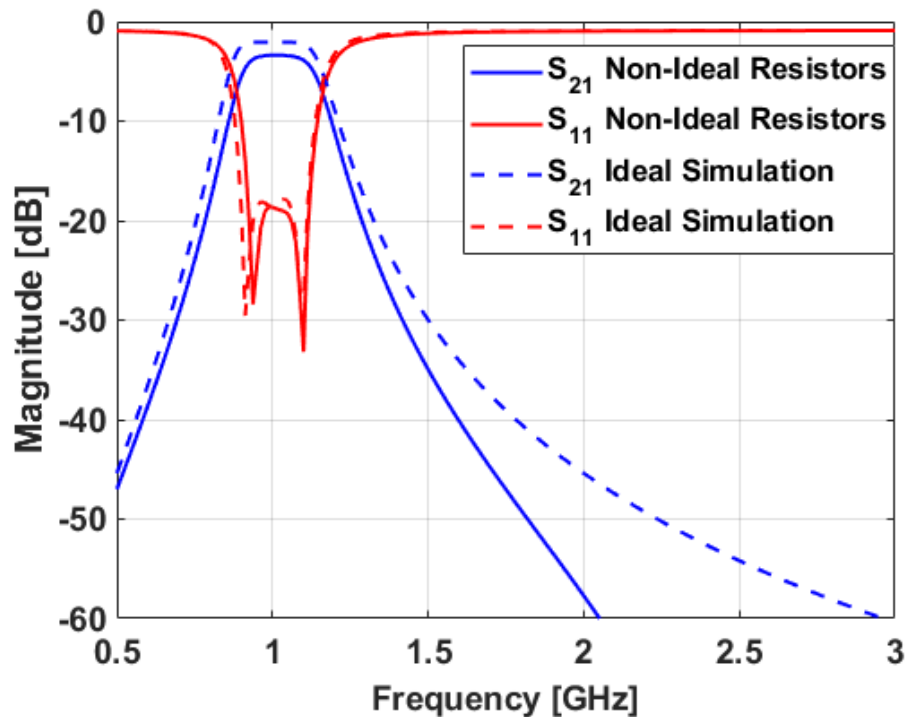


Figure 3.15: S-parameters for the ADS simulation after adding resistor equivalent circuit compared to the ideal simulation

capacitance added to the overall circuit is minimal in comparison to the component values used in the resonators.

3.2.5 Effects of Traces Between Series Resonators

An interesting issue was discovered when first simulating the filtenuator after adding microstrip traces to the design. The filter response became distorted and poorly matched. This was found to be due to the microstrip traces that were added to the circuit and in particular, between the inductor and capacitor of the series resonators. Upon further inspection, it was found that the segment of transmission line between the LC components of the resonator was adding enough inductance to shift the resonant frequency of the series resonators and causing the performance of the circuit to degrade.

The traditional series LC resonator consists of an inductor and capacitor in series. In general, an inductor will act as a short circuit at lower frequencies while at higher frequencies it will act as an open circuit while a capacitor will act as an open circuit at lower frequencies and at higher frequencies it will act as a short circuit. However, at a certain frequency, these components will resonate and allow

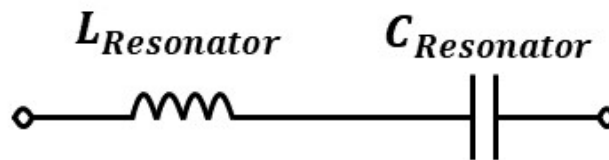


Figure 3.16: Ideal circuit of the series LC resonator

a “center” frequency to pass while attenuating higher and lower frequencies. The ideal circuit schematic of an LC resonator is shown in Figure 3.16 while the S-parameters of the ideal LC resonator are shown in Figure 3.17. The series resonator is shown to have an ideal response with the designed resonant frequency of 1 GHz. S_{11} has a very narrow response which indicates a high Q. This makes sense because ideal LC components have no added resistance and thus high Q.

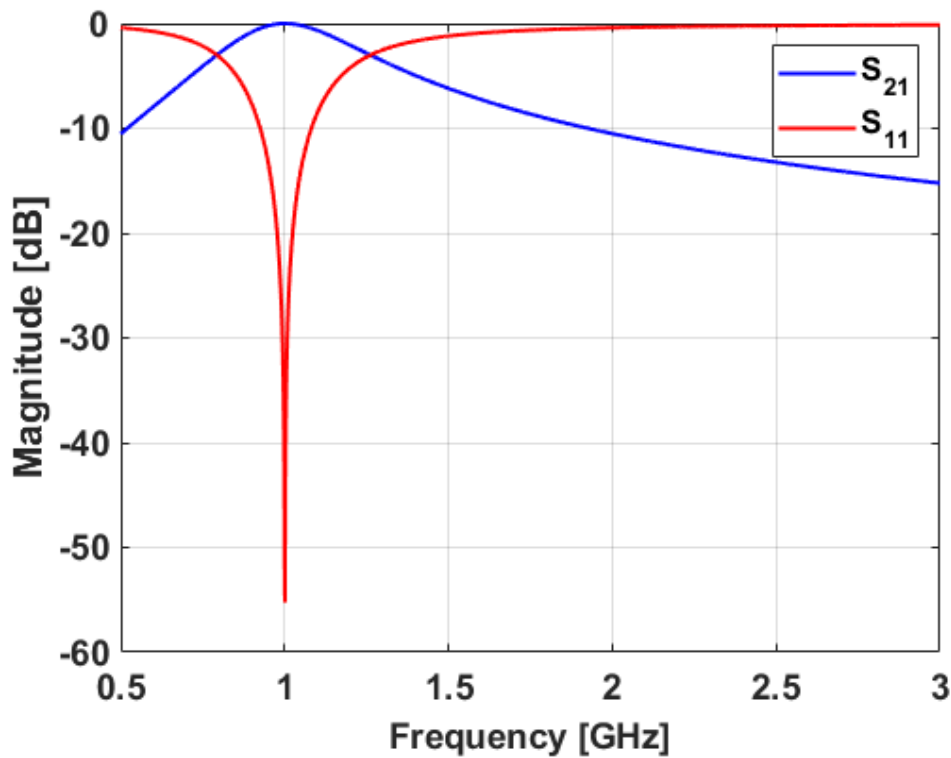


Figure 3.17: Simulated S-parameters of the ideal series LC resonator

Although it would be nice to have ideal inductors and capacitors that can be placed directly next to each other, in practical circuits, there is a small amount of transmission line between components. This transmission line can have a great effect on the circuit and the LC resonator. The schematic of the model of the LC resonator with a microstrip line between components is shown in Figure 3.18.

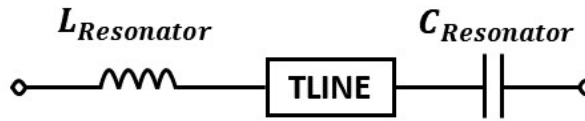


Figure 3.18: Schematic of the series LC resonator with a transmission line in-between components

The S-parameters of the LC resonator with added microstrip line between components is shown in Figure 3.19. The resonator shows a slight decrease in its center frequency which is caused by the additional inductance and capacitance of the

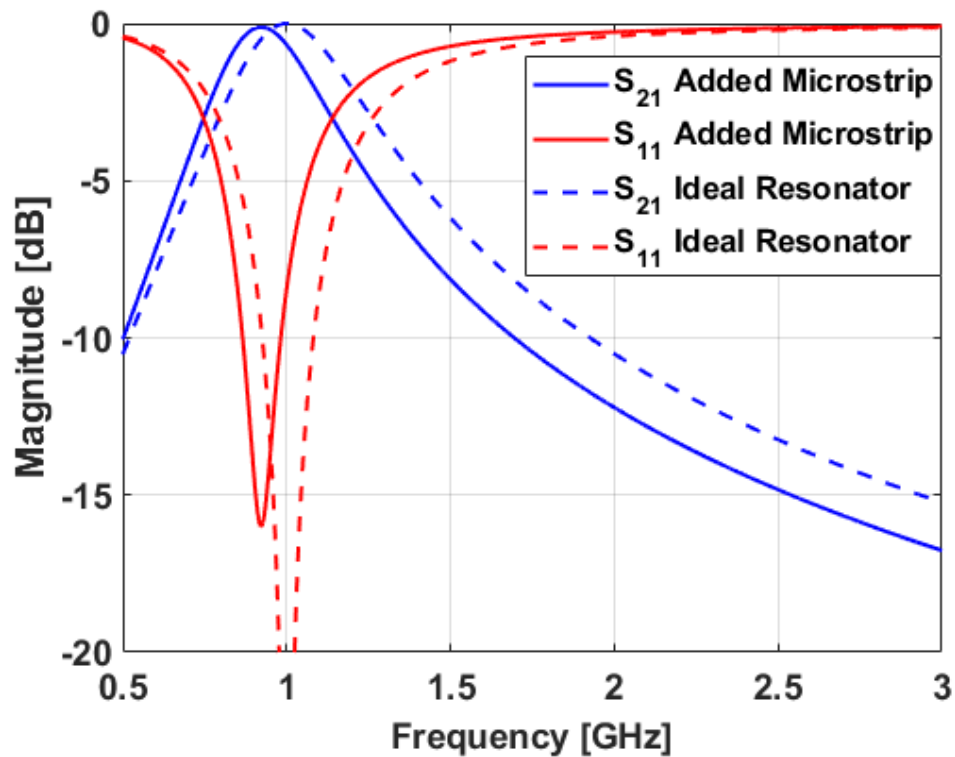


Figure 3.19: Simulated S-parameters of the series LC resonator with a transmission line in-between components compared to the ideal LC resonator

added transmission line. There is also a decrease in return loss and bandwidth which can be observed in S_{11} . This degradation in performance is caused by the slight added resistance and conductance of the microstrip line model used in simulations causing a decrease in the Q of the resonator.

To compensate for the length of transmission line added to the series resonator, the classic model of a lossless transmission line will be used to determine the equivalent inductance and capacitance that is added to the resonator by the transmission line. In this model, there is a series inductor followed by a shunt capacitor. The series inductance can be easily calculated and used to change the inductance of the series resonator ($L_{resonator}$). The model of the series resonator used in ADS and its LC equivalent model is shown in Figure 3.20.

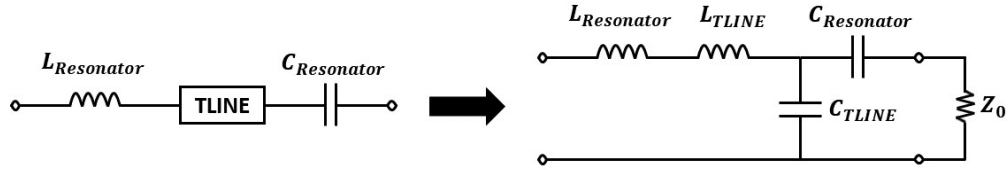


Figure 3.20: Equivalent circuit of the series resonator with transmission line

The transmission line is assumed to be $Z_0 = 50$ ohms, 12.7 mm long, and have a dielectric constant (ϵ_r) of 3. The first step in solving this problem is calculating the velocity of propagation (v_p) of the line using

$$v_p = \frac{c}{\sqrt{\epsilon_r}} \quad (3.7)$$

where c is the speed of light. This result is then used to calculate the capacitance per unit length

$$C_{meter} = \frac{1}{v_p Z_0} = 115.47 \text{ pF/m} \quad (3.8)$$

and the inductance per unit length

$$L_{meter} = Z_0^2 C_{meter} = 288.68 \text{ nH/m} \quad (3.9)$$

of the transmission line segment. To find the total capacitance of the length of transmission line, (3.8) is multiplied by the total length of the transmission line in meters which yields

$$C_{line} = C_{meter} 0.0127 = 1.4665 \text{ pF}. \quad (3.10)$$

To find the total inductance of the length of transmission line, (3.9) is multiplied by the total length of the transmission line in meters which yields

$$L_{line} = L_{meter} 0.0127 = 3.662 \text{ nH}. \quad (3.11)$$

The amount of parasitics added from the addition of a transmission line is a significant amount, especially the parasitic inductance. There are several ways to minimize the effects of these parasitics such as reducing the length of the transmission line or designing the circuit on a thicker substrate; however, reducing the length of the transmission line between components can only minimize the parasitics and has practical limitations due to the need to solder components, while designing on a thicker substrate may not be possible due to system design constraints. A possible solution is to compensate for the parasitic effects of the transmission line in the LC components.

The inductance is the simplest parasitic to compensate for since the inductors are in series and inductors in series add. The new inductor value needed for the resonator is calculated as

$$L_{new} = L_{resonator} - L_{line} = 33.96 \text{ nH} - 3.662 \text{ nH} = 30.298 \text{ nH}. \quad (3.12)$$

This new inductance value is then put into the ADS simulation with the added microstrip line to assess the effect tuning the inductor value has on the resonator. The S-parameters of the LC resonator after compensating for the microstrip line by changing the series inductor value in the LC resonator are shown in Figure 3.21. Although the frequency is still slightly shifted, the S-parameters of the series resonator is much closer to the ideal 1 GHz that it was designed to operate at. This shows that the addition of transmission lines has a mostly inductive effect on the LC resonator. The return loss and bandwidth of the resonator are still degraded compared to the ideal LC resonator. This degradation is due to the added resistance and conductance of the non-ideal transmission line model in ADS.

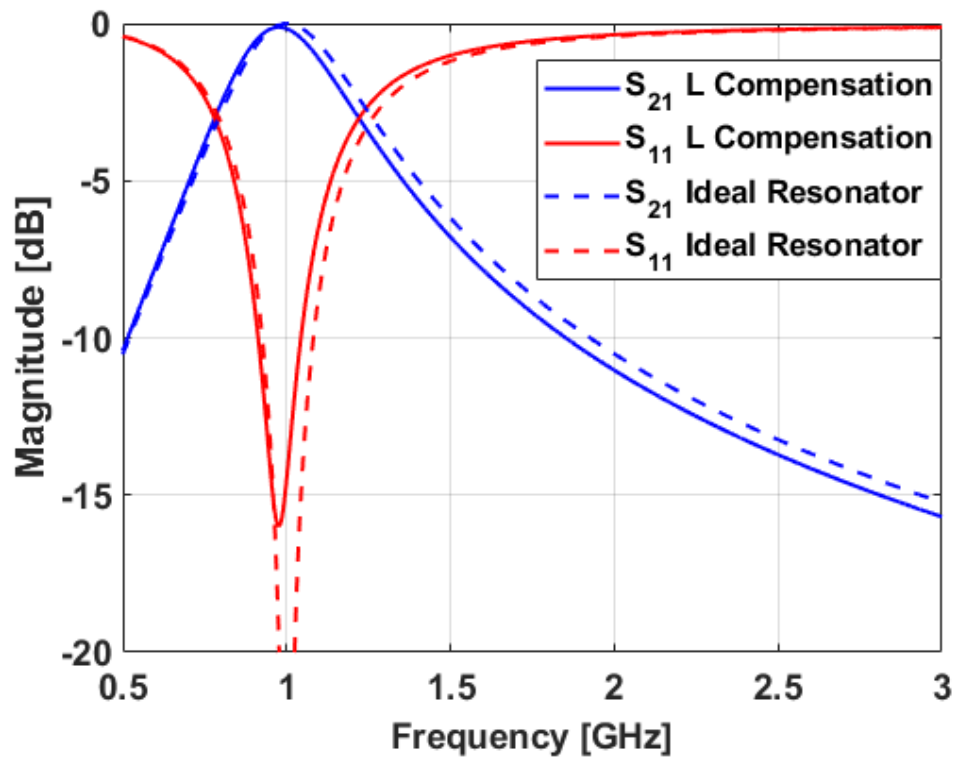


Figure 3.21: Simulated S-parameters of the series LC resonator with the added inductance compensated for compared to the ideal LC resonator

Although compensating for the inductance of the added transmission line can mostly fix the LC resonator, microwave filters are very sensitive to inductor and capacitor values. Due to this fact, it is necessary to also compensate for the parasitic capacitance added by the transmission line. This process involves solving the equivalent circuit of the series resonator for its input impedance and then finding the value of $C_{Resonator}$ that resonates with $L_{Resonator}$ at 1 GHz. The equivalent circuit used to solve for the input impedance of the resonator circuit is shown in Figure 3.22.

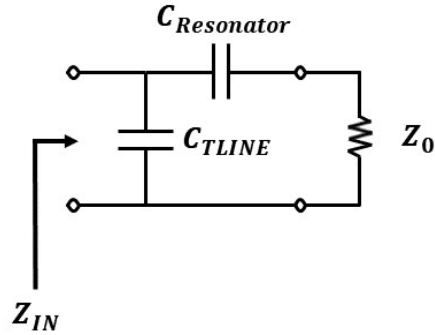


Figure 3.22: Model of the series resonator used to solve for C_{new}

On inspection, it is seen that Z_0 is in series with $C_{Resonator}$ which is in parallel with C_{TLINE} . The input impedance looking into the resonator is then solved for as

$$Z_{IN} = (Z_0 + Z_{C_{resonator}}) || Z_{C_{line}} . \quad (3.13)$$

After using some algebra and rearranging (3.13) the expression for the impedance of the capacitor in the resonator is

$$\frac{Z_{IN}Z_0 + Z_{IN}Z_{C_{line}} - Z_0Z_{C_{line}}}{Z_{C_{line}} - Z_{IN}} = Z_{C_{resonator}} . \quad (3.14)$$

Evaluating the impedances in (3.14) at the center frequency of 1 GHz results in

$$Z_{L_{Resonator}} = j213.38 \Omega, Z_{C_{line}} = -j109 \Omega, Z_{IN} = j213 \Omega, \text{ and } Z_0 = 50 \Omega.$$

These values can then be plugged into (3.14) to yield

$$\frac{(j213 \cdot 50) + (-j213 \cdot j109) - (50 \cdot -j109)}{-j109 + j213} = Z_{C_{resonator}} = 50 - j223 \Omega . \quad (3.15)$$

This results in a real part of 50 ohms and an imaginary part of -223 ohms. Since the transmission line is supposed to be 50 ohms, the real part of $Z_{C_{Resonator}}$ can be ignored. The imaginary part of (3.15) can then be put into the equation for the impedance of a capacitor evaluated at 1 GHz to yield

$$Z_{C_{new}} = \frac{1}{j\omega C_{new}} = -j223 \Omega . \quad (3.16)$$

Equation 3.16 is then rearranged and evaluated at 1 GHz to solve for the new capac-

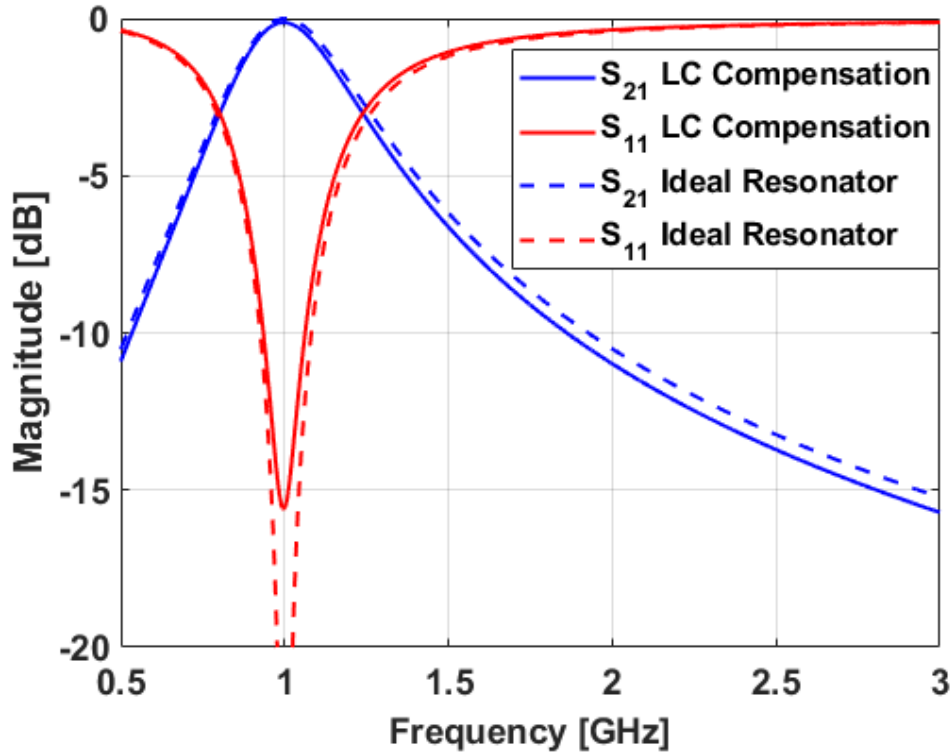


Figure 3.23: Simulated S-parameters of the series LC resonator with the added capacitance compensated for compared to the ideal LC resonator

ittance needed for the resonator to operate at that center frequency. The calculation of the new capacitance value is

$$C_{new} = \frac{1}{j\omega Z_{C_{new}}} = \frac{1}{j2\pi F_0 Z_{C_{new}}} = \frac{1}{j2\pi 10^9 223} = 0.713 \text{ pF} . \quad (3.17)$$

This new capacitor value is then put into the ADS simulation of the series resonator. This tuning of the capacitor to compensate for the transmission line shifts the frequency of the resonator back to 1 GHz. The resulting S-parameters are shown in Figure 3.23.

3.2.6 Adding Microstrip Traces and Vias

The last step in the design process is to add models of microstrip traces between components and models of vias to ground where necessary. It was decided to make a 75-mil-wide (50 ohm) line at the input and output of the filtenuator and then taper the line down to a 32-mil-wide microstrip so that the traces were the same size as the pads of the lumped components. The vias to ground were designed with a diameter of 20 mil and a square pad of 75 mils on a side. These decisions were made to simplify the design of the layout. The ADS simulation after adding microstrip and via models is shown in Figure 3.24. The S-parameters of the ADS simulation with models of microstrip lines and vias to ground added to it are shown in Figure 3.25. The S_{21} has about 3 dB of loss at the passband. This is the same amount of loss as before adding the microstrip lines and vias. The response does become frequency shifted down to around 960 MHz due to the combination of component availability and parasitics from the added microstrip lines. The addition of vias to ground does not seem to have any noticeable impact on the response. The S_{11} is still matched across the passband; however, it also shows more degradation and loses much of

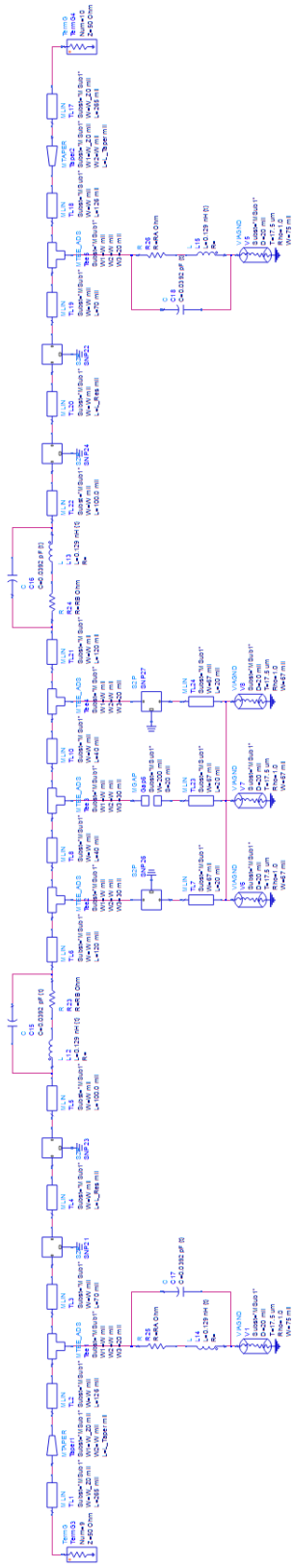


Figure 3.24: S-parameters for the fully non-ideal ADS simulation

its Chebyshev shape. This is due to the reduction in Q from the series resonators because of the addition of microstrip lines to the resonators.

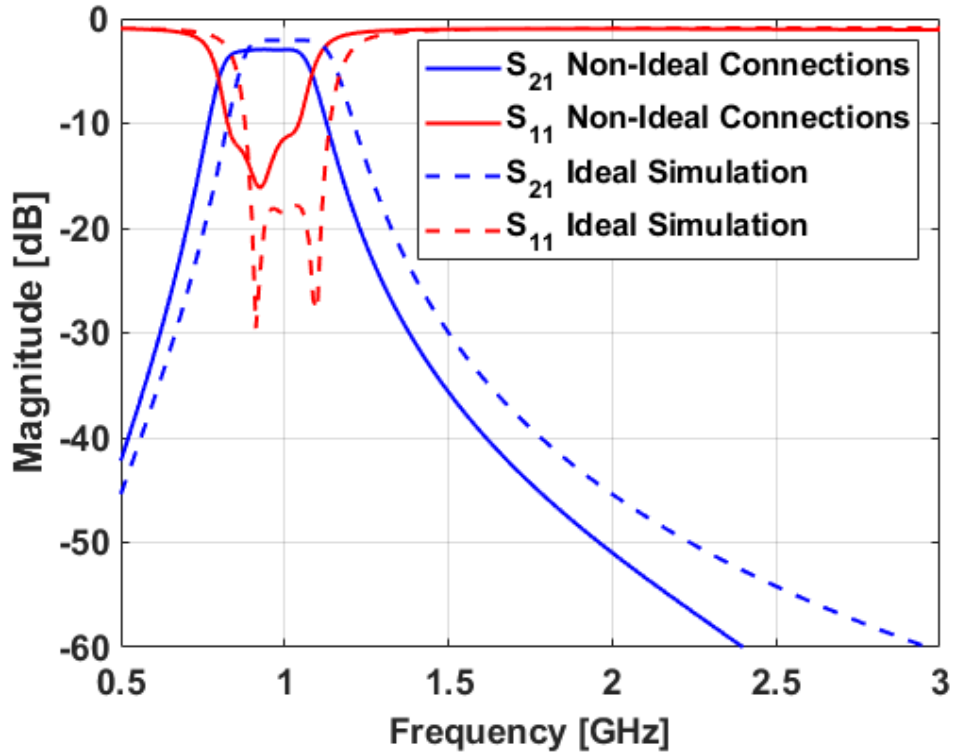


Figure 3.25: S-parameters for the ADS simulation after adding microstrip traces compared to the ideal simulation

3.3 Fabrication

The filtenuator is implemented on a 30-mil-thick Rogers 3003® laminate substrate with 1/2 oz. copper thickness [20]. The circuit is designed as a standard two-copper-layer printed circuit board (PCB) with the top layer being the signal layer containing all of the components and the bottom layer being a ground plane. The input and output traces of the filtenuator are 50 ohm microstrip transmission lines connecting to standard edge-launch SMA connectors [21]. The 50 ohm input traces are then tapered down to 32-mil-wide microstrip traces so that they can be

run straight into the component pads. The vias have a diameter of 19.7 mil (0.5 mm) to facilitate the application of the LPKF ProConduct conductive polymer as well as being a standard drill size. A single $200 \times 87 \text{ mil}^2$ pad was designated for the shunt components to make room for the possibility of adding capacitors in parallel to tune the shunt resonator. Three vias to ground were arranged on the shunt resonator pad to ensure that the pad was equally grounded everywhere. The top layer of the PCB is patterned using an LPKF ProtoLaser U4 and the vias are drilled using an LPKF ProtoMat S104 and plated using the LPKF ProConduct process. The EAGLE layout of the filtenuator PCB is shown in Figure 3.26.

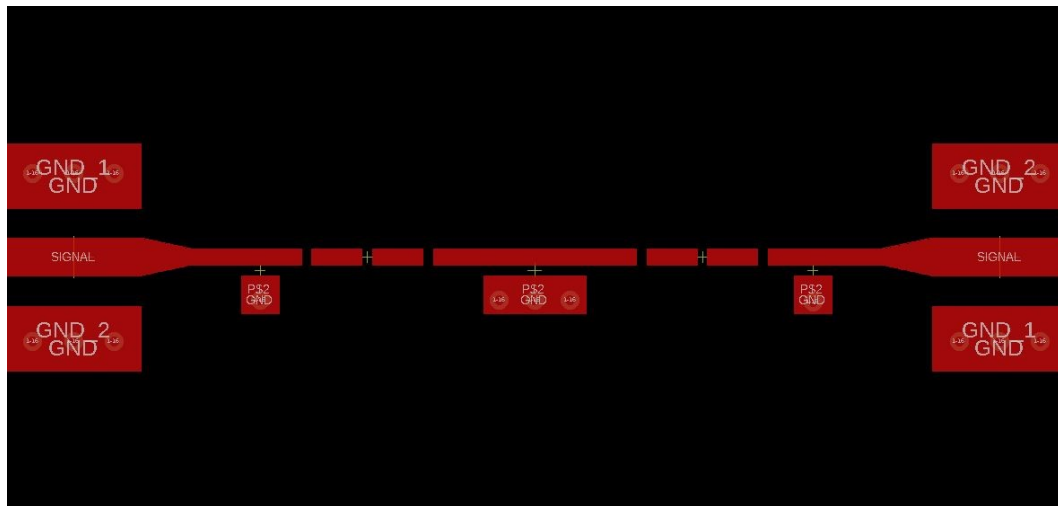


Figure 3.26: EAGLE layout of the static filtenuator

The final step of the fabrication process is soldering the lumped-element RLC components to the PCB. The resistors, capacitors, and inductors are soldered to the board using a reflow process and a silver-impregnated solder paste. It is very important during the reflow process that care is taken to ensure that the components do not drift very much from their desired locations as this drift can change the effective length of the transmission line between the inductors and capacitors in the series resonators. This can cause a small change in effective inductance of the res-

onator which can lead to an impactful difference in resonant frequency and overall frequency response. The inductors used in the design are the Coilcraft CT series 0603 inductors [22], the capacitors are Murata high-Q GJM series 0402 capacitors [23], and the resistors are Vishay high-frequency FC series 0402 resistors [24]. The total area of the fabricated PCB is $25 \times 50 \text{ mm}^2$. The final fabricated and populated filtenuator is shown in Figure 3.27.

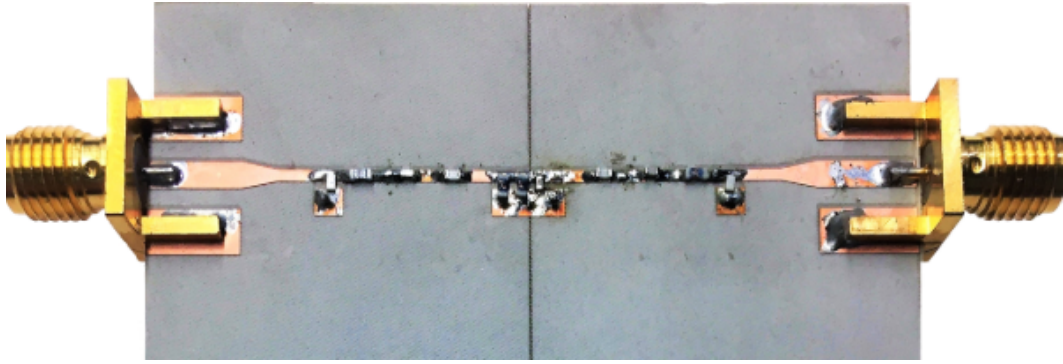


Figure 3.27: Fabricated and populated PCB of the static filtenuator

3.4 Measured Results

The proposed filtenuator design is measured using an Agilent Technologies N5225A precision network analyzer calibrated using an Agilent N4692-60006 electronic calibration module. The measured S-parameters are then compared to the simulated S-parameters. The S-parameters of the simulated results compared with the measured results of a 3 dB static filtenuator are shown in Figure 3.28. The center frequency for both the simulated and measured results is around 960 MHz due to component availability while the S_{21} passband attenuation is 3 dB for both simulated and measured results. The bandwidth of the filtenuator is slightly more narrow in the measured results than in simulation which could be because the loss in components and traces is not as large in the fabricated circuit as in the simu-

lated one. Another explanation could be that component tolerances were slightly off in a way that effected the bandwidth but not the center frequency. The S_{11} at the passband shows slightly more degradation in the measured results than in the simulated results but still results in a match at the passband. However, the simulated and measured results show excellent agreement.

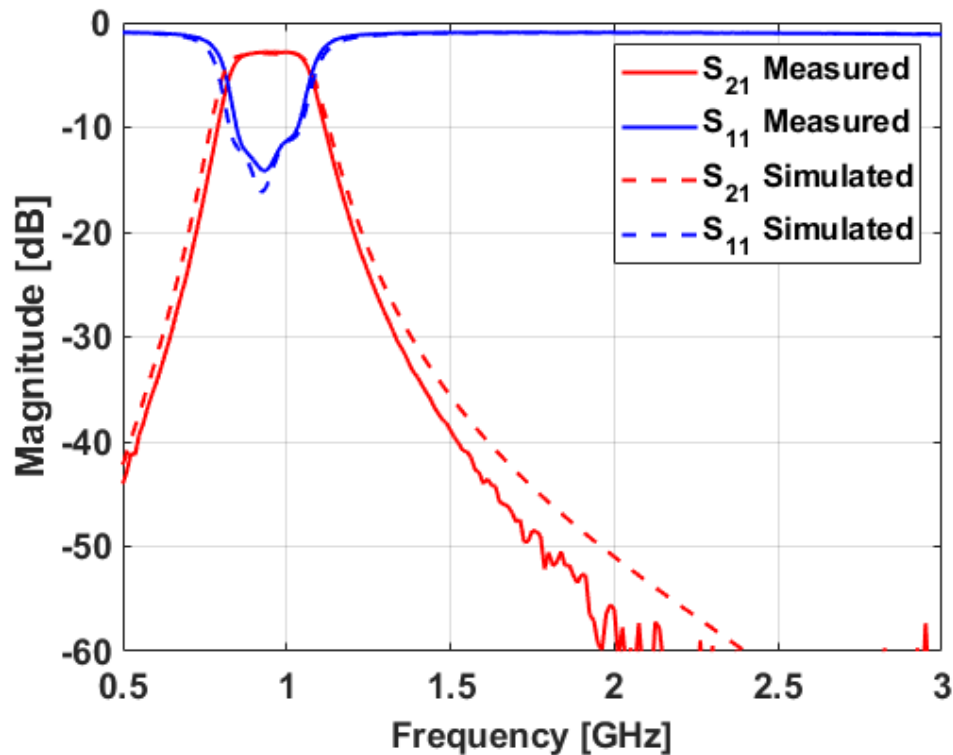


Figure 3.28: Measured results of the static filtenuator compared to ADS simulation

Now that the simulated and measured results for a 3 dB filtenuator design are shown to be in good agreement, attenuation levels of 3, 4, 5, 6, and 7 dB are simulated and fabricated. A table of resistor values used in the simulated and fabricated filtenuators and their associated passband attenuation are shown in Table 3.2.

Table 3.2: Table of values used for the static filtenuator

Loss (dB)	R_A (Ω)	R_B (Ω)
3	1000	10
4	330	10
5	330	15
6	200	20
7	132	20

The measured S_{11} of the static filtenuators with 3, 4, 5, 6, and 7 dB of loss are shown in Figure 3.29. The return loss of the measured filtenuator is sufficient to be matched across the passband for all measured levels of attenuation. Of note is that the S_{11} out of band is the same for the 4 dB and 5 dB measured filtenuators.

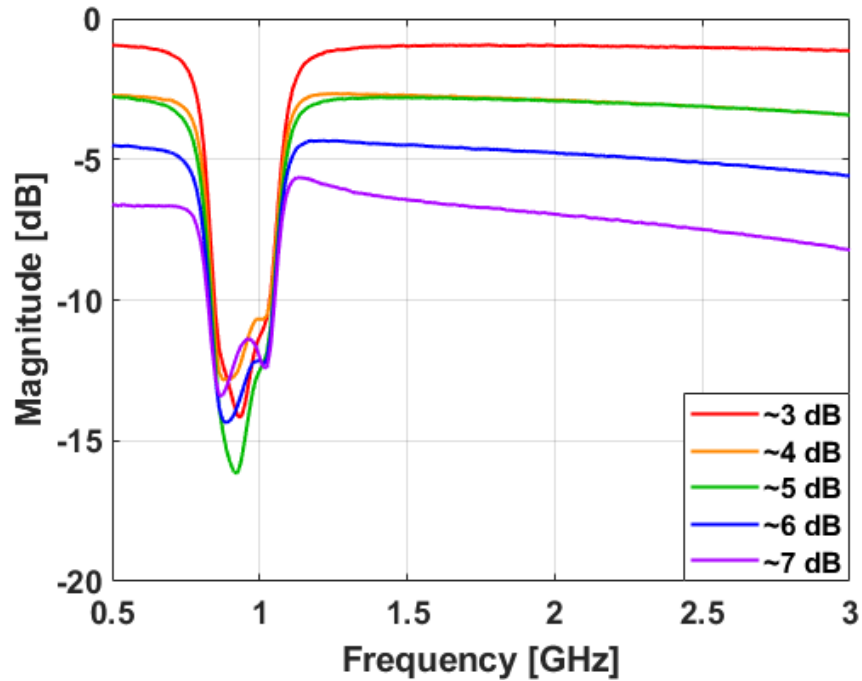


Figure 3.29: Measured S_{11} of the static filtenuator with 3, 4, 5, 6, and 7 dB of passband attenuation

This is due to the same resistance value for R_A being used for both cases and only varying the series resistance R_B . This was done due to the limited values of the high-frequency resistors available that would result in a matched passband. The measured S_{21} of the static filter attenuators with 3, 4, 5, 6, and 7 dB of attenuation are shown in Figure 3.30. The S_{21} of the fabricated filter attenuator shows that the filter attenuator has a center frequency of around 960 MHz and multiple levels of attenuation for each iteration. The passband also remains relatively flat for all measured levels of attenuation. The 3, 4, 5, 6, and 7 dB of attenuation that the filter attenuator is designed for is also met.

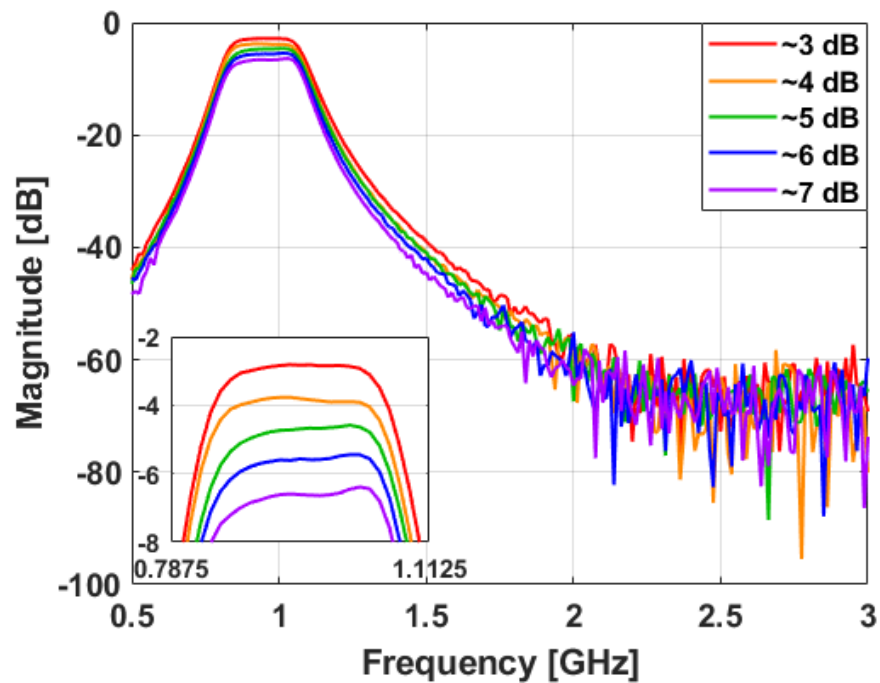


Figure 3.30: Measured S_{21} of the static filter attenuator with 3, 4, 5, 6, and 7 dB of passband attenuation

The group delay of the measured filter attenuator is then calculated using the measured S_{21} shown in Figure 3.30. The group delay at the center frequency of the filter attenuator stays constant for all levels of passband attenuation measured. This is ideal for

RF systems as a single system delay calibration can be conducted and used for all attenuation scenarios. The group delay as a function of passband attenuation is shown in Figure 3.31.

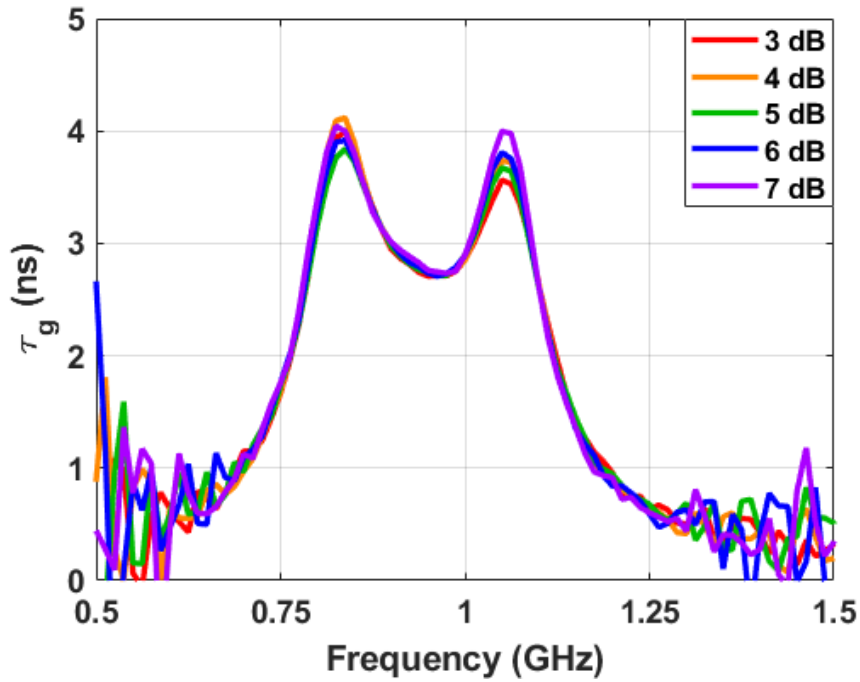


Figure 3.31: Measured group delay of the static filtenuator with 3, 4, 5, 6, and 7 dB of passband attenuation

3.5 Summary

In this chapter, a proof-of-concept static third-order bandpass filtenuator was designed, simulated, and fabricated. This circuit was then designed step-by-step in ADS using non-ideal component models. The circuit is finally fabricated and tested to validate the filtenuator theory outlined in Chapter 2. Now that a proof-of-concept static filtenuator circuit has been fabricated and measured, and the filtenuator concept and theory are validated, a continuously tunable filtenuator can be designed.

Chapter 4

Tunable Filtenuator Design

In Chapter 3 a static filtenuator was designed, simulated, and fabricated based on the theory detailed in Chapter 2 using lumped-element inductors, capacitors, and resistors. Although this served as a good proof-of-concept design for the filtenuator concept, the utility of a static design is limited. Although a fixed attenuation filtenuator serves to reduce the number of components necessary in RF receivers, multiple filtenuators would be necessary to fulfill the needs of modern RF receivers. A filtenuator capable of continuously and electronically tuning the passband attenuation would be ideal to decrease the SWaP of future RF receivers while also increasing the dynamic range of future systems.

4.1 Tunable Resistors

Tunable resistors are very useful devices and are found in many applications such as tunable circuits and switches. There are many different kinds of tunable resistors and methods of tuning resistance such as: trimmer potentiometers [25, 26], field effect transistors [27], varactor diodes [19], and PIN diodes [19, 28, 29, 30].

Trimmer potentiometers (trim pots) are simple devices which can be used as a variable resistance within a circuit. Trim pots are normally adjusted using a screw-

driver and as such need to be manually adjusted. They are also generally much larger than other lumped circuit elements that are used in RF circuit design.

Another device that could be used as a variable resistance are field effect transistors (FETs). They can be used as variable resistors by tuning the voltage difference from the gate to the source (V_{GS}) of the FET and thereby changing the resistance from the drain to the source (R_{DS}) of the FET. One of the drawbacks of using a FET as a variable resistance is that they have a large parasitic capacitance that can become difficult to design around.

Another device that could be used as a variable resistance are varactor diodes. Varactor diodes are used often in tunable filter designs; however, they are usually employed as variable capacitors by using the varactors in a reverse biased configuration. They can be used as a tunable resistance by using them in a forward biased configuration; however, they have a large parasitic capacitance and a minimized resistance.

The final candidate for a variable resistance is PIN diodes. PIN diodes are oftentimes used in electronic switching circuits and attenuators and are commonly used as variable resistances in these applications [29]. They can also be used as a variable capacitor by using them in a reverse biased configuration like varactor diodes are oftentimes used; however, PIN diodes are designed with a minimized junction capacitance. Because of this, they are not good tunable capacitors. They do, however, function well as variable resistances. They can be used as variable resistances by putting them into a forward biased configuration. Their minimized capacitance and good resistance make PIN diodes an ideal candidate for use as electronically tunable resistors. For these reasons, PIN diodes will be used as the tunable resistance for the filter attenuator.

4.2 Simulation

For the design of an electronically tunable filtnuator, the same general topology used in the design of the static filtnuator in Chapter 3 will be used with a few slight alterations. The first alteration to be made is to replace the resistors in the static design with tunable resistors. For this design, Skyworks SMP-1304 PIN diodes [30] will be used as electronically tunable resistors. The filtnuator circuit with PIN diodes added to it is shown in Figure 4.1.

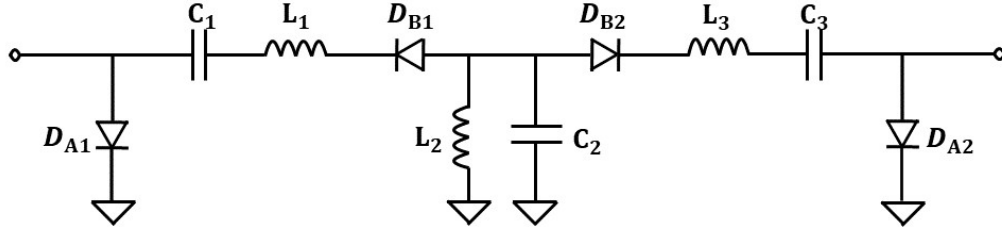


Figure 4.1: Filtnuator schematic with diodes added

4.2.1 Adding Non-Ideal Diode Models

The first step in the design process is to simulate the circuit with a non-ideal model of the PIN diodes in ADS. For this simulation, the priority will be on keeping the filtnuator at the correct frequency and level of attenuation while also remaining well matched in S_{11} . PIN diodes in forward bias can be modelled as a series combination of inductance and resistance. The datasheet for the PIN diodes indicate that they have a series inductance of 0.7 nH at 1 GHz. This series inductance will mainly have an effect on the inductance of the series resonators. This can be easily compensated for by subtracting 0.7 nH from the ideal resonator inductance value.

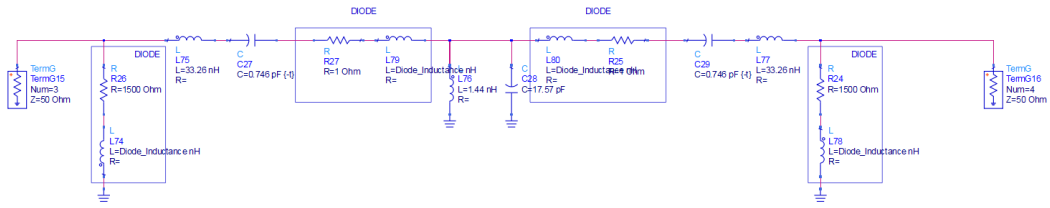


Figure 4.2: Filtnuator ADS schematic after adding PIN diode equivalent circuit

For the initial simulations, a single attenuation value will be designed for to keep the design process as simple as possible. The shunt resistance R_A will be set to 1752 ohms and the series resistances R_B will be set to 1.5 ohm. These values were selected because the datasheet for the PIN diodes show a table with a max resistance of 1752 ohms while the smallest value on the table is 1.5 ohm. These

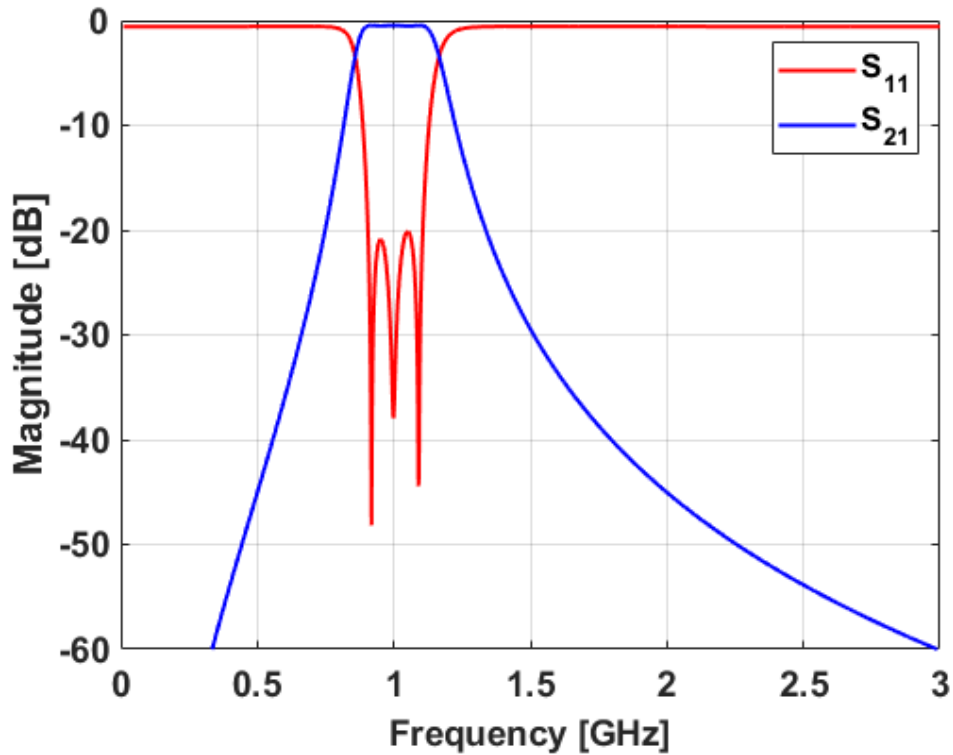


Figure 4.3: Filtnuator simulation S-parameters after adding PIN diode equivalent circuit

values indicate that a loss of 0.5 dB at the passband while remaining matched is the lowest achievable loss for this design using PIN diodes. The ADS simulation with the PIN diode equivalent circuit added is shown in Figure 4.2 while the S-parameters of the ADS simulation after adding the PIN diode equivalent circuit to the simulation is shown in Figure 4.3. The S_{21} of the filter shows the attenuation value of 0.5 dB which has been designed for while the S_{11} shows that the filter is well matched across the passband although the return loss ripple is slightly off from the ideal filter, however, the return loss meets the initial specification of 20 dB.

4.2.1.1 Diode Biasing

Although the PIN diodes are modeled as a series inductor and resistor, it is also necessary to include biasing circuitry to ensure that the diodes operate as designed within the circuit [28]. For the diodes to operate in a forward bias configuration, a positive DC bias should be applied to the anode of the diode while the cathode of the diode is grounded. The shunt diodes can be connected directly to ground while the series diodes need an RF choke to be connected to ground so that the DC power goes to ground while preventing the RF power from going to ground. In an active circuit, it is necessary to keep the RF and DC supplies separated so that they can both operate properly. This can be facilitated by inserting an RF choke between the DC power and the anode of the diodes. This RF choke provides isolation between the RF and DC sections of the circuit while also allowing the diodes to remain forward biased. For this application, an inductor is commonly used as an RF choke as it has frequency-dependent properties and is a low-impedance at DC while acting as a high-impedance at RF [31]. The filter schematic with biasing circuitry added is shown in Figure 4.4.

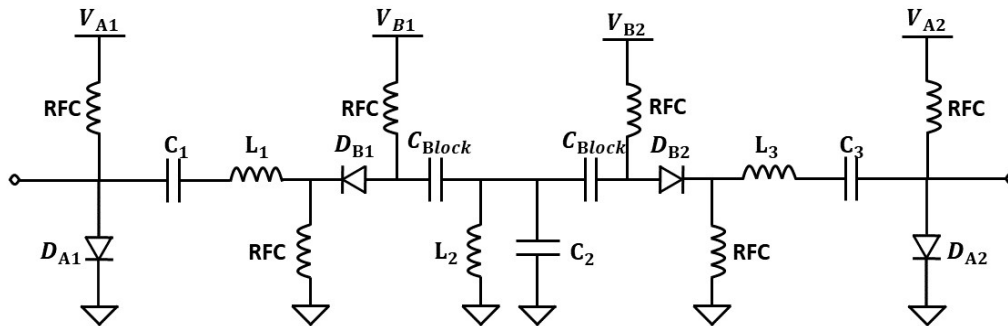


Figure 4.4: Filtnuator schematic with biasing circuitry added

When analyzing the circuit at DC, the RF chokes and inductors look like shorts while the capacitors look like opens. This causes the bias lines of the shunt diodes to have a direct path through the diode to ground. The series bias lines also have a path to ground through the diode, however, they also have a free path to ground through the inductor of the shunt resonator. Due to this it becomes necessary to block the DC from this path to ground so that the DC power goes to the diode as desired. This is done by adding a DC blocking capacitor between the series bias lines and the shunt resonator. The DC analysis of the circuit in Figure 4.4 is shown in Figure 4.5.

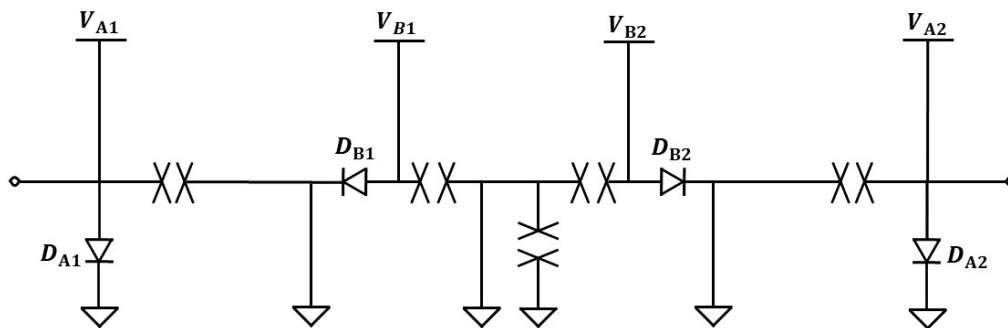


Figure 4.5: DC analysis of filtnuator schematic with biasing circuitry

4.2.2 Adding Non-Ideal RF Choke Models

Now that the necessary biasing circuit has been determined, the simulation is updated to include the biasing components. Coilcraft 0402DF series ferrite chip inductors are used for the RF chokes. These inductors have a low DC resistance and a self-resonant frequency (SRF) of 1070 MHz for the 470 nH models used. These RF chokes were modeled in ADS using measured component S-parameters from Coilcraft. The DC blocking capacitors will be modeled using built-in ideal capacitor models for now. The ADS simulation with the biasing components added is shown in Figure 4.6.

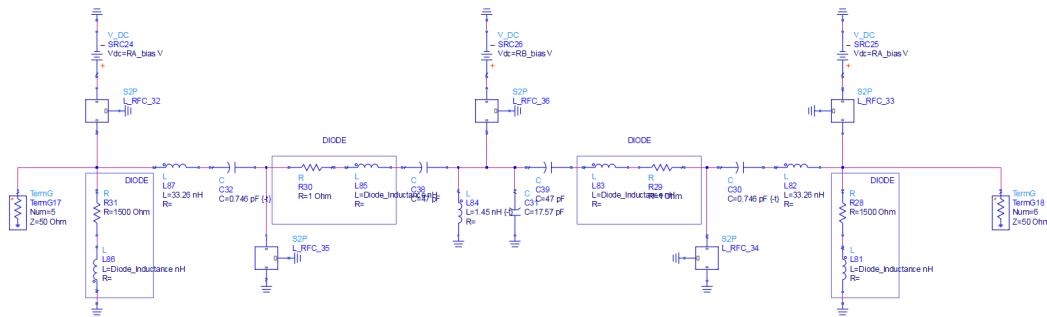


Figure 4.6: Filtenuator ADS schematic after adding biasing circuitry

The S-parameters of the ADS simulation after adding biasing circuitry to the simulation are shown in Figure 4.7. The insertion loss of the filter has increased from the ideal 0.5 dB to about 0.7 dB. This increase is due to the DC resistance of the RF chokes adding some loss to the filtenuator simulation. The S_{11} shows that the filtenuator is well matched across the passband with the designed 20 dB of return loss. A slight degradation in the filter ripple is also observed.

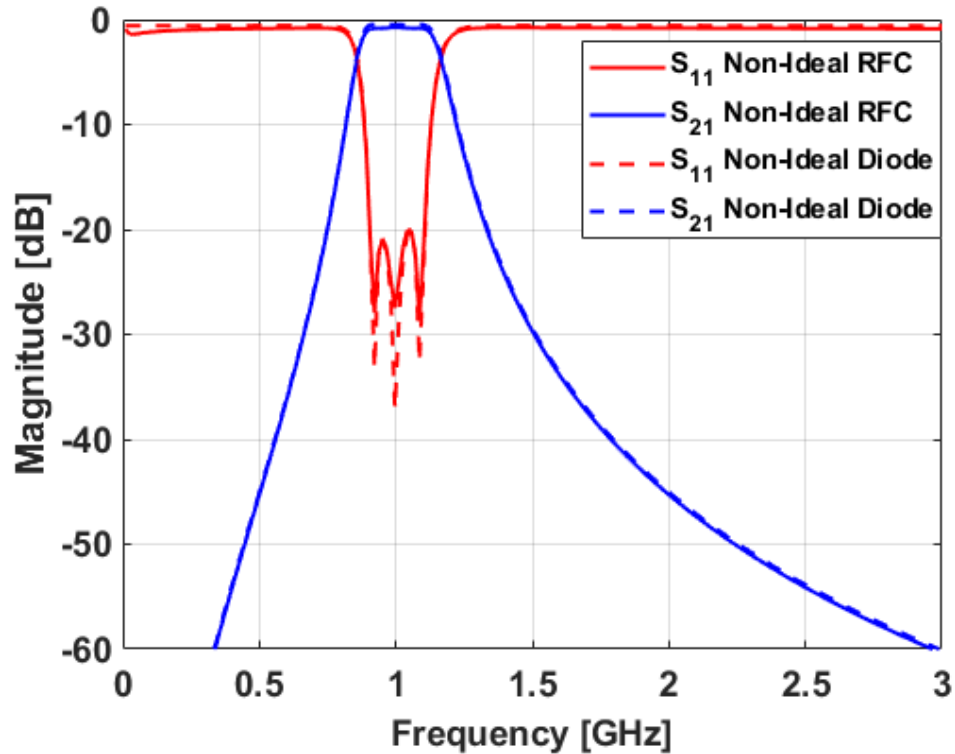


Figure 4.7: Filtenuator simulation S-parameters after adding RF choke measured S-parameters compared to non-ideal diode S-parameters

4.2.3 Adding Non-Ideal Inductor Models

The next step in the design process is to add real measured inductor S-parameters to the ADS simulation. These are added to the simulation first because it is more difficult to find specific values of inductors than it is to find other component values. This scarcity makes it much more difficult to tune the values of inductors than of capacitors. The ADS simulation after adding real measured inductor S-parameters is shown in Figure 4.8.

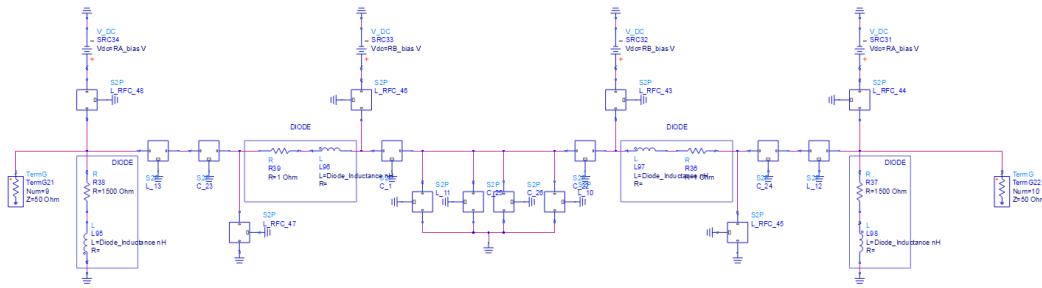


Figure 4.8: Filtenuator ADS schematic after adding measured inductor S-parameters

The S-parameters of the ADS simulation after adding real measured inductor S-parameters are shown in Figure 4.9. The insertion loss of the filter has increased from 0.7 dB to 1.8 dB. The passband of the filtenuator also has a more rounded

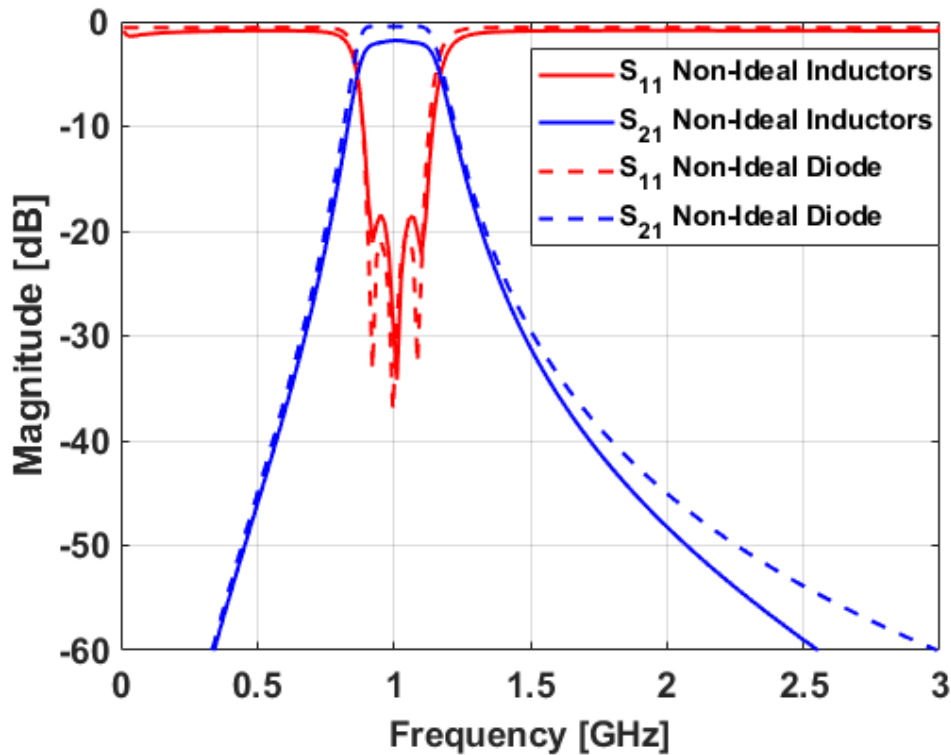


Figure 4.9: Filtenuator simulation S-parameters after adding measured inductor S-parameters compared to non-ideal diode S-parameters

passband edge. This is due to the DC resistance of the inductors adding additional loss to the filter and contributing to a decrease in resonator Q. The return loss of the filter also shows a degradation of the filter ripple.

4.2.4 Adding Non-Ideal Capacitor Models

The next step in the design process is to add real measured capacitor S-parameters to the ADS simulation. The capacitors are added after the inductors because there is greater availability of capacitor values to choose from, which makes it much easier to tune the capacitors than the inductors. There being limited choices of inductor values causes the center frequency of the filter to be slightly shifted. This frequency shift necessitated tuning the capacitor values to attain the desired center frequency. The ADS simulation after adding real measured capacitor S-parameters is shown in Figure 4.10.

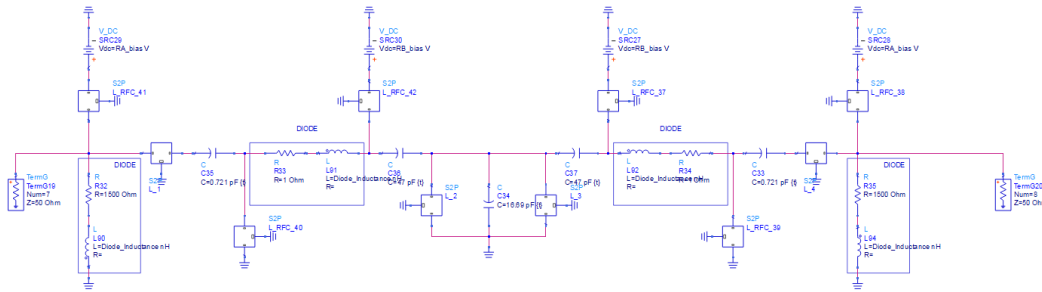


Figure 4.10: Filtenuator ADS schematic after adding measured capacitor S-parameters

The S-parameters of the ADS simulation after adding real measured capacitor S-parameters are shown in Figure 4.11. The insertion loss of the filter has increased from 1.8 dB to 2 dB. There is also a slight reduction in bandwidth which is likely due to tuning the capacitors to compensate for the non-ideal inductor values used. The return loss of the filter continues to show ripple degradation.

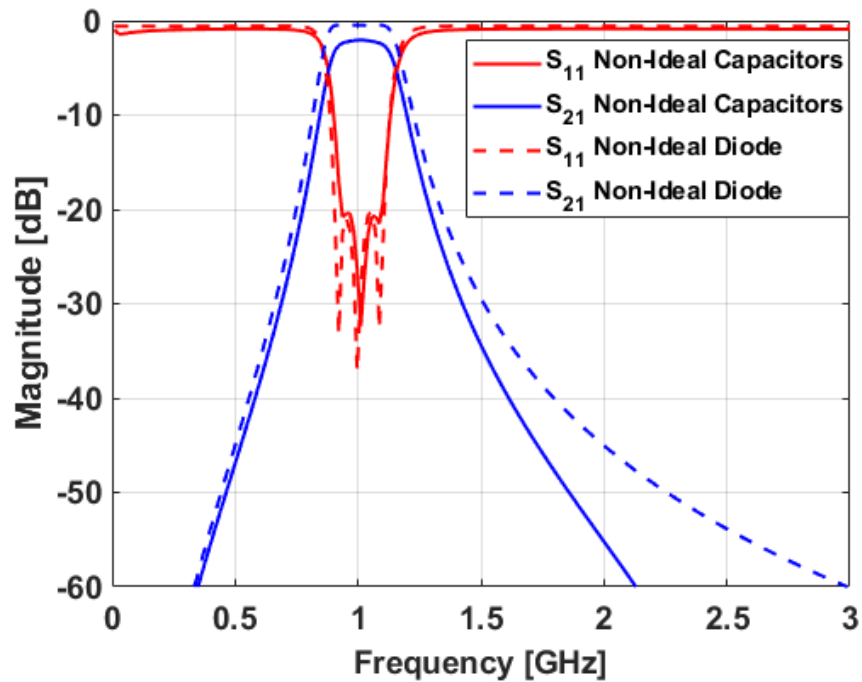


Figure 4.11: Filtenuator simulation S-parameters after adding measured capacitor S-parameters compared to non-ideal diode S-parameters

4.2.5 Adding Microstrip Traces and Vias

Finally, the last step in the design and simulation process is to add models of microstrip traces between components and models of vias to ground where necessary. It is decided to make a 75-mil-wide (50 ohm) line at the input and output of the filtenuator and then taper the line down to a 32-mil-wide microstrip so that the traces were the same size as the pads of the lumped components. The vias to ground are designed with a diameter of 20 mils and a $75 \times 75 \text{ mil}^2$ pad. These decisions are made to simplify the design of the layout. The ADS simulation after adding microstrip and via models to the simulation are shown in Figure 4.12 while the S-parameters of the ADS simulation after adding microstrip lines and vias to ground are shown in Figure 4.13. The insertion loss of the filter has stayed the same with

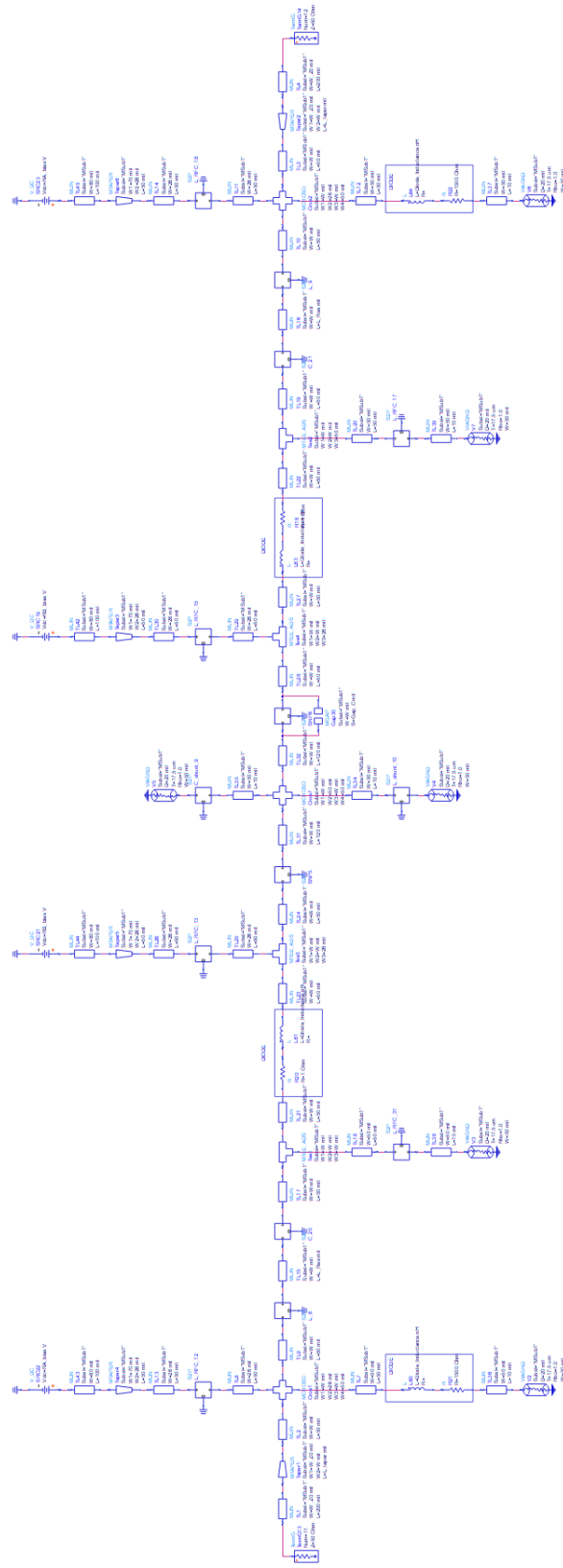


Figure 4.12: Filtenuator ADS schematic after adding microstrip trace and via models

about 2 dB of attenuation at the passband. The addition of vias to ground does not seem to have any noticeable impact on the response. The S_{11} is still matched across the passband; however, there is also more degradation and it loses much of its Chebyshev shape. This could be due to a reduction in Q in the resonators due to the addition of microstrip lines to the resonators. It should also be noted that the baseline loss of the filtenuator is 2 dB. Because of this intrinsic loss of the filtenuator, to create a 3 dB filtenuator it is necessary to design the resistive-network to add 1 dB of loss to the 2 dB of intrinsic loss. This needs to be done for all successive levels of passband attenuation.

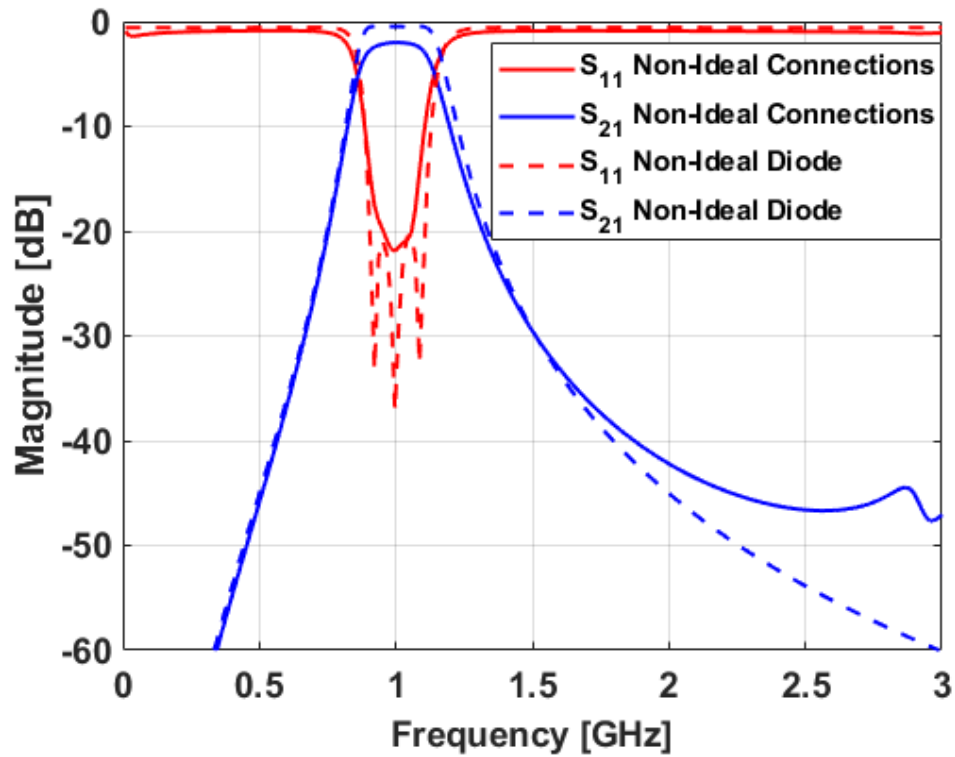


Figure 4.13: Filtenuator simulation S-parameters after adding microstrip trace and via models

4.2.6 Multiple Levels of Attenuation

Once the filtenuator for the lowest loss case has been designed, additional levels of attenuation are designed and simulated. These additional levels of attenuation are obtained by using the previous simulation and tuning the resistance values of the PIN diodes. The S_{21} of the simulated filtenuator with multiple levels of passband attenuation is shown in Figure 4.14. The passband attenuation of the filter is tuned from 3 to 7 dB. The center frequency of the filter is around 1 GHz, although it is shifted slightly down due to component tolerances. Near 2.8 GHz a resonance appears that is attributed to the measured inductor and capacitor S-parameters used in the ADS simulation and their respective self-resonant frequencies.

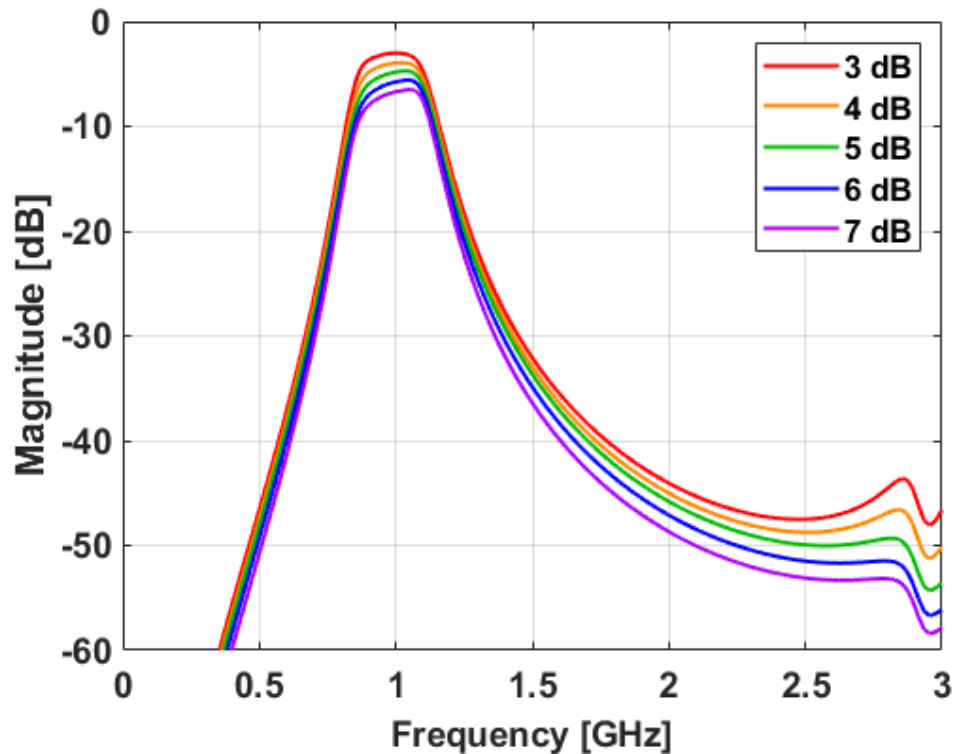


Figure 4.14: S_{21} of the final ADS simulation with 3, 4, 5, 6, and 7 dB of loss

The zoomed-in plot of the simulated S_{21} is shown in Figure 4.15. When looking at a zoomed-in plot of the simulated filter attenuator S_{21} , the center frequency of the filter attenuator is verified to be shifted down about 10 MHz. The trend is also observed that with increased attenuation, the passband flatness of the filter response becomes compromised. This is due to the shunt resonator not being centered at exactly 1 GHz due to component tolerances.

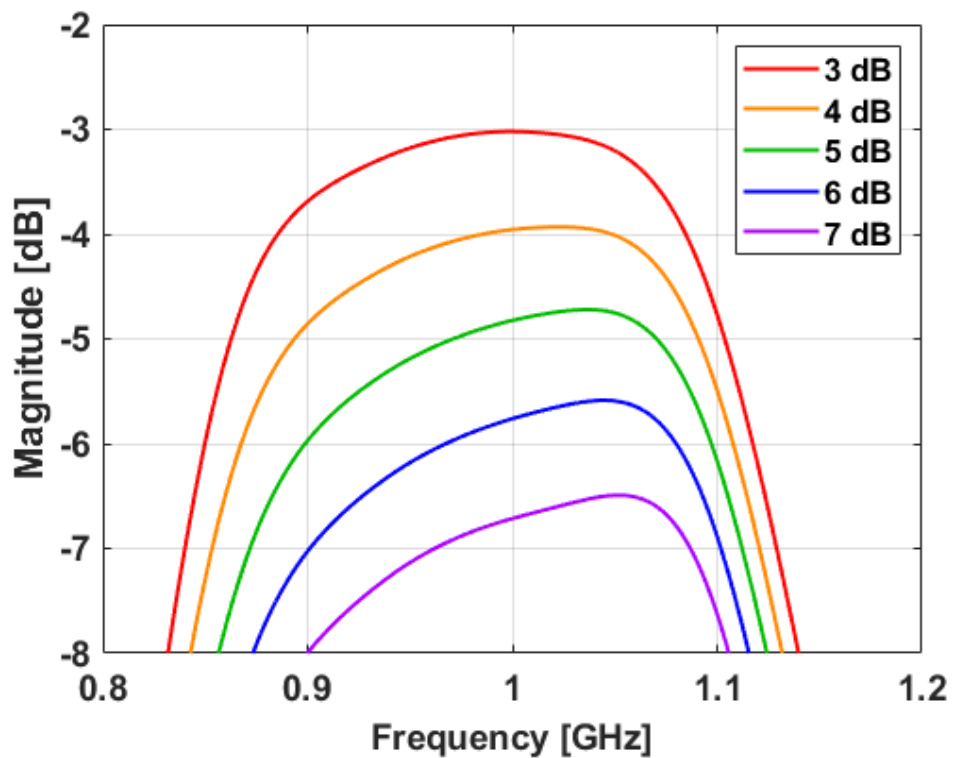


Figure 4.15: Zoomed-In S_{21} of the final ADS simulation with 3, 4, 5, 6, and 7 dB of loss

The S_{11} of the simulated filter attenuator with multiple levels of passband attenuation is shown in Figure 4.16. The filter attenuator is shown to be well-matched with at least 14 dB of return loss at the passband for all levels of passband attenuation. The out-of-band return loss is shown to decrease as the attenuation is increased, which coincides with a decrease in the shunt resistance. This verifies that this decrease in

out-of-band return loss is due to the shunt resistance in theory.

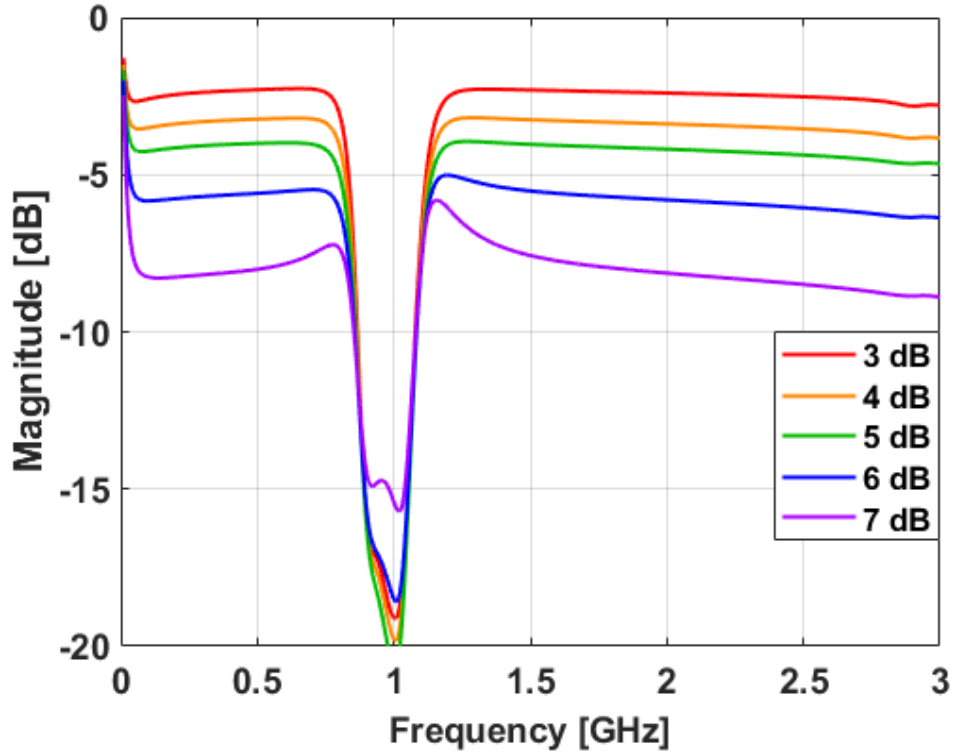


Figure 4.16: S_{11} of the final ADS simulation with 3, 4, 5, 6, and 7 dB of loss

4.3 Fabrication

The filtenuator is implemented on a 30-mil-thick Rogers 3003® laminate substrate [20] with 1/2 oz. copper thickness. The circuit is designed as a standard two-copper-layer printed circuit board (PCB) with the top layer being the signal layer containing all of the components and the bottom layer being a ground plane. The input and output traces of the filtenuator are 50 ohm microstrip transmission lines connecting to standard edge-launch SMA connectors [21]. The 50 ohm input traces are then tapered down to 32-mil-wide microstrip traces so that they can be run straight into the component pads. The vias have a diameter of 19.7 mils (0.5

mm) to facilitate the application of the LPKF ProConduct conductive polymer in addition to being a standard drill size. The inductor and capacitor of the shunt resonator are given separate pads that are each equidistant from the input traces. This is done to ensure the symmetry and reciprocity of the filter's response. The top layer of the PCB is patterned and the vias are drilled using an LPKF ProtoMat S104. The vias are then plated using the LPKF ProConduct process. The layout of the filter PCB is shown in Figure 4.17.

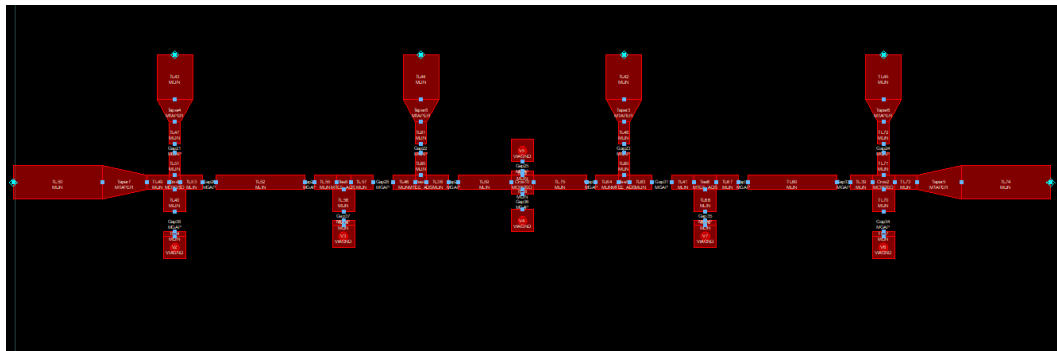


Figure 4.17: Layout of the tunable filter

The final step of the fabrication process is soldering the lumped RLC components to the PCB. The resistors, capacitors, and inductors are soldered to the board using a reflow process and silver solder paste. To minimize drift of components from their desired locations during the reflow process, a small length of transmission line was added to all shunt component pads. The specific inductors used for the resonators are the Coilcraft CT series 0603 inductors [22], the capacitors are Murata high-Q GJM series 0402 capacitors [23], the RF chokes are 0402DF series ferrite chip inductors [32], and the diodes used are SMP1304 SC-79 PIN diodes [30]. The final fabricated and populated filter is shown in Figure 4.18.



Figure 4.18: Fabricated and populated PCB of the tunable filter

4.4 Measured Results

The proposed tunable filter design is measured using an Agilent Technologies N5225A precision network analyzer calibrated using an Agilent N4692-60006 electronic calibration module. The S-parameters for the initial tunable filter

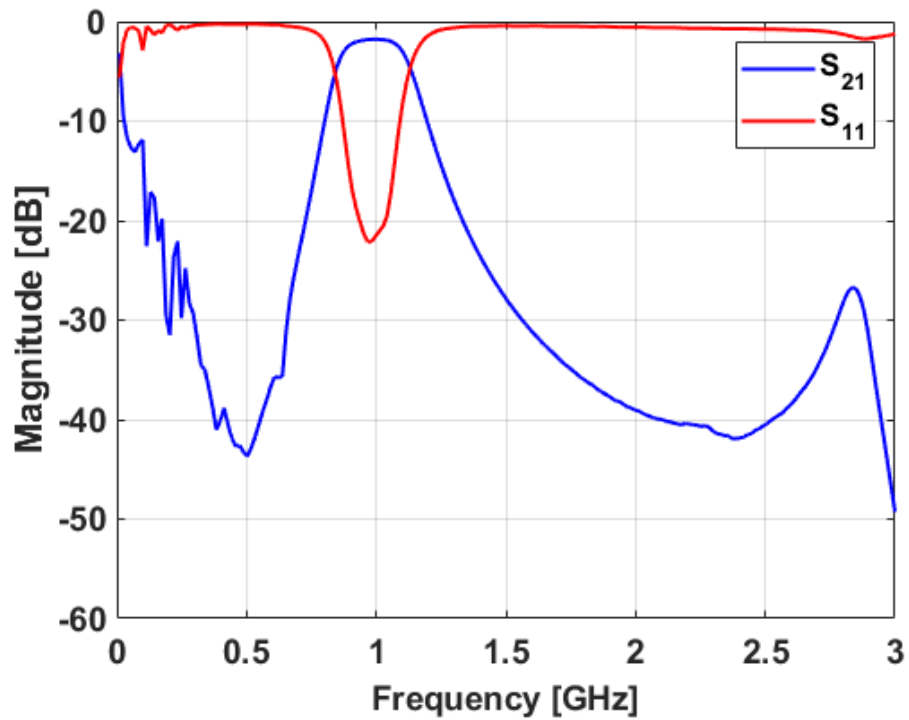


Figure 4.19: Measured S-parameters of the filter with both diodes sharing a power supply

are shown in Figure 4.19. The initial measured results show that the designed tunable filtenuator functions as designed in-band, however, there are a few out-of-band issues with the results. At frequencies lower than 500 MHz, wideband noise appears in the response. There is also a resonance around 2.8 GHz that also appears in the ADS simulation.

There are several things that could cause the low-frequency noise to appear in the measurements. One of these things could be that in the initial measurements, the shunt diodes shared the same DC power supply for their bias. The effect of this was replicated in the ADS simulation by connecting the bias lines for the shunt diodes. After connecting the bias lines, the simulation shows the same trend in the low-frequency response as in the measured results, although there is no noise added

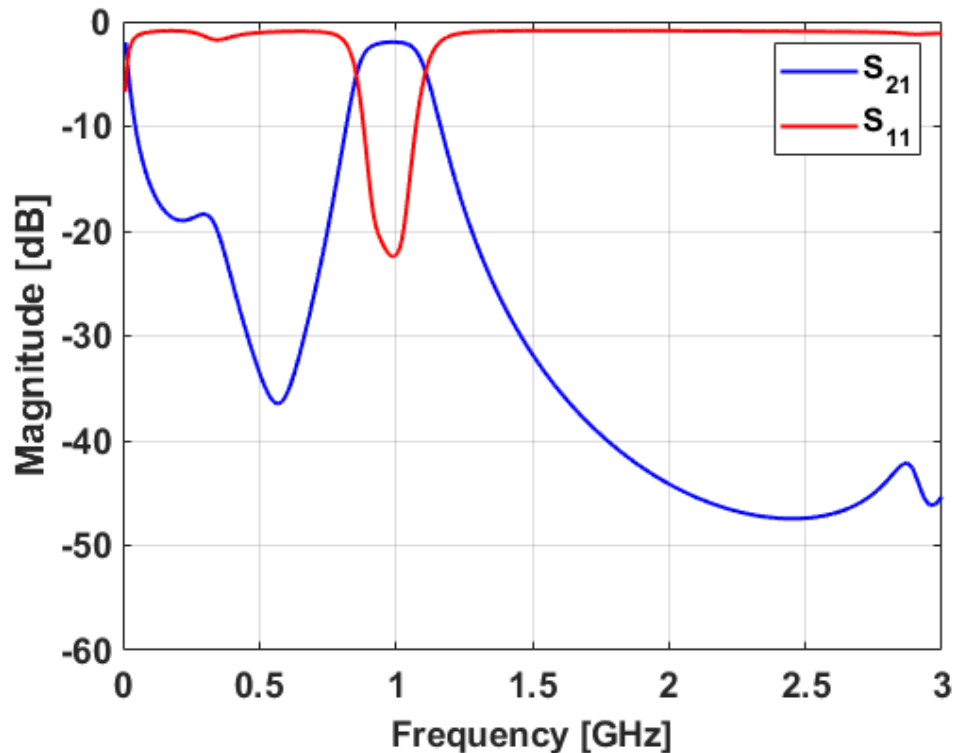


Figure 4.20: S-parameters of the filtenuator ADS simulation with both diodes sharing a power supply

to the bias lines in the simulation. The S-parameters for the shunt diodes sharing the same power supply in ADS are shown in Figure 4.20.

Now that it has been determined that sharing the same power supply will cause the lowpass filtering characteristics of the RF choke to become degraded due to the effective series combination of the inductors that are being used as RF chokes, separate power supplies are used for the shunt diode DC bias. The filtenuator was tested to verify this hypothesis. The S-parameters for the shunt diodes using separate power supplies are shown in Figure 4.21. There is a great improvement in the low-frequency performance of the filter, however, there is still -20 dB of noise below 250 MHz.

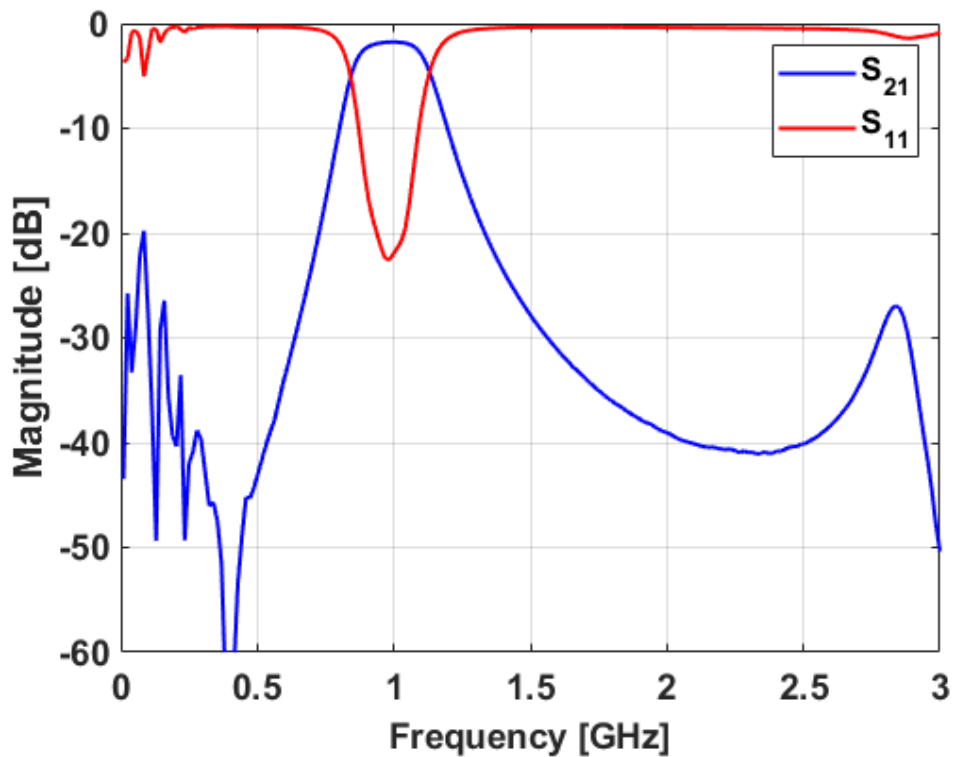


Figure 4.21: Measured S-parameters after using separate power supplies for shunt diodes

Another issue that could cause the remaining low-frequency noise is that the roll-off of the single series inductor is not steep enough to effectively attenuate the noise. To increase the steepness of the roll-off, a 10 nF bypass capacitor shunted to ground is added to the bias line. This addition effectively makes the lowpass filter on the bias line a second-order filter and thus results in a steeper roll-off compared to a first-order filter. The S-parameters comparing the response of the single RF choke and the RF choke with an added bypass capacitor are shown in Figure 4.22.

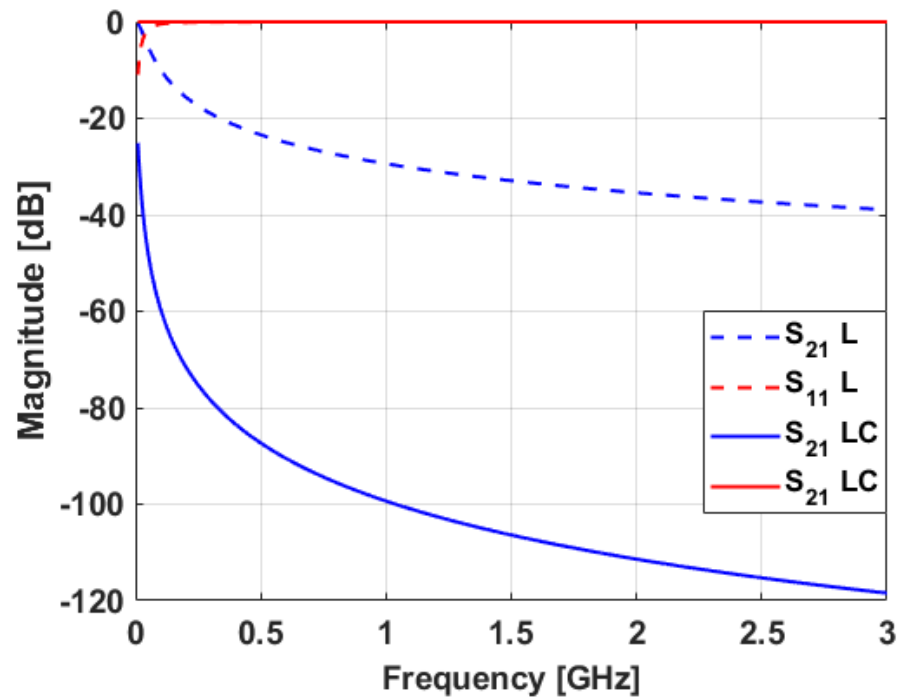


Figure 4.22: Simulated S-parameters of the single inductor bias line compared to the inductor and capacitor bias line

A 10 nF bypass capacitor is added to the bias line to further isolate the DC power supply from the RF circuit. The filtenuator circuit is then measured again and the low-frequency noise is found to be even more attenuated than it was previously with at least 40 dB of rejection below 500 MHz. The S-parameters of the filtenuator after adding a bypass capacitor to the bias lines are shown in Figure 4.23.

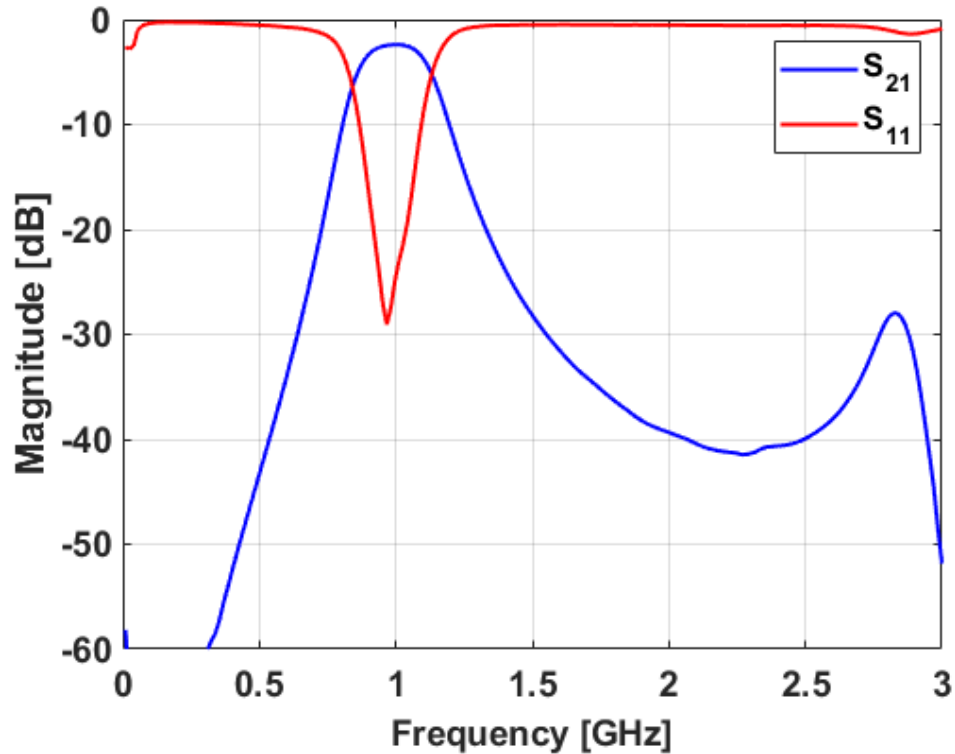


Figure 4.23: Measured S-parameters after adding bypass capacitor to bias lines

The measured S-parameters with the low-frequency issue fixed will now be compared to the simulated S-parameters. The S-parameters of the simulated results compared with the measured results of the filtenuator at the lowest attenuation level are shown in Figure 4.24. The center frequency for both the simulated and measured results is around 990 MHz due to component availability, while the pass-band attenuation is 2 dB for both simulated and measured results. The bandwidth of the filtenuator is slightly wider in the measured results than in the simulation. This could be because the loss in components and traces is slightly less in the fabricated circuit than in the simulated one. The S_{11} at the passband looks similar in simulation and measurements, however, the out-of-band measured results show less return loss. This could be because the PIN diodes used have a different resistance range

than indicated by the datasheet. However, there is excellent agreement between the simulated and measured results.

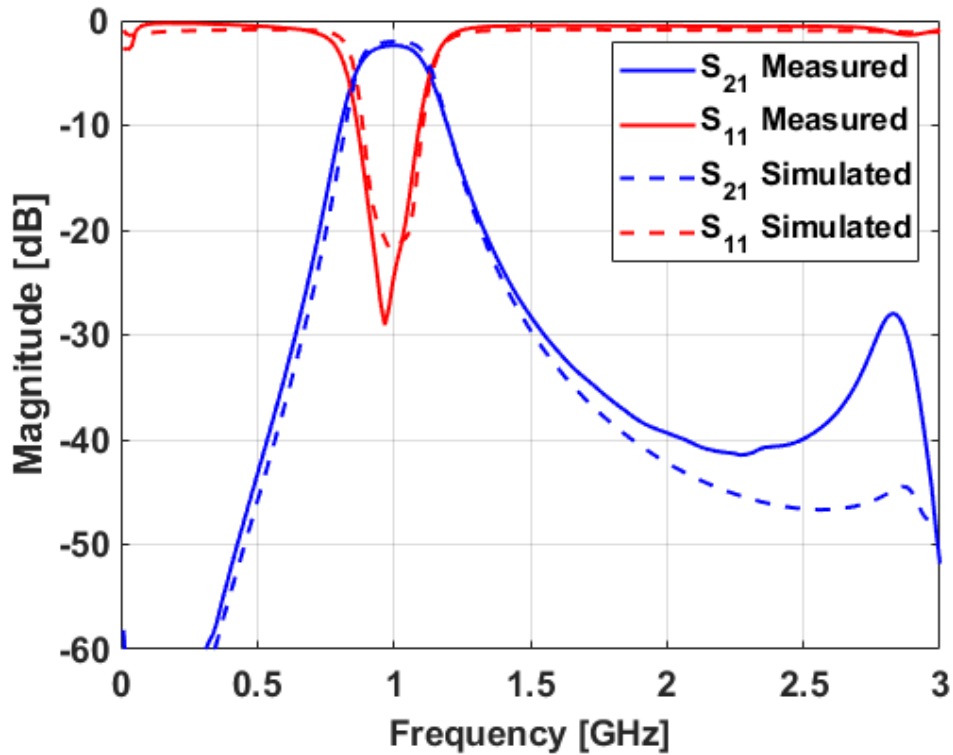


Figure 4.24: S-parameters of the filtenuator simulation compared to the measured results

Now that the low-frequency noise has been mitigated and the simulated and measured results of the lowest attainable attenuation level have been compared and found to be in good agreement, multiple additional levels of passband attenuation will be tested. The passband attenuation of the filtenuator is tuned from 3-7 dB. The resonance near 2.8 GHz is observed to slowly go away as the attenuation is increased. The S_{21} showing 3, 4, 5, 6, and 7 dB of attenuation are shown in Figure 4.25.

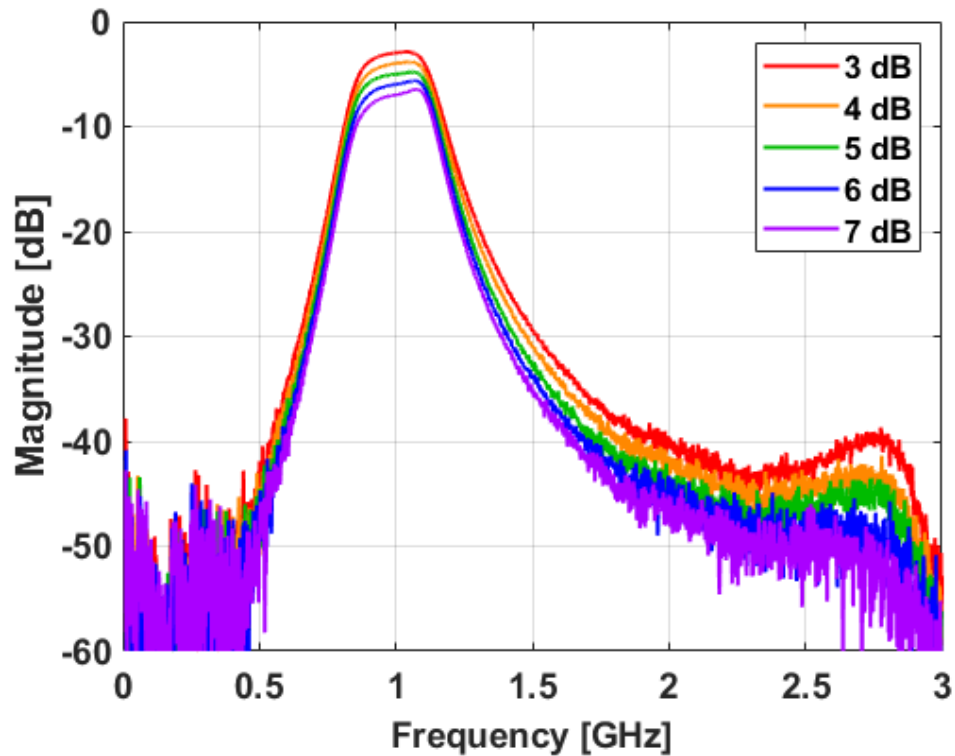


Figure 4.25: S_{21} of the final filtenuator measurements with 3, 4, 5, 6, and 7 dB of loss

The zoomed-in plot of the measured filtenuator S_{21} is shown in Figure 4.26. When looking at a zoomed-in plot of the filtenuator S_{21} the center frequency is shifted down to 990 MHz for all measured levels of attenuation. It is also observed that with increased passband attenuation, both the filter bandwidth and passband flatness suffer some degradation. This is due to the shunt resonator not being centered at exactly 1 GHz due to component tolerances.

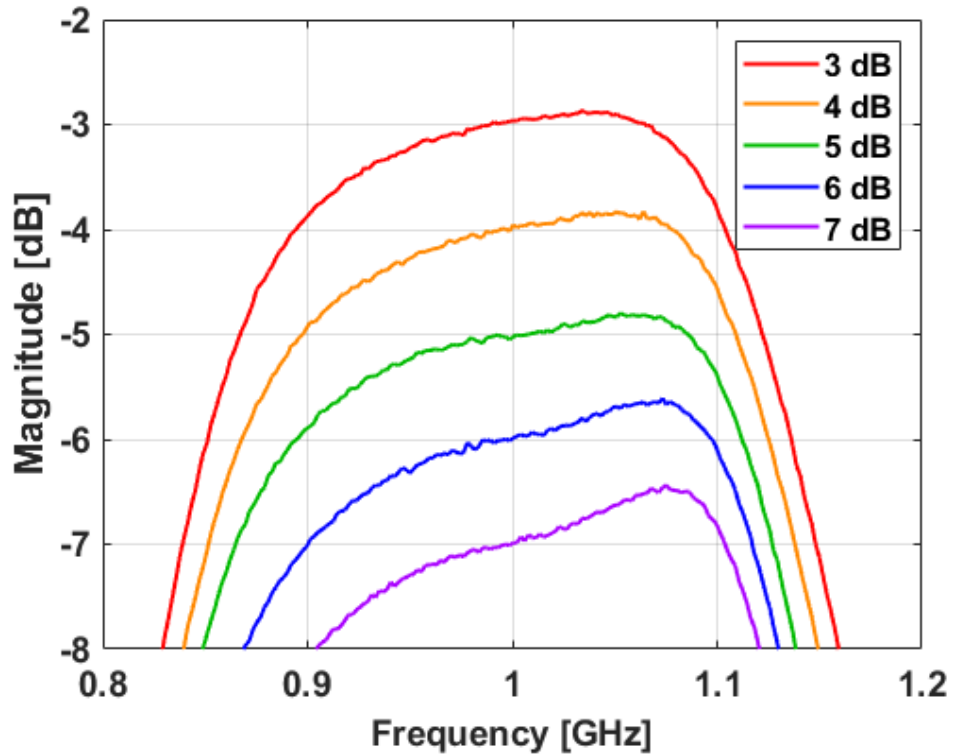


Figure 4.26: Zoomed-In S_{21} of the final filter measurements with 3, 4, 5, 6, and 7 dB of loss

The S_{11} of the measured filter is shown in Figure 4.27. The filter is shown to be well-matched with at least 12 dB of return loss at the passband for all levels of passband attenuation. The out-of-band return loss also decreases as the passband attenuation is increased, which coincides with a decrease in the shunt resistance. This observation verifies that this decrease in out-of-band return loss is due to the shunt resistance.

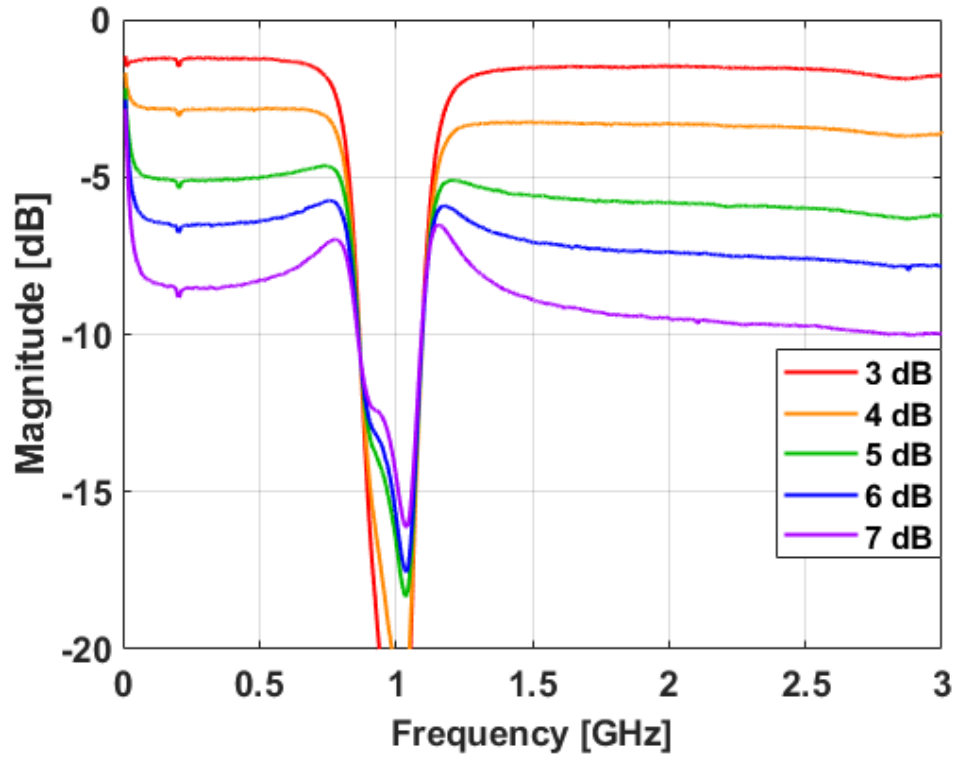


Figure 4.27: S_{11} of the measured results with 3, 4, 5, 6, and 7 dB of loss

The group delay of the tunable filter is calculated using the measured S_{21} found in Figure 4.25. The group delay as a function of passband attenuation is shown in Figure 4.28. Similar to the static filter in Chapter 3, the group delay at the center frequency of the filter stays constant for all levels of passband attenuation measured. This is ideal for RF systems as a single system delay calibration can be conducted and used for all attenuation scenarios.

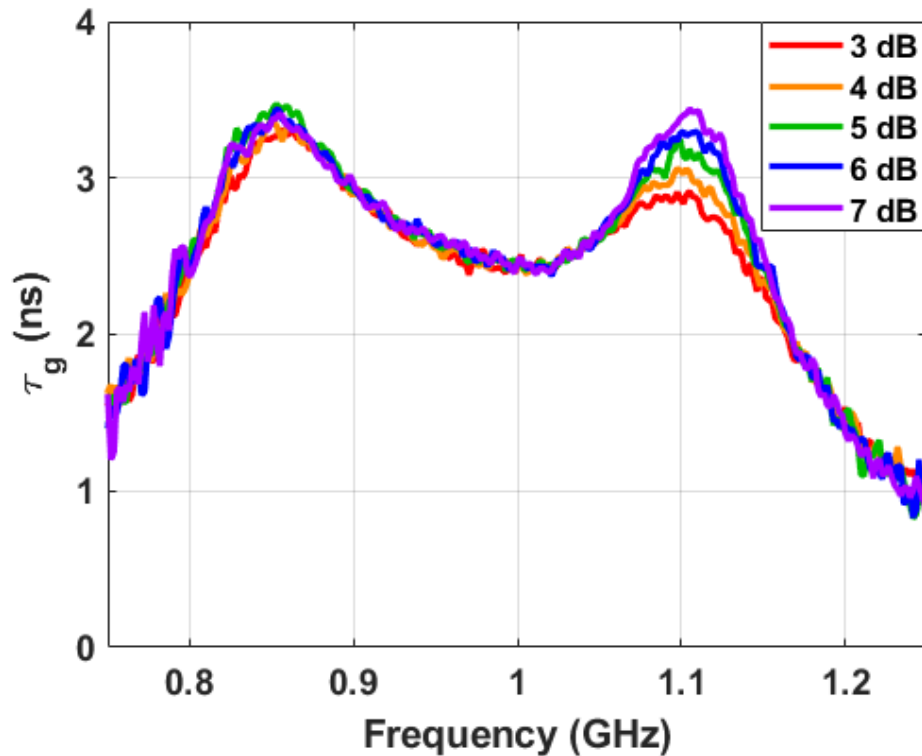


Figure 4.28: Group delay of the measured filtenuator with 3, 4, 5, 6, and 7 dB of loss

Several interesting observations are made while tuning the PIN diodes. It is found that one of the shunt diodes draws more current for the same voltage being applied. The voltage difference needed to obtain the same amount of current is about 15 mV. This difference is due to differences in the DC resistance of the RF chokes and the diodes used. It is also found that the diode resistance becomes much more sensitive to changes in voltage and current when not being observed at the on or off states. A table of values showing the filtenuator loss at the center frequency, the voltages, and the currents used to obtain the measured results are shown in Table 4.1.

Table 4.1: Table of filtenuator losses and the corresponding biasing voltages and currents

Loss (dB)	V_{A1} (V)	I_{A1} (mA)	V_{A2} (V)	I_{A2} (mA)	V_B (V)	I_B (mA)
1.72	0	0	0	0	1	100
2.02	0.030	0.00065	0.032	0.00065	0.82	18.7
2.98	0.505	0.036	0.520	0.036	0.766	8.13
4.00	0.560	0.100	0.575	0.1	0.751	6.32
5.01	0.595	0.200	0.610	0.2	0.750	6.2
6.00	0.610	0.265	0.625	0.267	0.733	4.6
6.99	0.625	0.340	0.640	0.34	0.722	3.79
8.02	0.635	0.420	0.650	0.42	0.709	2.99
9.00	0.640	0.470	0.655	0.44	0.693	2.24
10.00	0.650	0.580	0.665	0.53	0.687	2

4.5 Summary

In this chapter, a tunable filtenuator circuit was designed, simulated, and fabricated. A third-order tunable bandpass filtenuator was designed using PIN diodes as tunable resistances. This circuit was then designed step-by-step in ADS using non-ideal component models. An evaluation of the effects of bias line configuration on the out-of-band performance of the filtenuator was also performed. The design was then fabricated and tested and found to be in excellent agreement with simulation with levels of attenuation from 2-7 dB demonstrated while maintaining a match at the passband. The group delay of the filtenuator was also shown to be constant at the designed center frequency of the filter for all measured levels of passband attenuation. This shows that not only is the filtenuator concept a boon for system C-SWaP and dynamic range, but could also be implemented within a system without further complicating the calibration of the overall system.

Chapter 5

Conclusions and Future Work

5.1 Conclusions

Due to the soaring demands of RF systems to become more compact while simultaneously retaining the ability to detect very small and very large signals at the same time, more adaptable RF systems are needed. Tunable systems offer a simple and effective solution to these issues. Although much of the research in the area of tunable filters involves tuning the frequency or bandwidth of the filter, there is little research concerning tuning the passband insertion loss of filters.

In this thesis, the theory, design, simulation, and fabrication of filtenuators has been demonstrated. The generalized theory and design equations for several different types of filtering attenuators were derived. The generalized theory was then expanded to higher-orders of filtenuators. A static, proof of concept filtenuator with multiple levels of attenuation using high-frequency resistors was designed, simulated, fabricated, and validated. A real-time, continuously tunable filtering attenuator utilizing PIN diodes was designed, simulated, fabricated, and validated through testing. This lays the groundwork for future filtenuator designs.

5.2 Scientific Impact

While several different variants of filtenuators have been demonstrated, to the authors' knowledge, this is the first work detailing a rigorous derivation of the theory for a generalized filtering attenuator structure. This structure allows for the design of a filtenuator with a lowpass, highpass, bandpass, or bandstop response as well as any frequency or system impedance. A proof-of-concept static filtenuator was implemented to verify the theory outlined in Chapter 2 and demonstrate a decrease in SWaP. Additionally, a continuously tunable filtenuator using lumped-element components was designed, simulated, and fabricated which has the potential to increase the dynamic range of future RF systems by allowing them to receive low powered signals as well as more high powered signals.

5.3 Future Work

Although the design, fabrication, and measurement of a continuously tunable filtenuator have great potential to decrease system SWaP as well as increase dynamic range, there are still areas of this work that can and need to be explored in the future.

One area of this work that could be further explored is the addition of frequency agility to the current design. This could be implemented by using varactors as electronically tunable capacitors and adding them to the design. The addition of frequency agility capabilities to the current continuously tunable filtenuator design would add another degree of flexibility to the filter and enable a further decrease in overall system SWaP.

Another area of this work that could be further explored is making the filtenuator

design reflectionless [33]. This addition would make the filtenuator matched outside of the passband and allow for the filtenuator to deal with potential ringing between an amplifier and the filtenuator within a system.

A final area of the filtenuator that could be explored is a further derivation of the S-parameters. In Chapter 2 a derivation of the S-parameters for a generalized filtenuator structure was performed, however, the circuit was assumed to be symmetric with R_{A1} being the same as R_{A2} and R_{B1} being the same as R_{B2} , however, there has been no work done on what can be done by making the filtenuator structure asymmetric.

The simulated group delay for a filtenuator circuit with 3, 7, and 10 dB of attenuation is shown in Figure 5.1. The group delay for the symmetric case of the filtenuator is shown to be flat at the center frequency of the filter.

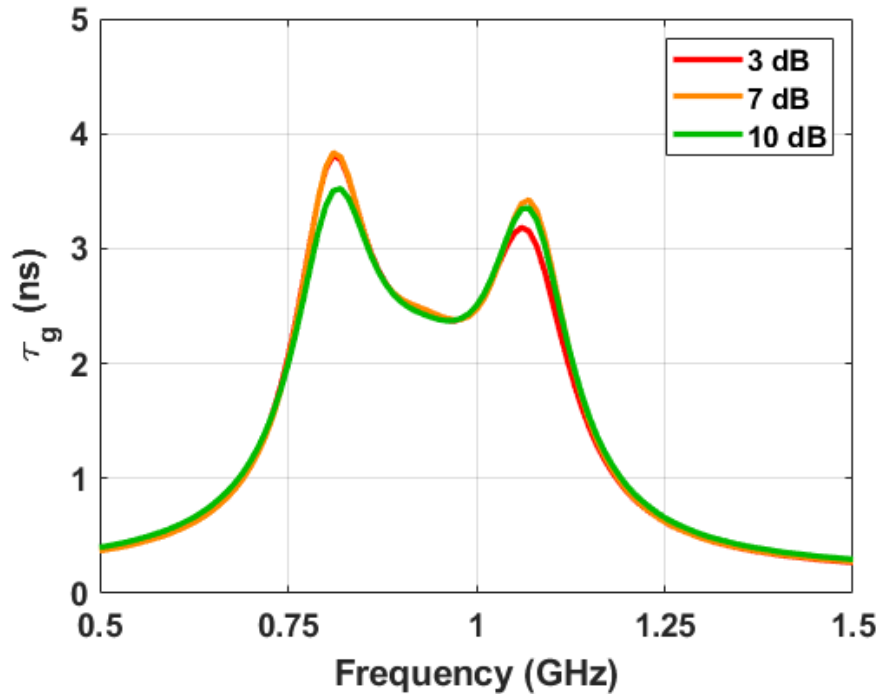


Figure 5.1: Calculated group delay of a symmetric filtenuator simulation with 3, 7, and 10 dB of attenuation

A simulation of the group delay for the asymmetric case of the filtenuator where R_B is not spread out along the resonators is shown in Figure 5.2. Although the group delay is flat for the symmetric filtenuator, the asymmetric case shows a decrease in center frequency group delay with increased attenuation.

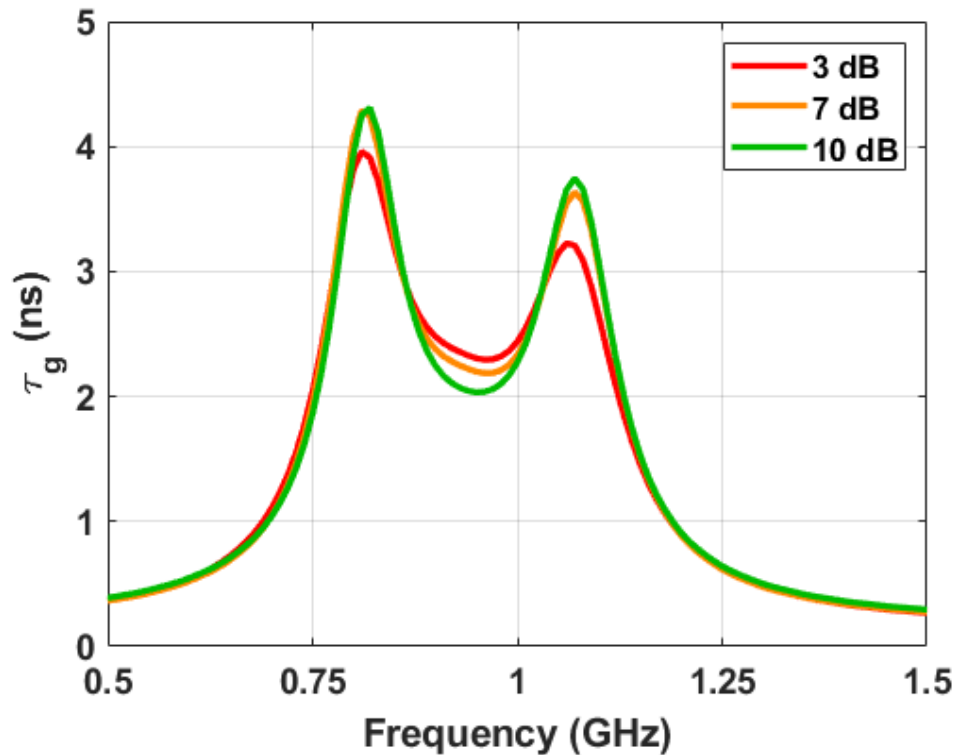


Figure 5.2: Calculated group delay of an asymmetric filtenuator simulation with 3, 7, and 10 dB of attenuation

This unusual behavior of the asymmetric filtenuator could be better understood with a further derivation of an even more generalized filtenuator structure and would provide more insight into these interesting results. Other useful and interesting insights could also be gained by pursuing this difficult yet worthwhile endeavor.

References

- [1] R. Keim, “What is a low pass filter? a tutorial on the basics of passive RC filters.” Available: <https://www.allaboutcircuits.com/technical-articles/low-pass-filter-tutorial-basics-passive-RC-filter/>, Accessed April 5, 2022.
- [2] I. Hunter, “Theory and design of microwave filters.” The Institution of Engineering and Technology, 2006.
- [3] H. Sigmarsson, “ECE 5733 RF microwave filter design lecture 12.” University of Oklahoma Lecture, 2021.
- [4] D. Pozar, “Microwave engineering.” Wiley, 1990.
- [5] “RF attenuators.” Available: everythingrf.com/browse/rf-attenuators, Accessed April 5, 2022.
- [6] M. Dishal, “Design of Dissipative Band-Pass Filters Producing Desired Exact Amplitude-Frequency Characteristics,” *Proceedings of the IRE*, vol. 37, no. 9, pp. 1050–1069, 1949.
- [7] G. Arıturk and H. H. Sigmarsson, “Lossy Microwave Filters With Active Shape Correction,” *IEEE Access*, vol. 9, pp. 35 075–35 087, 2021.
- [8] J. Bae and C. Nguyen, “A 44 GHz CMOS RFIC Dual-Function Attenuator with Band-Pass-Filter Response,” *IEEE Microwave and Wireless Components Letters*, vol. 25, no. 4, pp. 241–243, 2015.
- [9] S. Daoud and P. Shastry, “A novel wideband MMIC voltage controlled attenuator with a bandpass filter topology,” in *European Gallium Arsenide and Other Semiconductor Application Symposium, GAAS 2005*, 2005, pp. 629–632.
- [10] C. Fan, B. Wu, N. Wu, M. Wu, and W. Su, “Dynamically Tunable Four Band Filtering Attenuator Based on Graphene Integrated Microstrip Multi-mode Resonator,” in *2019 Photonics Electromagnetics Research Symposium - Fall (PIERS - Fall)*, 2019, pp. 1033–1039.

- [11] B. Wu, C. Fan, X. Feng, Y.-T. Zhao, J. Ning, D. Wang, and T. Su, “Dynamically Tunable Filtering Attenuator Based on Graphene Integrated Microstrip Resonators,” *IEEE Transactions on Microwave Theory and Techniques*, vol. 68, no. 12, pp. 5270–5278, 2020.
- [12] Y. Yi and A.-Q. Zhang, “A Tunable Graphene Filtering Attenuator Based on Effective Spoof Surface Plasmon Polariton Waveguide,” *IEEE Transactions on Microwave Theory and Techniques*, vol. 68, no. 12, pp. 5169–5177, 2020.
- [13] M. Yasir, S. Bistarelli, A. Cataldo, M. Bozzi, L. Perregrini, and S. Bellucci, “Enhanced Tunable Microstrip Attenuator Based on Few Layer Graphene Flakes,” *IEEE Microwave and Wireless Components Letters*, vol. 27, no. 4, pp. 332–334, 2017.
- [14] C. Fan, B. Wu, and S. Sun, “Controllable Design of Filtering Attenuators Based on Graphene Integrated Dual-Mode Microstrip Resonator,” in *2021 IEEE 4th International Conference on Electronic Information and Communication Technology (ICEICT)*, 2021, pp. 833–835.
- [15] D. R. Jachowski and C. Rauscher, “Frequency-agile bandstop filter with tunable attenuation,” in *2009 IEEE MTT-S International Microwave Symposium Digest*, 2009, pp. 649–652.
- [16] D. R. Jachowski, “Frequency-agile frequency-selective variable attenuator.” U.S. Patent 8,305,164 B1, November 6, 2012.
- [17] E. J. G. Matthaei, L. Young, “Microwave filters, impedance-matching networks, and coupling structures.” Artech House, 1980.
- [18] M. Steer, “Microwave and RF design: A systems approach.” Scitech Publishing, 2015.
- [19] G. B. Reinhold Ludwig, “RF circuit design: Theory and applications.” Pearson, 2009.
- [20] R. Corporation, “Datasheet RO3000 series circuit materials,” 2019.
- [21] Amphenol, “SMA end launch connectors datasheet,” 2012.
- [22] Coilcraft, “Datasheet 0603CT chip inductors,” July 22, 2021.
- [23] Murata, “Datasheet 0402GJM,” December 27, 2021.
- [24] Vishay, “High frequency (up to 40 GHz) resistor, thin film surface mount chip,” 2021.

- [25] Bourns, “3224- 4 mm SMD trimpot trimming potentiometer,” March 31, 2015.
- [26] “Chapter 3-resistor types: Trimpot.” Available: <https://eepower.com/resistor-guide/resistor-types/trimpot/>, Accessed April 5, 2022.
- [27] “Solid-state switches.” Available: <https://www.microwaves101.com/encyclopedias/solid-state-switches>, Accessed April 5, 2022.
- [28] Skyworks, “A wideband general purpose PIN diode attenuator,” October 4, 2011.
- [29] —, “Design with PIN diodes,” August 30, 2021.
- [30] —, “SMP1304 series: Low-distortion attenuator plastic packaged PIN diodes,” July 1, 2016.
- [31] Coilcraft, “Inductors as RF chokes,” October 4, 2017.
- [32] —, “Datasheet 0402DF chip inductors,” October 28, 2021.
- [33] M. A. Morgan, “Reflectionless filters.” Artech House Publishers, 2017.